University of Strathclyde
Department of Pure and Applied Chemistry

Optimisation of Surace Enhanced Raman Scattering from Gold and Silver Nanoparticle Solutions

By

Johan Lundahl

Thesis submitted to the Department of Pure and Applied Chemistry, University of Strathclyde, in fulfilment of the requirements for degree of Doctor of Philosophy.

September 2008

PAGE NUMBERING AS ORIGINAL

I would like to thank professor Ewen Smith and professor Duncan Graham for help and support during my PhD. I would also like to thank professor Klaas Wynne for assistance in the physics related parts of my research.

Also thanks to all members of the Raman group for help and company, espescially Dale Cunningham who provided me with a running group, showed me how evil a Nello can be, and introduced me to the world of Delta Tre athletics.

Finally, thanks to my Family for not letting me forget my roots.

Optimisation of Surface Enhanced Raman Scattering from Gold and Silver Nanoparticle Solutions

Thesis

Johan Lundahl

December 2007

ABSTRACT

The efficiency of Surface enhanced resonance Raman spectroscopy (SERS or SERRS) as a technique is entirely dependent on controlling the parameters responsible for the enhancement effects. In this thesis, some of the critical parameters have been investigated. It is concluded that it is possible to predict and to some degree manipulate the maximum enhancement of the Raman scattering in an experimental setup.

By applying the findings presented in this thesis it is possible to optimise an experimental setup according to a desired purpose where silver or gold nanoparticle solutions are used as the source of surface enhancement. Many of the findings herein are also expected to be applicable to other SER(R)S-systems, and also to be of interest in related techniques, such as metal enhanced fluorescence and surface plasmon resonance.

Methods for the controlled synthesis of silver and gold nanoparticles are presented and techniques for the characterisation of their physical properties are evaluated. Further, a technique enabling the separation of the relative contribution of absorption and scattering to the extinction profile is presented.

Further, the effect of the nanoparticles physical properties on their suitability as SERS substrates is investigated. In particular, the effect of nanoparticle size and nanoparticle solution state of aggregation is investigated in order to optimise the SERS intensity at the detector. The results show that the SERS intensity is critically dependent on these properties, and that it is possible to predict the optimal combination of nanoparticle size, wavelength of the excitation source and aggregation state of the nanoparticle solution.

Finally, the effect of a molecular resonance on the SERRS intensity is demonstrated and confirmed as a significant effect.

TABLE OF CONTENTS

CHAPTER PAGE

CHAPTER 1

INTRODUCTION AND THEORY

TABLE OF CONTENTS

CHAPTER PAGE

1.1 General Introduction

Due to continuous improvements in equipment and instrumentation, Raman spectroscopy has become a well-established analytical technique within both industry and research with hundreds of publications on the subject every year. This, combined with the potential of huge enhancement of the inherently weak Raman signal by surface enhancement, has allowed Raman spectroscopy to develop into an ultra-sensitive analytical technique[1-4], with reports of single molecule detection[5-7]. Two different enhancement effects are involved to achieve this kind of sensitivity, resonance Raman scattering and surface enhanced Raman scattering (SERS). Combining these gives the technique called surface enhanced resonance Raman spectroscopy (SERRS) with the potential of enhancing Raman scattering by a factor of 10^{11} or higher[8-10]. To fully exploit these potentials, the combination of surface enhancement substrate, chromophore and excitation source must be optimal. This requires a thorough understanding of the fundamental principles involved.

In this thesis, the effects of particle plasmon resonance and molecular chromophore resonance on Raman scattering on SER(R)S are investigated in silver and gold nanoparticle solutions. It is demonstrated how to choose the experimental parameters to maximize the SER(R)S signal at the collection point.

1.2 ELECTROMAGNETIC RADIATION

Electromagnetic radiation (light) is created as soon as an electric charge is accelerated. All charges are associated with a constant radial electric field **E**. At the instance the charge is accelerated, the electric field in its vicinity is changed, and this change is propagated out in space. Maxwells's Equations state that every time varying **E**-field generates a magnetic, equally time varying **B**-field that is perpendicular to the direction of **E**, and vice versa. This means that as soon as such an electromagnetic wave has been created, it will continue to regenerate itself through space as an electromagnetic wave (figure 1.1).

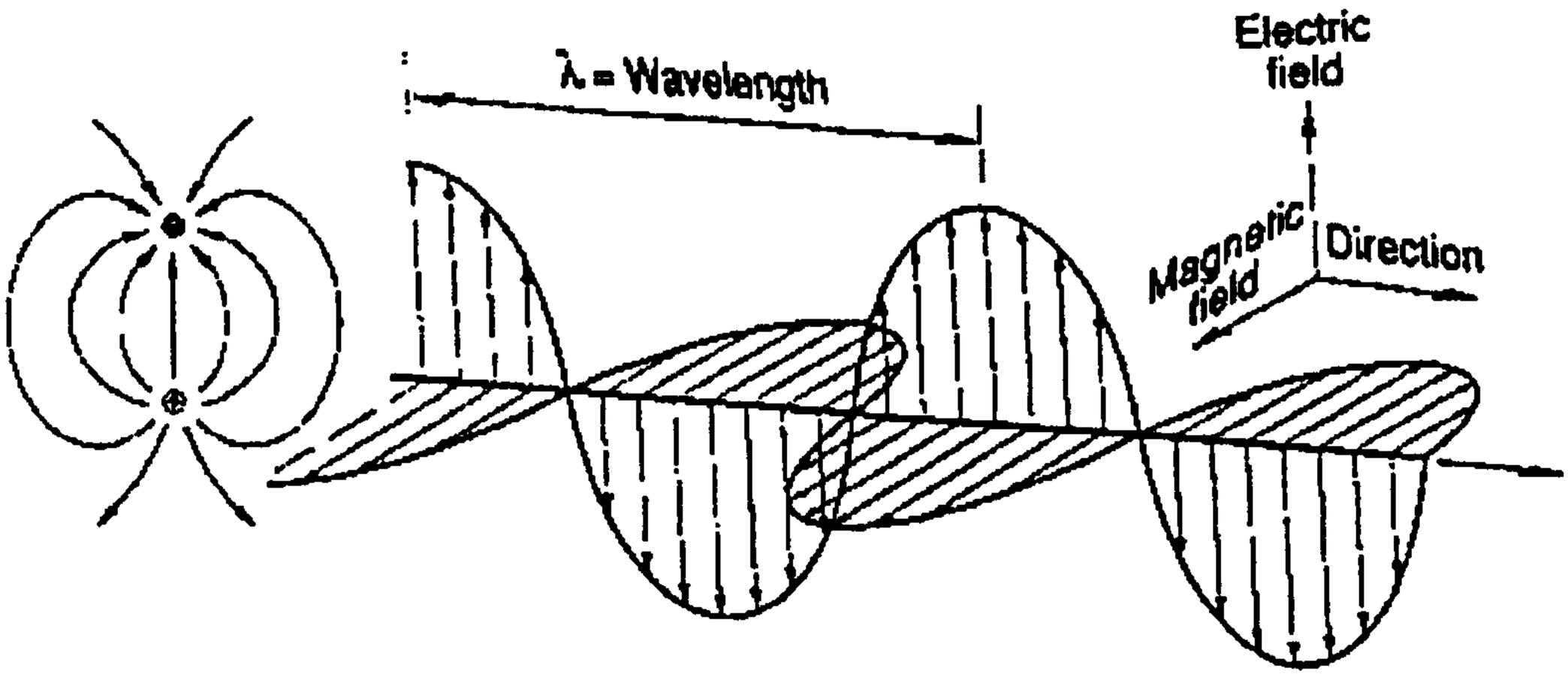

FIGURE 1.1. An oscillating dipole creating an electromagnetic wave. The electric field and the magnetic field are directed perpendicular to each other, and the direction of the light is perpendicular to both the magnetic and electric field. The wavelength of the light is determined by the frequency of the oscillating dipole.

The intensity, or irradiance, *I*, of the light from a radiation source illuminating a surface is

$$I = \varepsilon_0 c \left\langle E^2 \right\rangle_T \tag{1.1}$$

$\left\langle E^2 \right\rangle_T$ is the time averaged electrical field intensity, ε_0 is the electric permittivity of free space and *c* the speed of light. The irradiance is in the direction of the light and

is what is usually referred to as the optical power. The total emissive power, P, from a classical oscillating dipole integrated over all angles is

$$P = \frac{\omega^4 |\vec{\mu}_{ed}|^2}{12\pi\varepsilon_o c^3} \tag{1.2}$$

Where ε_o is the electric permittivity of free space and $\vec{\mu}_{ed}$ is the induced electric dipole moment.

1.3 Raman Scattering

When light interacts with a molecule it can be absorbed, absorbed then emitted or scattered. Elastic scattering is called Rayleigh scattering and inelastic is called Raman scattering, named after Sir C.V. Raman who first reported the phenomena in 1928. If the Raman scattered photon has gained energy, it is called anti Stokes scattering, and if it has lost energy, it is called Stokes scattering (figure 1.2). For anti Stokes scattering to occur, the incoming photon must find the molecule in an excited vibrational electronic state. At room temperature this is far less likely to be the case than to find the molecule in its ground state, as dictated by the Bolzman distribution.

$$\frac{N_n}{N_m} = \frac{g_n}{g_m} e^{\left[\frac{-(E_n - E_m)}{kT}\right]} \tag{1.3}$$

N_n and N_m are the number of molecules in the corresponding energy state E_n and E_m. g is the degeneracy of levels, T absolute temperature and k is the Bolzmann's constant.

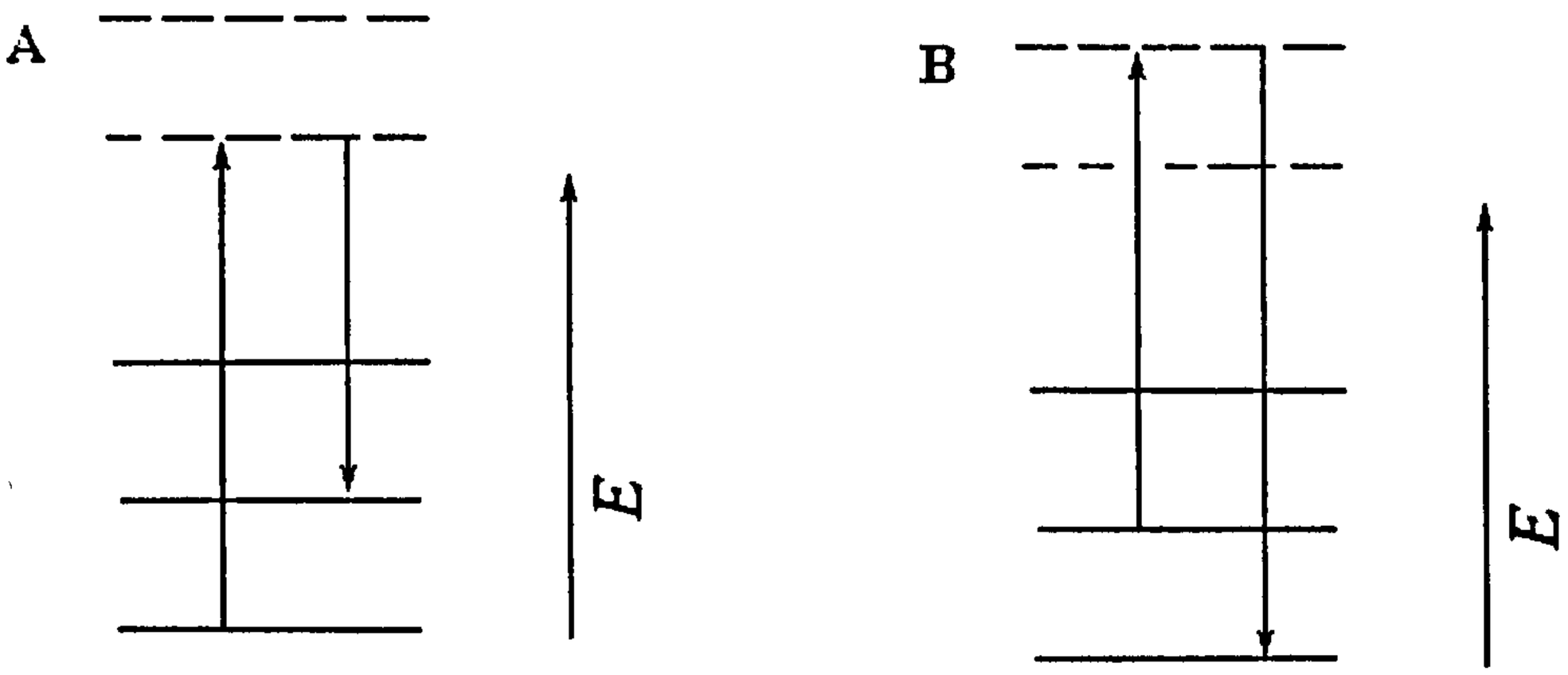

FIGURE 1.2. Schematic of Stokes (A) and anti Stokes (B) scattering. Solid lines represent real vibrational levels within this electronic state, and dotted lines represent virtual vibrational levels and E is the energy level of the state of the molecule.

Since a molecule is more likely to be in its ground state under normal conditions, Stokes scattering is much more intense than anti Stokes scattering under normal conditions. About one incident photon in a million is Raman scattered, and about one in a thousand is Rayleigh scattered.

In Raman scattering, energy is transferred between the photon and the nucleus of the molecules so that the photon is scattered, within a picosecond, either as Stokes or anti Stokes Raman scattering. The Raman scattering intensity can be directly related to the polarisability of the molecule as

$$\vec{\mu} = \vec{\alpha} \cdot \vec{E}(r) \tag{1.4}$$

Where $\vec{\mu}$ is the induced electric dipole moment and $\vec{\alpha}$ (in the units Cm^2V) is a matrix with the molecule polarisability in all directions relative to the coordinate system (x,y,z) chosen. $\vec{\alpha}$ can also be illustrated as an ellipsoid (with the coordinate system directed along the long axis of the ellipsoid) by

$$\vec{\alpha} = \alpha_{xx}x^2 + \alpha_{yy}y^2 + \alpha_{zz}z^2 \tag{1.5}$$

The scattering intensity, I_{Sca}, from an oscillating dipole can be written as:

$$I_{Sca} = k\omega^4 \vec{\alpha}^2 I_0 \tag{1.6}$$

where I_0 is the input irradiance.

The basic selection rule for Raman scattering is that the molecule needs to undergo a change in polarisability for it to occur. This means that symmetric vibrations will give the most intense scattering intensities, as they stretch the polarisability tensor the most.

If the energy of the incident radiation coincides with a transition of the molecule to an excited electronic vibrational state, the Raman scattering can be enhanced with around 2-4 orders of magnitude. This is called resonance Raman scattering (figure 1.3). In many cases it is accompanied by an increase in fluorescence.

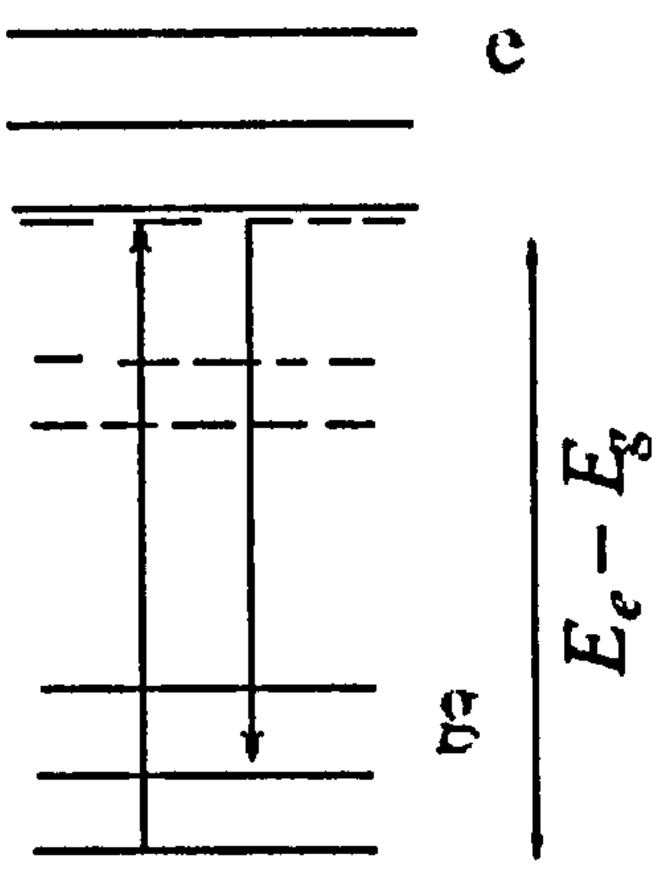

FIGURE 1.3. Schematic of the resonance Raman process. The electron is excited to a virtual vibrational state that coincides with a real vibrational state. **e** represents the first excited electronic state of the molecule and **g** the ground state.

1.4 Optical properties of Gold and Silver

Gold and silver have the same type of electron configuration (together with copper), $d^{10}s^1$, where the completely filled d-shell efficiently screens the valence electron in the s-shell from the atom core. When these metals form clusters, the valence electron is donated to the aggregate, with the atomic nuclei's acting as a positive background charge. In interaction with light, the metals will behave in different ways depending on the energy of the light. The UV-visible energy range of light can be divided in to two general regions for silver and gold. At lower energies they will display free electron like behaviour, and at higher energies, interband transitions will dominate. In addition collective electron oscillations (plasmons) due to interaction with an electromagnetic field can occur in one or both regions. The threshold energy for interband transitions to occur is 3.9 eV and 1.7 eV for silver and gold respectively.

1.5 Lorenz-Drude model for the dielectric constant of noble metals

The interaction of small particles with electromagnetic radiation is dictated by the dielectric constants of the particle and the surrounding matrix.

In the Lorenz model for an oscillator in a local field **E**, basic Newtonian mechanics are applied to a system like the one shown in figure 1.4:

$$e\mathbf{E} = m\ddot{\mathbf{x}} + b\dot{\mathbf{x}} + K\mathbf{x} \qquad (1.7)$$

E is the applied electrical field, **x** is the distance between the charges, e and m are the charge and mass of the electron, K is the "spring constant" between the charges, and b is the damping term.

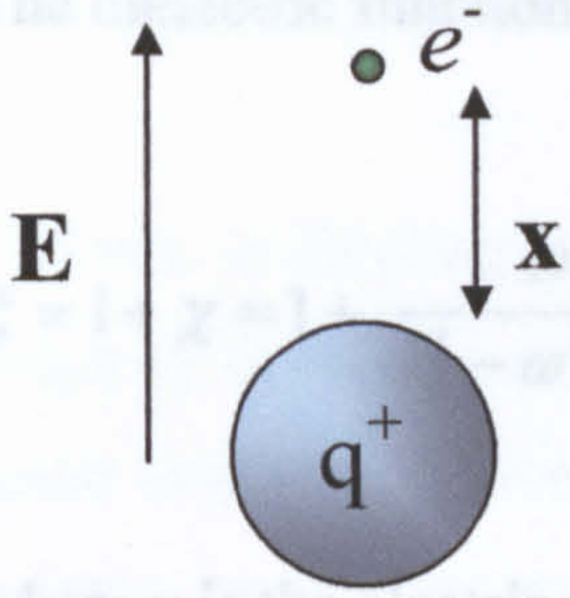

FIGURE 1.4. The system described by equation 1.7. **E** is the applied electrical field, **X** is the distance between the charges $\mathbf{q}^+$ and $\mathbf{e}^-$.

Now, if **E** is time harmonic with frequency ω, then $\mathbf{E} = \mathbf{E}_0 e^{i\omega t}$ and $\mathbf{x} = \mathbf{x}_0 e^{i\omega t}$

$$e/m\,\mathbf{E} = -\omega^2\mathbf{x} + i\gamma\omega\mathbf{x} + \omega_0^2\mathbf{x} \tag{1.8}$$

And this can be rearranged to

$$\mathbf{x} = \frac{(e/m)\mathbf{E}}{\omega_0^2 - \omega^2 + i\gamma\omega} \tag{1.9}$$

where $\gamma = b/m$ and $\omega_0 = \sqrt{k/m}$

$\sqrt{k/m}$ here corresponds to the resonance frequency of a Newtonian "spring and mass" system. The induced dipole moment, **p,** of an oscillator is the charge times the displacement, *e***x. P**, the sum polarisation of the metal sphere is then, with η as the number density of electrons, $\eta\mathbf{p}=\eta e\boldsymbol{x}$ and from this follows, with ε_0 as the electric permittivity of free space

$$\mathbf{P} = \frac{\omega_P^2}{\omega_0^2 - \omega^2 + i\gamma\omega}\varepsilon_0\mathbf{E} \tag{1.10}$$

$$\omega_p^2 = \eta e^2/m\varepsilon_0$$

The dielectric function, ξ, is defined as

$$\xi = 1 + \chi = 1 + \frac{\omega_p^2}{\omega_0^2 - \omega^2 + i\gamma\omega} \tag{1.11}$$

where χ is the electric susceptibility. The real (ξ') and imaginary parts (ξ'') are obtained by multiplying (1.11) with the complex conjugate of its denominator

$$\xi' = 1 + \chi' = 1 + \frac{\omega_p^2(\omega_0^2 - \omega^2)}{(\omega_0^2 - \omega^2)^2 + \gamma^2\omega^2} \tag{1.12}$$

$$\xi'' = \chi'' = 1 + \frac{\omega_p^2\gamma\omega}{(\omega_0^2 - \omega^2)^2 + \gamma^2\omega^2} \tag{1.13}$$

In the Drude model, electrons in metals essentially behave like free electrons. This corresponds to setting the spring constant, K, to 0. From this

$$\xi = 1 + \chi = 1 - \frac{\omega_p^2}{\omega^2 + i\gamma\omega} \tag{1.14}$$

$$\xi' = 1 + \chi' = 1 - \frac{\omega_p^2}{\omega^2 + \gamma^2} \tag{1.15}$$

$$\xi'' = \chi'' = \frac{\gamma\omega_p^2}{\omega(\omega^2 + \gamma^2)} \tag{1.16}$$

1.6 SURFACE MODES IN SMALL SPHERES

Spheres, small compared to the wavelength of light, can interact with incident light, either by absorption or through scattering of the incident photon. For absorption to occur in gold and silver nanoparticles, interband or intraband transitions from valence band electrons to higher energy electron bands of the particle have to be possible. The interaction is dictated by the materials dielectric constants, where the imaginary part corresponds to absorption processes, and the real part corresponds to scattering processes. Gustav Mie 1908 developed a general theory of light scattering that applies to spherical particles of any size that can absorb as well as scatter light[11]. From Mie theory applied to spheres which are small compared to the wavelength of light, an expression for the scattered irradiance and absorption efficiencies of these particles, with ξ_m as the dielectric constant of the surrounding medium, can be derived as

$$Q_{abs} = 4x\,\mathrm{Im}\frac{\xi-\xi_m}{\xi+2\xi_m}, \qquad Q_{sca} = \frac{8}{3}x^4\left|\frac{\xi-\xi_m}{\xi+2\xi_m}\right|^2 \tag{1.17}$$

$x = \frac{2\pi Na}{\lambda}$, with N the refractive index of the surrounding medium, and a is the particle radius. This is equivalent to writing

$$C_{abs} = \pi a^2 k\,\mathrm{Im}\{\alpha\}, \qquad C_{sca} = \frac{k^4}{6\pi}|\alpha|^2 \tag{1.18}$$

In other words, Q is the scattering cross section of the particle, divided by its geometrical cross section. From 1.17 it follows that Q_{abs} and Q_{sca} are at a maximum when $\xi = -2\,\xi_m$. The solution to this equation is $\xi' = -2\,\xi_m$; $\xi'' = 0$, where we also have taken the permeability of the sphere to be equal to that of the surrounding medium. It is useful to note that, at the resonance frequency Q_{abs} and Q_{sca} can take on values higher than 1.

Extending this to an ellipsoid of volume v, and with L as the geometrical factor [0,1], the polarisability becomes

$$\alpha = v\frac{\xi - \xi_m}{\xi_m + L(\xi - \xi_m)} \tag{1.19}$$

$$\alpha_{\max} \leftrightarrow \xi = \xi_m\left(1 - \frac{1}{L}\right)$$

We see that an ellipsoid will have two resonance frequencies. One along its long axis and one along its short axis, with the long axis resonance shifted towards lower energies.

1.7 PLASMONS

In the previous section the conditions for surface plasmon resonance are described. Under these conditions, the electrons of the metal move collectively due to the electric field induced in the particle. This causes the electrons to gather on one side of the particle, building up a charge difference towards the opposite side. The restoring forces due to the charge difference will drive the electrons to equalize this charge by shifting back to the positively charged side of the particle, thus causing the electrons to oscillate. If the exciting light has a frequency coinciding with the eigenfrequency of the particle of this collective oscillation, even weak exciting light sources can cause the plasmon to oscillate, radiating electromagnetic waves. When the nanoparticle is small compared to the wavelength of light, it will behave as if it was in a uniform electric field and the plasmon will oscillate as a dipole.

The resonance wavelength of gold nanoparticles is at around 520 nm (2.4 eV) in water and the lowest interband transition for gold is at 1.7 eV (730 nm). This causes the plasmon resonance of gold to be considerably dampened at this frequency, because a large fraction of the incident photons will be transformed to heat via electron-phonon scattering which leads to a quicker dephasing of the plasmon

oscillation since this provides an additional dephasing process[12-14]. In silver on the other hand, the resonance wavelength is at about 400 nm (3.1 eV) in water, with the lowest interband transition energies beginning at 3.9 eV (320 nm). This causes the plasmon response to be much sharper than for gold. Computationally, these properties are described by the dielectric constant of each metal, section 1.5.

As the particle becomes larger, the particle polarisability will increase, and the resonance frequency of the dipole will shift towards lower energies. When the particle grows further, it will no longer behave as if in a uniform electric field, and higher order oscillations will start to appear at higher energies (shorter wavelengths), illustrated in figure 1.5. These higher order oscillations will mostly be nonradiative because they occur at higher energy where absorption processes dominate[10].

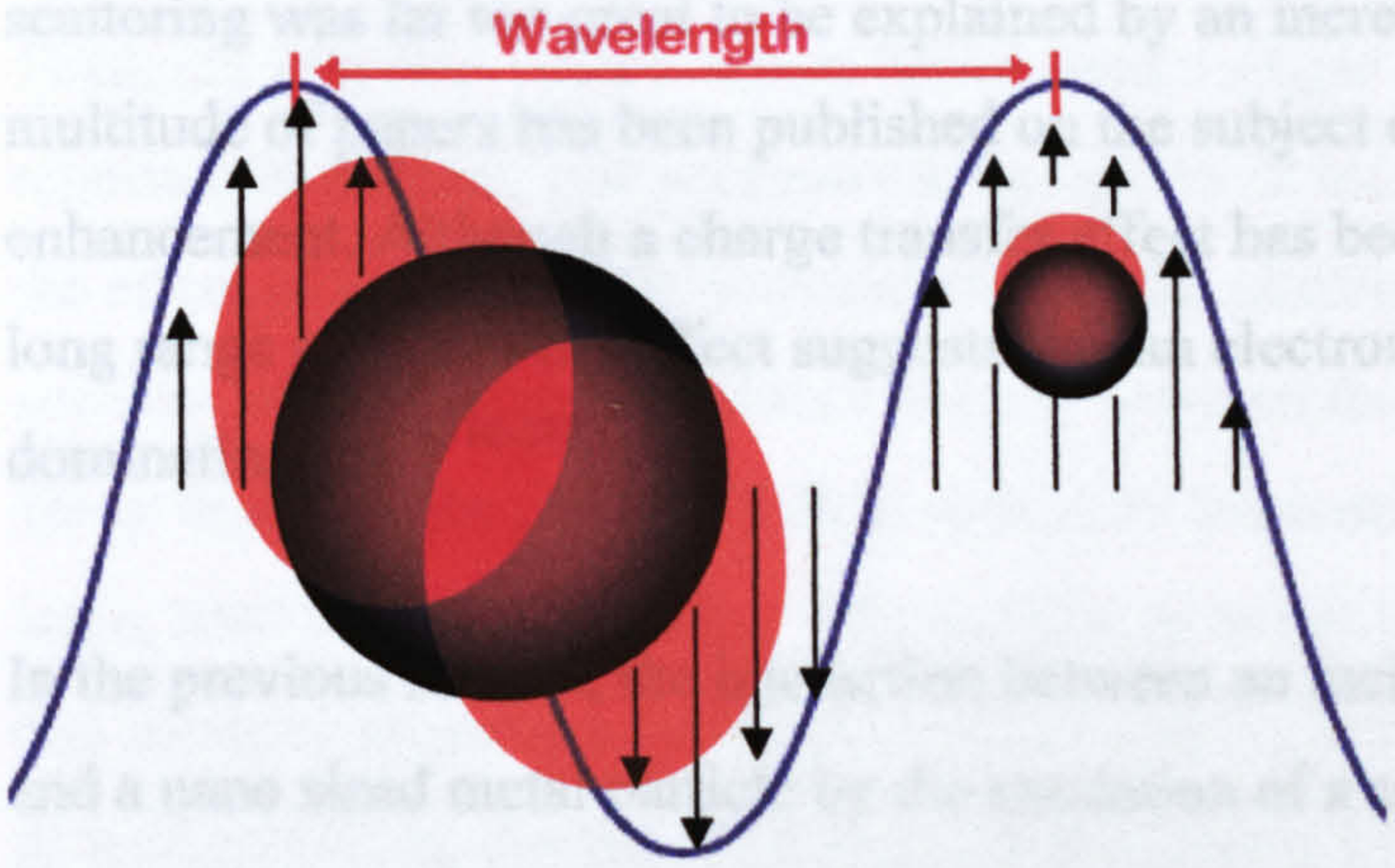

FIGURE 1.5. Schematic of the formation of a quadrupole to the left, and a dipole to the right. The dipole will have a single oscillation in the direction of the E-field. The quadrupole will have one component in the direction of the E-field, and one component in the direction of the propagation of the light wave.

1.8 LIMITATIONS OF THE MEAN FREE PATH

When particles decrease in size, the effect of electrons colliding with the surface will have an effect on the dielectric function. The effect on the real part will be limited,

whilst the effect on the imaginary part will be significant. The effect of this is a broadening of the spectra and a decrease in peak height. The effect on gold will be slightly less dramatic as the damping term from interband transitions is much more significant than for silver, i.e. the free electron part of the dielectric function does not dominate as much for gold as for silver.

1.9 SURFACE ENHANCED RAMAN SCATTERING

The phenomena of surface enhanced Raman scattering (SERS) was first observed in 1974[15], with pyridine adsorbed on to a roughened silver surface, but was incorrectly put down to an increase in surface area. 1977 Creighton et al.[16] and Jeanmarie et al.[17] independently of each other came to the conclusion that the increase in scattering was far too great to be explained by an increased surface area alone. A multitude of papers has been published on the subject of the nature of the enhancement. Although a charge transfer effect has been suggested to play a role, the long range nature of the effect suggests that an electromagnetic effect is the dominating one[8, 18-21].

In the previous section, the interaction between an incident electromagnetic wave and a nano sized metal particle by the excitation of a surface plasmon was described. Under these conditions, the local electromagnetic field at the metal surface can be dramatically enhanced due to the localization of the incident electromagnetic field to the metal surface[8, 10, 18]. This is the basis for the electromagnetic SERS effect. This effect will work on both incident and scattered field.

Considering the Stokes case the expression will look like

$$M^{EM} = \left[\frac{E^L(\omega_I)}{E^I(\omega_I)}\right]^2 \cdot \left[\frac{E^L(\omega_I - \omega_v)}{E^I(\omega_I - \omega_v)}\right]^2 \qquad (1.20)$$

With indexes I and L denoting incident and local electromagnetic field respectively and ω_I, ω_v being the frequency of the incident field and vibrational frequency. If $\omega_I >> \omega_v$, equation (1.20) can be written as

$$M^{EM} = \left[\frac{E^L(\omega_I)}{E^I(\omega_I)}\right]^4 \tag{1.21}$$

This means that the electromagnetic enhancement effect in SERS is expected to be maximised at the frequency close to the surface plasmon resonance frequency of the metal particle. This is the reason why gold and silver are by far the most commonly used metals in SERS, as they have resonance frequencies in the visible region, where lasers are available at relatively low cost.

There are very few reports where SERS from a single spherical particle has been reported. In general, it is necessary to bring two or more surfaces together. This has the effect of localizing the potential drop of the electromagnetic field between to surfaces with the Raman scatterer trapped between them. If the surfaces are brought closer together, the capacitive field sensed by the scatterer could be made arbitrarily large, until a limit where other effects, such as tunnelling of electrons between the two surfaces becomes a factor. As both α and E are vector functions, the orientation of both molecule, electric field and SERS substrate will be crucial to obtain a strong enhancement of the Raman scattering. The enhancement factor derived from the electromagnetic effect has been calculated to be of the order of 10^{11} for the right orientations[8].

As there have been claims of single molecule detection using SERS, the remaining enhancement has sometimes been assigned to a "chemical" enhancement effect. The theory for this usually builds on the formation of a charge transfer complex between molecule and metal. This would increase the polarisability of the adsorbed molecule, and by doing so, the Raman scattering would be further enhanced.

1.10 ELECTRONIC SPECTRA AND SERS

Figures 1.6 and 1.7 illustrate the connection between the electronic response of nanoparticle solutions and surface enhancement of Raman scattering from an analyte in the close vicinity of the nanoparticles. At the particle plasmon resonance frequency, the extinction cross section of the particles is maximised. This means that at this frequency, the localization of the electromagnetic field from the incident irradiation to the surface of the particle is maximised as well. A molecule close to the surface will experience a much increased oscillating electromagnetic field. Van Duyne et al. has shown on nanolithographically produced surfaces that the maximum SERS enhancement can be achieved by exciting the SERS substrate so that the particle plasmon resonance is between the excitation frequency and the frequency of the Raman emission peak[22].

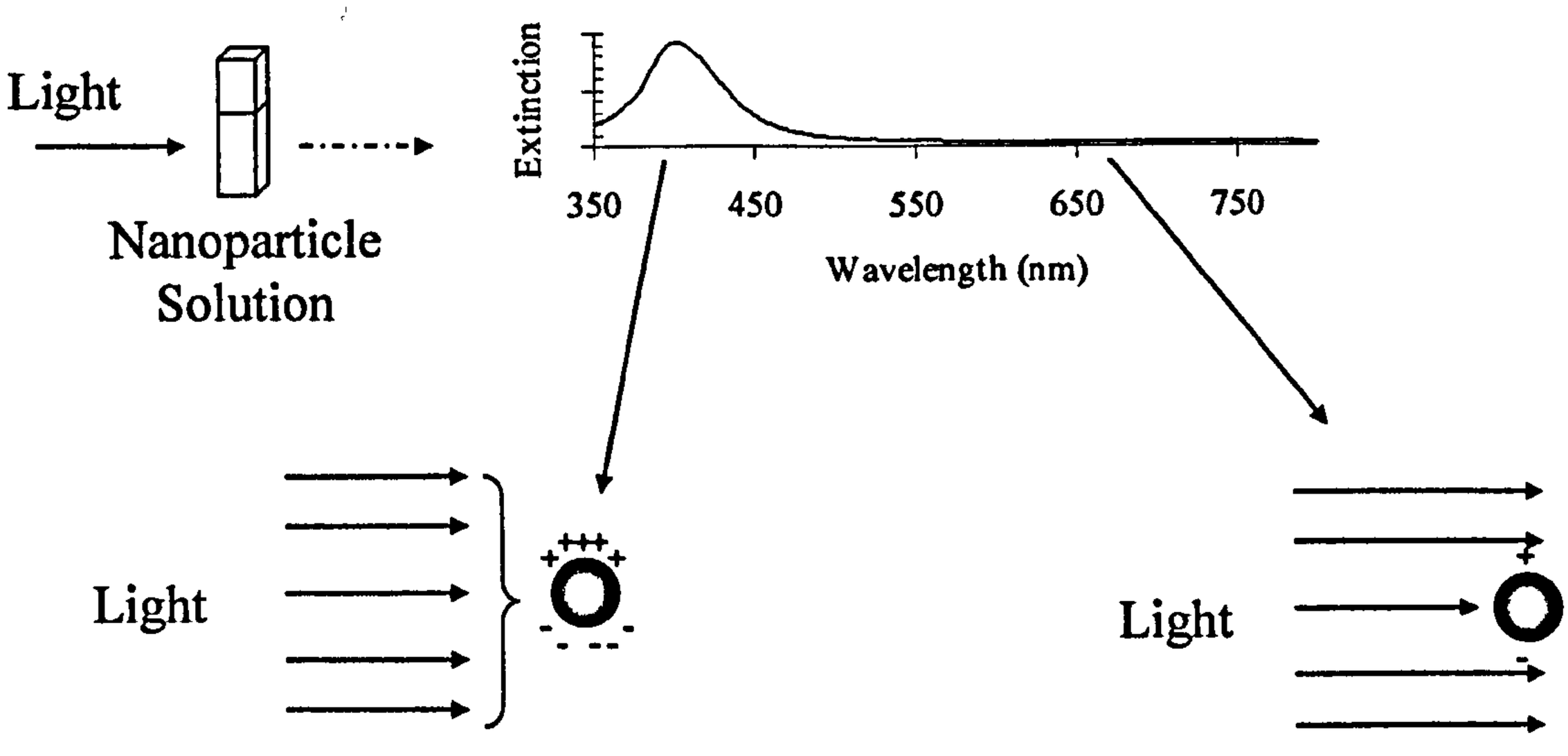

FIGURE 1.6: Scheme illustrating the connection between SERS and electronic spectra for unaggregated silver nanoparticles. At the wavelength of the peak extinction, the cross section of the nanoparticle is large and a large portion of the incident light is localised to the particle surface as a particle plasmon (blue arrows). Off resonance the extinction cross section decreases and less light is localised to the surface.

When the particle solution is aggregated, cluster of particles are formed. The shape and size of these clusters may vary significantly depending on aggregating conditions and aggregating agent. The electronic response of the clusters will also be heavily dependent on these properties. Because of these variables, and the dynamic process

of aggregation, the electronic response of the aggregated nanoparticles is often broadened and red shifted. The red shift is due to coupling between particle plasmons as the particle distance decreases[8, 23-25]. As the distance becomes smaller, the red shift of the plasmon increases. It can thus be concluded that the structure of the clusters are imperative to their optical response. This may not however necessarily mean that when aggregated nanoparticles are used as a SERS substrate, the enhancement is directly dependent on its electronic response in the same way as for the single particle system, due to the many additional processes that occur in such complex systems.

As the particles come together, additional effects occur, such as confining the potential drop of the electromagnetic field outside the particle between two surfaces. This brings potentially huge signal enhancements of a Raman scatterer trapped between the two particles, making detection of extremely low concentrations of a targeted substance possible.

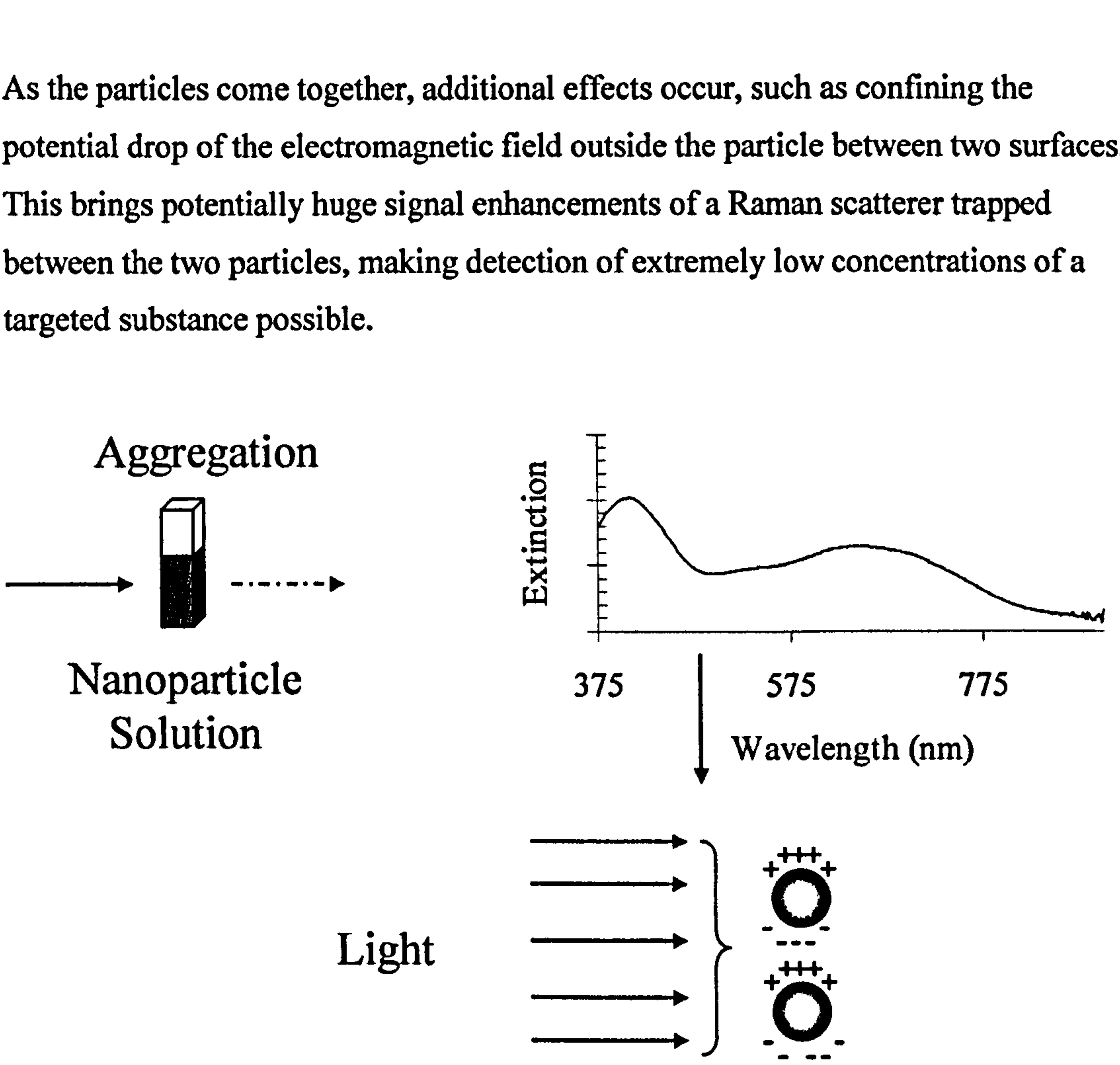

FIGURE 1.7. Scheme illustrating the connection between SERS and electronic spectra for aggregated silver nanoparticles. The first peak remains approximately at the resonance frequency for single particles and a red shifted peak emerges. The redshift is due to coupling between particle plasmons as they come close to each other and is dependant on interparticle distance, particle size, and number of particles in the clusters formed.

[1] K. Faulds, L. Fruk, D. C. Robson, D. G. Thompson, A. Enright, W. E. Smith, D. Graham, *Faraday Discussions* **2006**, *132*, 261.

[2] K. Faulds, W. E. Smith, D. Graham, *Analyst* **2005**, *130*, 1125.

[3] A. E. Grow, L. L. Wood, J. L. Claycomb, P. A. Thompson, *J. Microbiolical Methods* **2003**, *53*, 221.

[4] A. J. Haes, W. P. Hall, L. Chang, W. L. Klein, R. P. Van Duyne, *Nano Letters* **2004**, *4*, 1029.

[5] S. Habuchi, M. Cotlet, R. Gronheid, G. Dirix, J. Michiels, J. Vanderleyden, F. C. De Schryver, J. Hofkens, *Journal of the American Chemical Society* **2003**, *125(28)*, 8446.

[6] K. Kneipp, Y. Wang, R. R. Dasari, M. S. Feld, *Applied Spectroscopy* **1995**, *49*, 780.

[7] S. Nie, S. R. Emory, *Science* **1997**, *275*, 1102.

[8] H. Xu, J. Aizpurua, M. Kall, P. Apell, *Physical Review E* **2000**, *62*, 4318.

[9] H. Xu, X.-H. Wang, M. P. Persson, H. Q. Xu, *Physical Review Letter* **2004**, *93*, 2430021.

[10] E. Hao, Schatz, G. C., *Journal of Chemical Physics* **2004**, *120*, 357.

[11] G. Mie, *Annalen der Physich* **1908**, *25*, 377.

[12] S. Link, M. A. El-Sayed, *Journal of physical Chemistry B* **1999**, *103*, 8410.

[13] M. Perner, P. Bost, U. Lemmer, G. von Plessen, J. Feldman, U. Becker, M. Mennig, M. Schmitt, H. Schmidt, *Physical Review Letters* **1997**, *78*, 2192.

[14] C. Sönnichsen, T. Franzl, T. Wilk, G. von Plessen, J. Feldmann, *Physical review letters* **2002**, *88*, 077402.

[15] C. V. Raman, K. S. Krishnan, *Nature* **1928**, *121*, 501.

[16] J. A. Creighton, C. G. Blatchford, M. G. Albrecht, *Journal of Chemical Society Faraday Transitions II* **1979**, *75*, 790.

[17] D. C. Jeanmarie, R. P. Van Duyne, *Journal Electroanalytical Chemistry* **1977**, *84*, 1.

[18] J. Gersten, A. Nitzan, *Journal of Chemical Physics* **1980**, *73*, 3023.

[19] M. Moskovits, *Journal of Chemical Physics* **1978**, *69*, 4159.

[20] K. L. Kelly, E. Coronado, L. L. Zhao, G. C. Schatz, *Journal Of Physical Chemistry B* **2003**, *107*, 668.

[21] M. Arnold, P. Bussemer, K. Hehl, H. Grabhorn, A. Otto, *Journal of Modern Optics* **1992**, *39*, 2329.

[22] J. A. Dieringer, A. D. McFarland, N. C. Shah, D. A. Stuart, A. V. Whitney, C. R. Yonzon, M. A. Young, X. Y. Zhang, R. P. Van Duyne, *Faraday Discussions* **2006**, *132*, 9.

[23] S. Y. Park, J. S. Lee, D. Georganopoulou, C. A. Mirkin, G. C. Schatz, *Journal Of Physical Chemistry B* **2006**, *110*, 12673.

[24] P. Nordlander, C. Oubre, E. Prodan, K. Li, I. Stockman, *Nano Letters* **2004**, *4*, 899.

[25] M. Moskovits, *103 Topics in Applied Physics* **2006**, 1.

CHAPTER 2

INSTRUMENTS THEORY OF OPERATION

TABLE OF CONTENTS

CHAPTER PAGE

2.1 LASERS

Diode lasers and ion lasers are the two most common types of lasers in the visible spectrum. The basic setup consists of a light amplifier and an optical cavity that stores light energy. When the amplifier provides enough gain to overcome the loss of the cavity, laser light will be produced. The gain in the case of an ion laser consists of a plasma tube containing gas at low pressure (figure 2.1). The plasma is created by an electrical discharge that is maintained through the gas in the tube, creating ionized gas particles and electrons. Under the right conditions (voltage, pressure, current), a situation is created where the number of electrons in the excited state will exceed the number electrons in a lower energy level. As an electron makes the transition from the excited energy level to the lower level, a photon will be emitted corresponding to the energy gap between the two states. The laser lines available from a laser system will thus depend on what ion gas is used in the plasma tube. The light energy released will be stored in the cavity. At each end of the plasma tube, there is a mirror with a dielectric coating. The back mirror will reflect all light of a chosen wavelength, whereas the front mirror will let through some light. This is what constitutes the laser beam.

The principal for a diode laser is similar, with the main difference being that the gain is created by a current flowing through a p-n junction. The photons are emitted when electrons from the n type semiconductor and electron holes (an electron deficiency in the p type semiconductor) combine. Diode lasers can be made much smaller and cheaper than ion lasers.

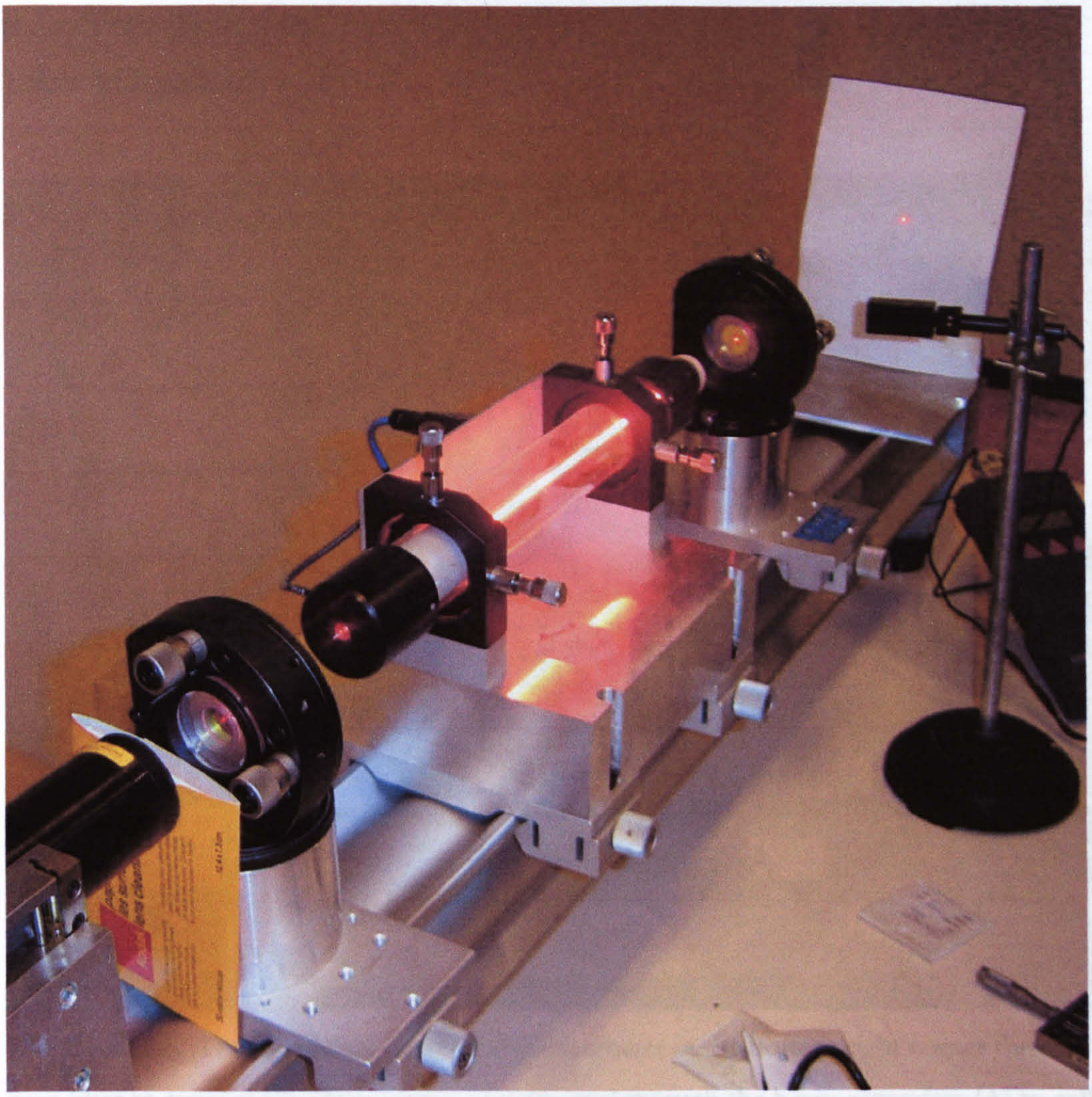

FIGURE 2.1. A stripped ion laser system. The red glow in the plasma tube is not the laser, but the ionized gas.

2.2 RAMAN INSTRUMENTATION

In a typical Raman experimental setup, the sample is irradiated by a single wavelength intense light source, such as a laser. The light scattered from the sample is collected and passed through a notch filter, only allowing the frequency shifted light to pass. This light then is dispersed by a grating on to a detector, typically a charged coupled device camera (CCD). The number of photons that hit each area of the CCD is then integrated and a Raman spectrum is generated from this. In this work, four main systems where used. Two were Renishaw Ramascope systems and one was a Renishaw inVia Raman

microscope. Both work in a similar way, with one of the Ramascope systems shown below in figure 2.2.

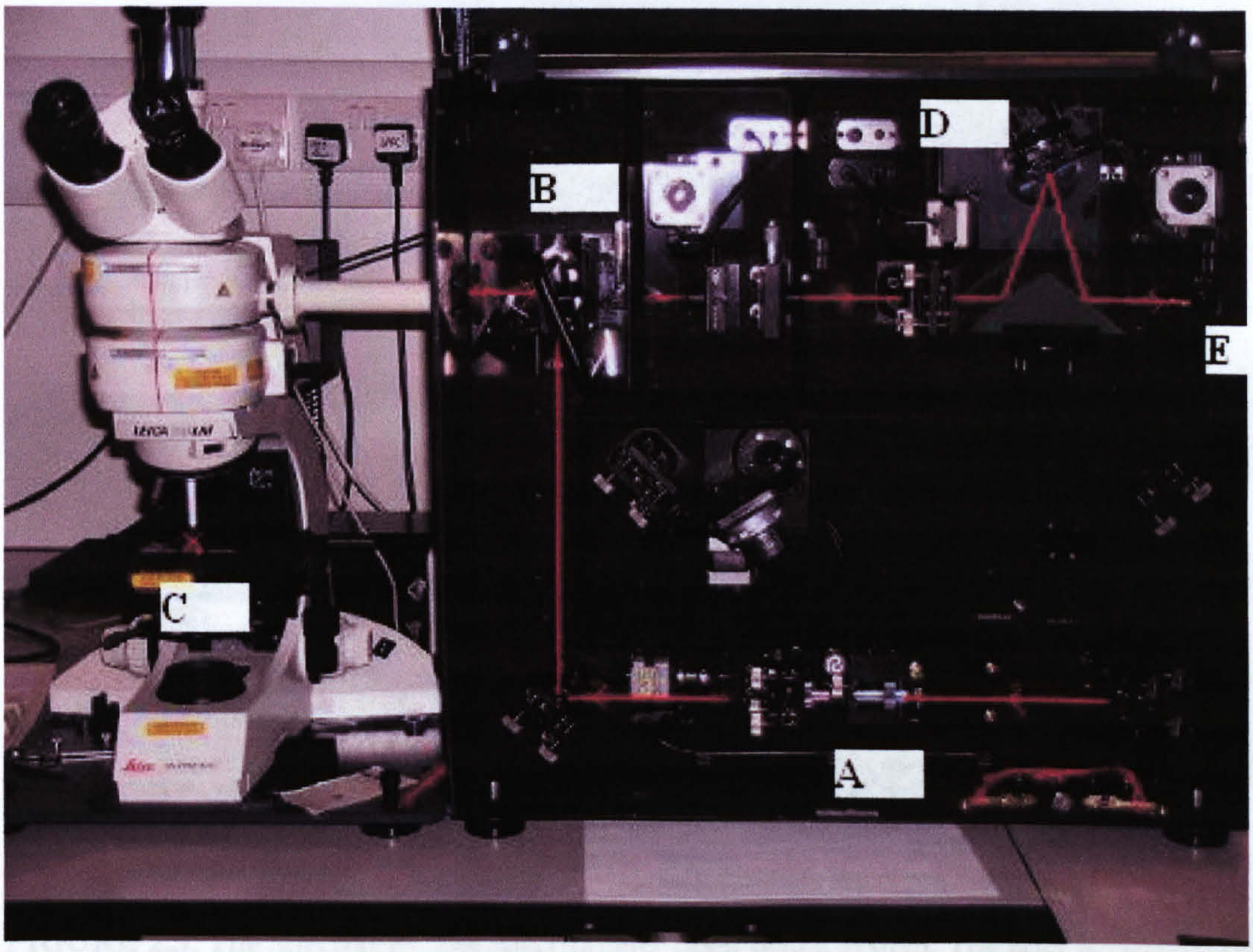

FIGURE 2.2. The laser beam enters the spectrometer in the bottom right corner through a band pass filter to remove any plasma lines. It is directed through the beam expanders (A) to collimate the beam, and then via mirrors, through the microscope onto the sample (C). The backscattered light is collected through the objective and is directed back through the notch filter (B), through the slits and on to the grating (D) and finally out onto the CCD (E).

A fourth system was set up in order to enable the use of greater number of laser lines in the experiments carried out in chapter 5 and chapter 6. For this purpose, an open bench system was setup, using a SpectraPro 300i Monochromator from Acton Research Corporation as spectrometer, shown in figure 2.3. Three laser systems were used. By changing the notch filter, laser lines at 375 nm, 407 nm, 413 nm, 442 nm, 457 nm, 476 nm, 488 nm, 514 nm, 568 nm, 647 nm and 671 nm could be used if desired. Further laser lines were available towards the red end of the spectrum. However the spectrometer CCD became very ineffective at lower energies. The CCD was calibrated to intensity and wavelength using both a Neon calibration lamp from Renishaw as well

as a cyclohexane standard using the Raman shifts and relative intensities suggested by the ASTM subcommitte on Raman spectroscopy (ASTM E 1840 Raman shift standard).

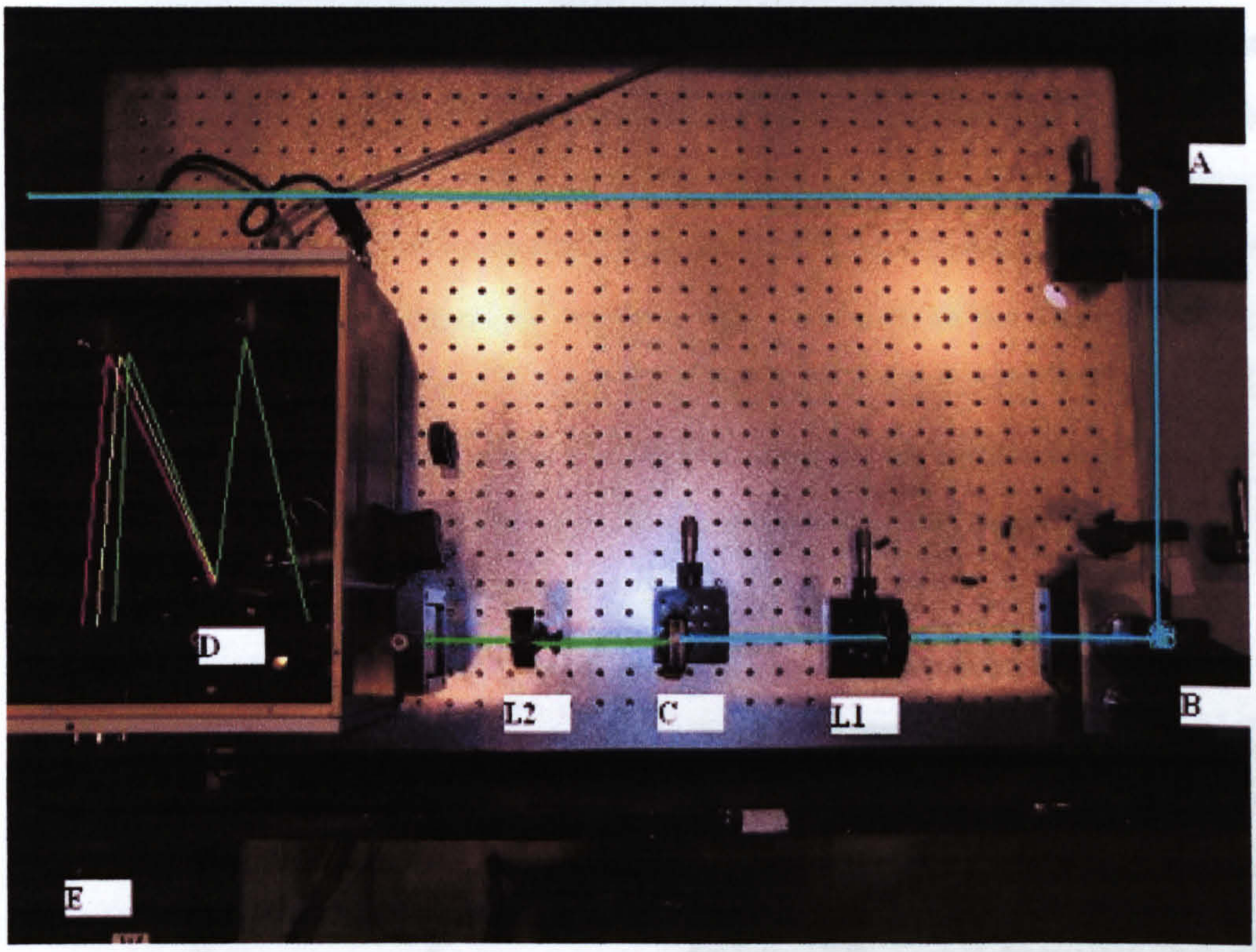

FIGURE 2.3. The SpectraPro 300i spectrometer open bench system. The laser is directed onto the sample (B) via a mirror (A). A lens (L1) collects the scattered light and directs it through the notch/longpass filter (C), and the second lens (L2) focuses the frequency shifted light through the slits. The light is the directed on to the grating (D) via two mirrors, and dispersed onto a third mirror, which sends it on to the CCD (E).

2.3 ATOMIC FORCE MICROSCOPY

An atomic force microscope (AFM) is based on tracking the movement of a flexible cantilever with a tip of a couple of nanometers moving across a surface as shown in figure 2.4,. When travelling across the surface it can either be in constant contact with the surface, or it can be in "close contact" or "tapping mode". The latter means that while the tip travels across the surface it is oscillating at a constant frequency. When the tip interacts with something on the surface, the oscillation of the cantilever changes. This is registered by the detector, and via a feedback loop, the tip is retracted until the oscillation is restored. The sharper the tip that is used, the higher the spatial resolution can be achieved, down towards a couple of nanometers, and in beneficial samples, single carbon atoms can be imaged.

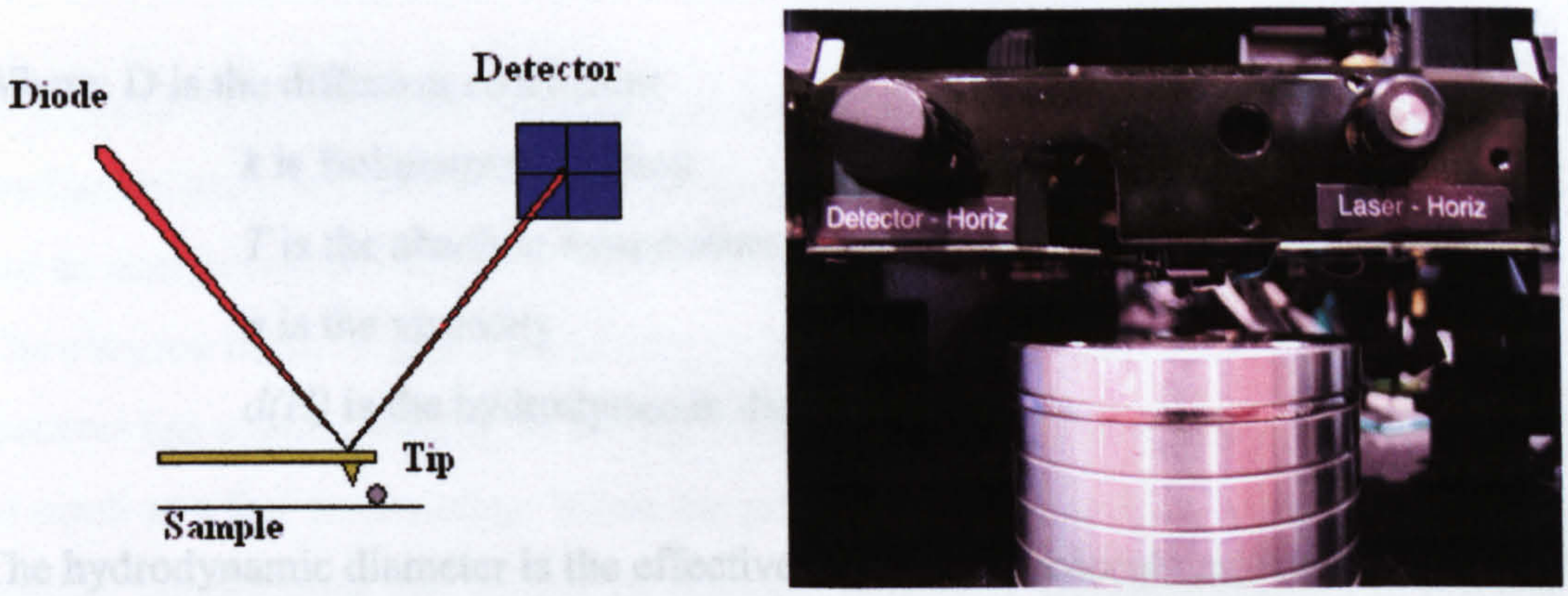

FIGURE 2.4. Schematic of an AFM and the actual AFM used in this work. The laser diode is directed onto the end of the tip and reflected on to a detector that tracks the tips movement. The sample is mounted on the metal cylinder and the tip is centred above the sample.

2.4 PARTICLE SIZE ANALYSIS THROUGH DYNAMIC LIGHT SCATTERING

Particle size analysis using dynamic light scattering is based on Brownian motion of particles in suspension. The Brownian motion is due to the random collisions of particles with the molecules of the liquid and is dependent on the size of the particle. By illuminating the particles with a laser and monitoring the intensity fluctuations of the scattered light the size of the particle can be estimated.

The relationship between size of a particle and its velocity due to Brownian motion is described by the Stokes Einstein equation.

$$d(H) = \frac{kT}{3\pi\eta D} \qquad (2.1)$$

Where: D is the diffusion coefficient

k is Bolzmanns constant

T is the absolute temperature

η is the viscosity

$d(H)$ is the hydrodynamic diameter

The hydrodynamic diameter is the effective size of the molecule as detected by its diffusion. From the equation it then follows, that if temperature and suspension medium is constant, $d(H)$ is directly connected to the diffusion rate of the particle.

The actual calculations carried out during the measurement are quite complicated. In short, the instrument measures the rate of change of light fluctuations from the particles through correlators. The correlator channels are set to count photons at set delay times. For short delay times, the change in light level will be small. The change in light levels will increase with longer delay times, and the correlation with the initial state will decrease. The larger the particle is, the slower the Brownian motion will be, and the correlation with the initial state will tail off slower. The size of the particle can then be derived.

2.5 Z-POTENTIAL MEASUREMENTS

Z-potential is defined as the charge difference between the surface of a particle and the charge at the distance from the particle where charges are no longer dragged along by the particle. In the Malvern Zetasizer, Z-potential is measured through laser Doppler electrophoresis. This technique measures the movement of small charged particles in an electric field. The mobility of the particles will be related to their surface charge, and thus their Z-potential.

2.6 SCANNING ELECTRON MICROSCOPY (SEM)

In a typical SEM, electrons are emitted via field emission or from a tungsten or lanthanum hexaboride cathode and are accelerated towards an anode. The electron beam has an energy range between a few eV up to 100 keV and is focused through two lenses. The electron beam is scanned over the sample in a pattern of parallel lines. Since an electron has a much shorter wavelength than a photon, the focal spot size can be made as small as a few nanometers. When the primary electron beam interacts with the sample, the electrons lose energy by repeated scattering and absorption. The interaction between sample and electron beam create an emission of photons and scattered electrons that can be detected to produce an image. The most common imaging mode monitors low energy (<50 eV) secondary electrons. The detector is a type of scintillator-photomultiplier and the resulting signal is rendered into a two-dimensional intensity distribution.

2.7 ELECTRONIC/ UV-VIS SPECTROSCOPY

In UV-Vis spectrometry monocromatic light is passed through a sample and the intensity of the light passing through the sample, I, is compared to the intensity of the incident light, I_0. The ratio I/I_0 is called the transmitted light, T. Usually the data is displayed as the absorption, or extinction, A. This is related to the transmitted light as

$$A = -\log_{10}\left(I/I_0\right) \tag{2.2}$$

Concentrations of an analyte, c, can be obtained from A via the Beer-Lambert law as

$$A = c \cdot l \cdot \varepsilon \tag{2.3}$$

Where l is the path length of the light through the sample, and ε is the molar extinction coefficient of the analyte.

2.8 SCATTERING MEASUREMENTS

The scattering data in chapter 3.5 were collected using a Varian Cary Eclipse Fluoresence Spectrophotometer. The sample is illuminated with a 1 cm wide monochromatic light beam, which also is the width of the sample. The collection of the scattered light was made at 90° angle from the incident radiation as shown in figure 2.5.

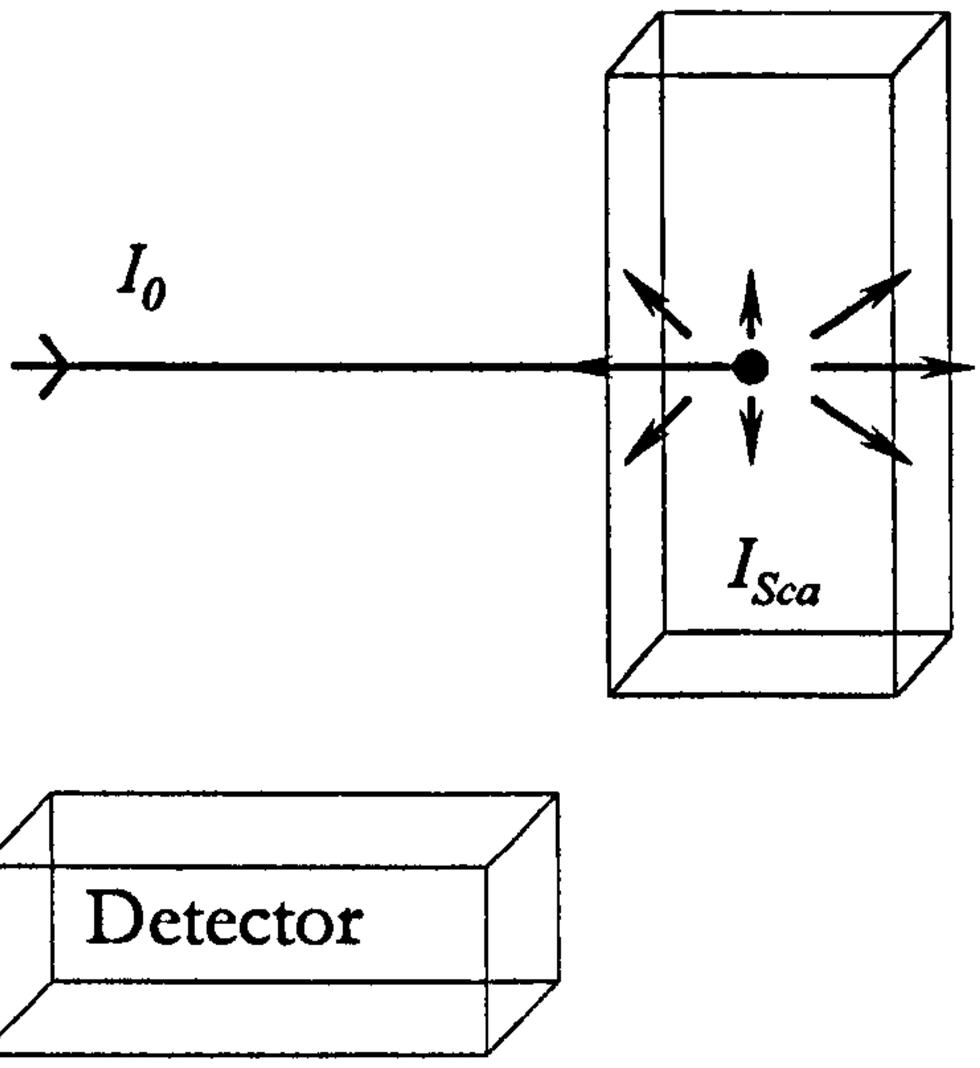

FIGURE 2.5. Schematic of the experimental setup of the scattering measurements. The samples are illuminated with a monochromatic light I_0 and the scattered light, I_{Sca} is detected at a 90° angle.

Because of the width of the illumination beam self absorption becomes a factor. The self absorption of scattered light by the sample was taken into account through the equation (from Beer-Lamberts law and integrating over the beam width):

$$A_{tot} = \int_0^l C \cdot \varepsilon \cdot x \cdot dx = C \cdot \varepsilon \int_0^l x \cdot dx \qquad (2.4)$$

where ε, x are extinction coefficient and path length respectively, A_{tot} is the effective loss of scattered light from the illuminated sample volume. l is the cuvette length and also width of the illuminating beam, 1 cm.

Particle concentrations, c, were calculated from extinction spectra and theoretical extinction coefficients using Beer Lamberts law

$$A = c \cdot l \cdot \varepsilon \tag{2.5}$$

where l is the path length of the light through the sample, A is the maximum extinction and ε is the molar extinction coefficient of the nanoparticle.

The fluorometer was calibrated using Perylene at 4.3 μmol dm^{-3}. The integrated fluorescence was taken as a scattering cross section equivalent. Since the number of Perylene molecules present in the sample was known, as well as its extinction coefficient and quantum yield, a "scattering" cross section for Perylene could be calculated from equation 2.6.

$$\sigma_{sca}^{P} = \varphi_{sca} \cdot \sigma_{ext}^{P} = 0.93 \cdot \frac{2.303 \cdot 38500 M^{-1} cm^{-1} \cdot 100 cm/m}{6.022 \cdot 10^{23} mol^{-1} \cdot 1000 L/m^{3}} \tag{2.6}$$

Note that the second term in equation 2.6 is mainly converting units. Using Perylene as standard scattering cross sections for the metal nanoparticles was given by

$$\frac{\sigma_{sca}^{NP}}{\sigma_{Sca}^{P}} = \left(\frac{I_{Sca}^{NP} / N^{NP}}{I_{Sca}^{P} / N^{P}} \right) \tag{2.7}$$

Where N^{NP} and N^{P} are the number of nanoparticles and the number of Perylene molecules, and I_{Sca}^{NP} and I_{Sca}^{P} the "scattering" intensities for the nanoparticle sample and Perylene sample respectively.

From the extinction spectra, extinction cross sections at any wavelength, w_1, could be calculated as

$$\sigma_{ext}^{w_1} = A^{w_1} / A^{w_{max}} \cdot \sigma_{ext}^{w_{max}} \tag{2.8}$$

where $A^{w_{max}}$ is the maximum extinction. From this and the scattering cross sections, absorption cross sections at the wavelength w_1 could be calculated as

$$\sigma_{abs}^{w_1} = \sigma_{ext}^{w_1} - \sigma_{sca}^{w_1} \tag{2.9}$$

This technique was used to probe the optical response of metal nanoparticles of different size.

Attempts were made to apply this technique to aggregated nanoparticle systems. They were unsuccesfull, mainly due to the time and concentration dependence of the aggregation process, and the need to keep the sample concentrations low during the measurements.

2.9 NORMALISATION OF RAMAN INTENSITIES

In many of the experiments described in this thesis, the Raman scattering intensity has been normalised to a cyclohexane standard in order to enable comparison between different spectrometers. This is necessary in order to correct for variations in e.g. gratings and CCD sensitivity over the spectral range. This was done by taking cyclohexane spectra before and after every sample, under the same acquisition conditions as the sample. The cyclohexane spectra were compared to the spectra produced by the ASTM E 1840 Raman shift standard (figure 2.6), which also shows relative intensities between the peaks of the cyclohexane spectrum. In short, these spectra has been produced from an average of cyclohexane spectra taken at six different labs (Perkin-Elmer, Bruker, etc), with both FT and dispersive Raman spectrometers, and can be used as a calibration tool for Raman spectrometers. To normalise the Raman scattering intensity of the sample, the cyclohexane spectra was first corrected for any CCD sensitivity variations. After this, the most intense peak of the sample spectrum was divided by the average intensity of the 1444 cm^{-1} peak of the cyclohexane spectrum taken before and after the sample.

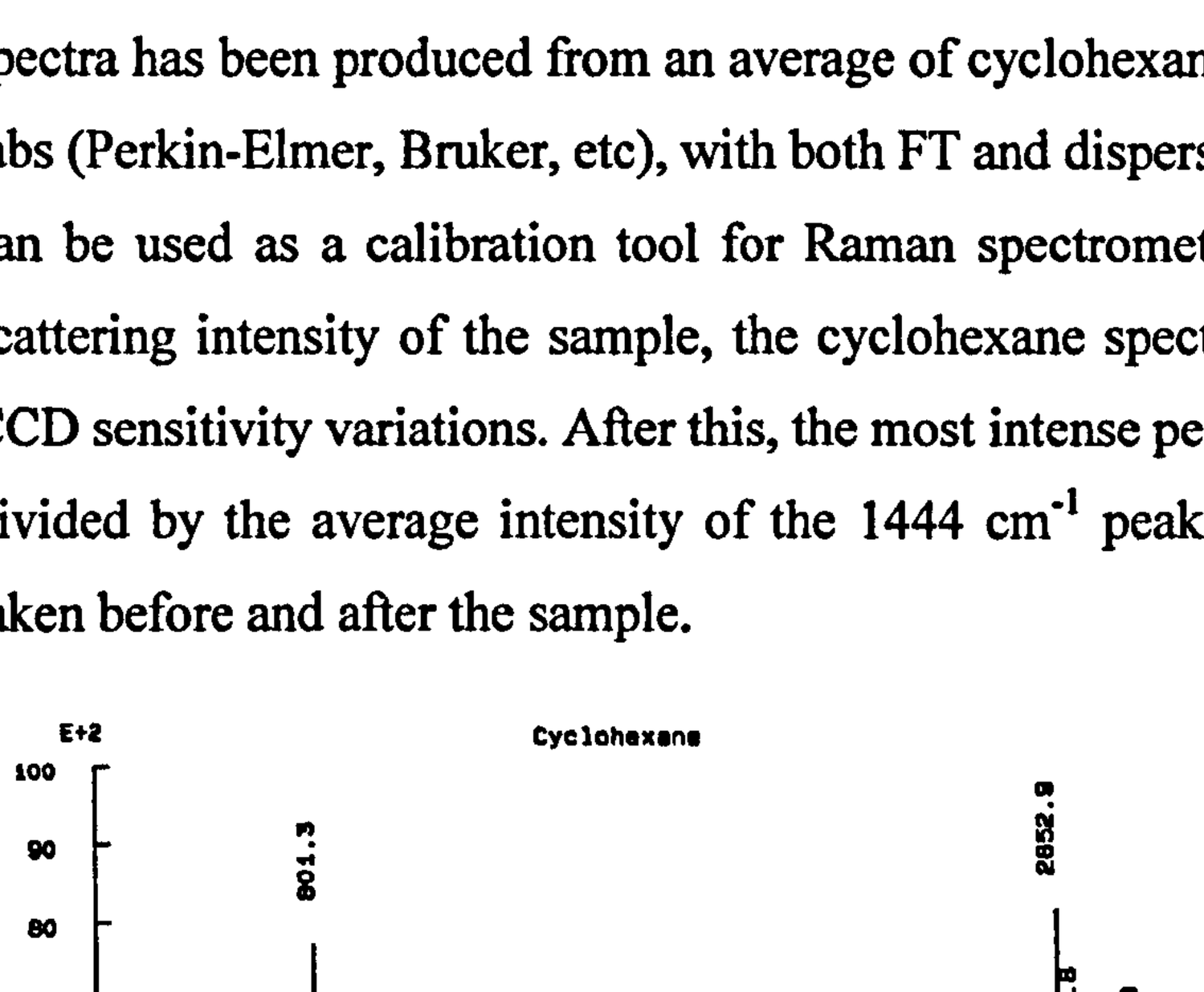

FIGURE 2.6. The cyclohexane spectra produced by the ASTM E 1840 Raman shift standard. The spectra has been produced from an average of cyclohexane spectra taken at six different labs with both FT and dispersive Raman spectrometers and can be used as a calibration tool for Raman spectrometers. It contains both Raman shifts and relative intensities of the peaks.

CHAPTER 3

SYNTHESIS AND CHARACTERISATION OF NANOPARTICLES

TABLE OF CONTENTS

CHAPTER PAGE

3.1 INTRODUCTION

The use of metal nanoparticles in various sensor applications such as plasmon resonance light scattering (RLS) and surface enhanced Raman spectroscopy (SERS) is a fast developing field.[1-3] The properties of these nanoparticles are strongly dependent on their size and shape.[4-8] Silver and gold nanoparticles with diameters between 5-100 nm have surface plasmon resonance (SPR) energies that coincide with that of visible light. In addition to this, the fact that they are both relatively stable results in these being the most commonly used metals for application into spectroscopic applications. The two properties of the nanoparticles that are generally the most important to control are the surface area and the (SPR derived) optical response. Gold nanoparticles are commercially available in different sizes, and there are a number of articles published on the controlled synthesis of gold nanoparticles of various sizes[9-11]. However, to achieve the same degree of control for silver nanoparticles appears to present more of a challenge. Two of the most commonly used methods for synthesis of silver nanoparticles are the citrate reduction of silver nitrate described by Lee and Meisel[12] and sodium borohydride reduction of silver nitrate according to Creighton et al.[13] These methods produce a very polydisperse product with a variety of shapes present, and in the latter case, an unstable suspension. This is often used as an argument for using gold rather than silver, in spite of the stronger optical response and narrower surface plasmon resonance of silver nanoparticles compared to gold.[2-4, 6]

This chapter consists of three sections. The first is a SEM-study of nanoparticles produced from already published material, or from variations of published methods. The second section presents a new method for synthesis of highly spherical and monodisperse silver nanoparticles of various sizes. This size-controlled synthesis of silver nanoparticles was achieved by seeded growth from EDTA-reduced nanoparticles[14], using reduction of silver nitrate with hydroxylamine hydrochloride.

In the last section a number of techniques to characterize physical dimensions of nanoparticles are evaluated. Also, a new method for separation of absorption and scattering contribution to the extinction of a nanoparticle solution is presented. The main improvement of this technique compared to previous ones is the simplicity in which it can be carried out, using only a standard fluorometer and a UV-Vis spectrometer.

3.2 INVESTIGATION OF ESTABLISHED PROTOCOLS FOR NANOPARTICLE SYNTHESIS

3.2.1 EXPERIMENTAL

All chemicals used were acquired from Sigma-Aldrich. All glassware was soaked in aqua regia and then thoroughly rinsed with distilled water before use. All water used in the nanoparticle synthesis was doubly distilled.

SEM grids were prepared by placing a small drop of nanoparticle solution on to the grid and then letting the water evaporate. The same samples were used for AFM. Further experimental conditions are given in each individual synthesis chapter.

3.2.2 CITRATE REDUCED SILVER NANOPARTICLES

Silver colloids where synthesized according to Lee and Meisel[12] with some modifications. The solution was stirred vigorously during the synthesis. 90 mG silver nitrate was suspended in 500 mL of distilled water at 40°C. After rapidly heating the solution to 98 °C, 10 mL of a 1% solution of trisodium citrate was added. After 90 minutes of keeping the solution at constant temperature the sol was allowed to cool to room temperature.

3.2.3 EDTA REDUCED SILVER NANOPARTICLES

EDTA reduced silver nanoparticles were prepared as described by Sanders et al[14]. A mixture containing 100 mL of 0.16 mM EDTA and 4 mL of 0.1 M NaOH was heated to boiling where upon 1 mL of 26 mM $AgNO_3$ is added under vigorous stirring.

3.2.4 CITRATE REDUCED GOLD NANOPARTICLES

The nanoparticle solution was prepared according to a method described by Grabar[10] et al. Sodium tetrachloroaurate (50 mG) was dissolved in 500 mL water. The solution was brought to boiling whilst stirring. Upon boiling, trisodium citrate (7.5 mL of a 1 % solution, Sigma) was added. The solution was maintained at boiling point for 15 minutes and then allowed to cool to room temperature under stirring.

3.2.5 HYDROXYLAMINE HYDROCHLORIDE REDUCED GOLD NANOPARTICLES ACCORDING TO DUFF[11] ET AL.

The synthesis was carried out over two days. Day one, 9 mL of 25 mM chloroauric stock solution was added to 491 mL of MQ water. To this solution, 122 mG of potassium carbonate was added. The solution was mixed thoroughly and then left overnight in darkness. The colour of the solution went from weak yellow to clear.

Day two, while stirring, 50 mL of the dark aged chloroauric solution prepared on day one, was added to a 250 mL round bottom flask. Then, 25 mL of a freshly prepared hydroxylamine hydrochloride solution (32 mG in 250 mL MQ water) was added dropwise over approximately 2 minutes under vigorous stirring. Upon addition, the colour of the solution changed from blue to a red-purple colour with some murkiness due to a more pronounced scattering in the yellow-red.

3.2.6 HYDROXYLAMINE HYDROCHLORIDE REDUCED GOLD NANOPARTICLES FROM SEEDED GROWTH BY A MODIFICATION OF THE APPROACH OF DUFF[11] ET AL.

The synthesis was carried out over two days, with a dark aged chloroauric/potassium carbonate solution prepared on day one as described in section 3.2.5.

On day two, while stirring, 40 mL of of the dark aged chloroauric solution prepared on day one, and 10 mL of citrate reduced gold nanoparticles described in chapter 3.2.4 was added to a 250 mL round bottom flask. Then, 10 mL of a freshly prepared hydroxylamine hydrochloride solution (32 mG in 250 mL MQ water) was added dropwise over approximately 2 minutes under vigorous stirring. Upon addition, the colour of the solution changed from the weak pink colour of the diluted citrate reduced gold colloids, to a deeper wine red colour.

This protocol was repeated with 5 mL of citrate reduced gold nanoparticles added instead of 10 mL. The final product was red/violet.

3.2.7 SYNTHESIS OF MONODISPERSED SILVER NANOPARTICLES OF CONTROLLED SIZES

The size controlled synthesis of silver nanoparticles was achieved by seeded growth of EDTA reduced nanoparticles (section 3.2.3), using reduction of silver nitrate with hydroxylamine hydrochloride. 100 mL of EDTA reduced colloid were diluted with 100 mL of water and added to a 500 mL round bottom flask. Aqueous silver nitrate (0.5 mM) was added in varying amounts to give the desired size of nanoparticle. In this study, 20 mL, 30 mL, 50 mL and 200 mL silver nitrate (preparations 1, 2, 3 and 4) were added to give four different sizes. Hydroxylamine hydrochloride was added causing the nanoparticle suspension to take on a strongly scattering red-brown colour. The suspension was then heated to around 80°C and kept at that temperature for ten minutes

during which the sol turned to a strongly blue/green scattering, yellow-red transmitting color. Finally, trisodium citrate solution was added to increase the stability of the nanoparticle and the suspension was allowed to cool to room temperature.

3.3 Results and Discussion

3.3.1 Citrate reduced silver nanoparticles

The properties of the citrate reduced silver nanoparticle suspension are very sensitive to the experimental conditions. The synthesis often results in a very polydisperse product and the variation between batches can be significant. The electronic spectra show a maximum at 410 nm, where the width of the peak can vary considerably from batch to batch (figure 3.2). There is often a high abundance of high aspect ratio particles and a large variety in sizes as can be seen in figure 3.1. In the electronic spectra this has the effect of an increase in background in the region 450 nm and onwards.

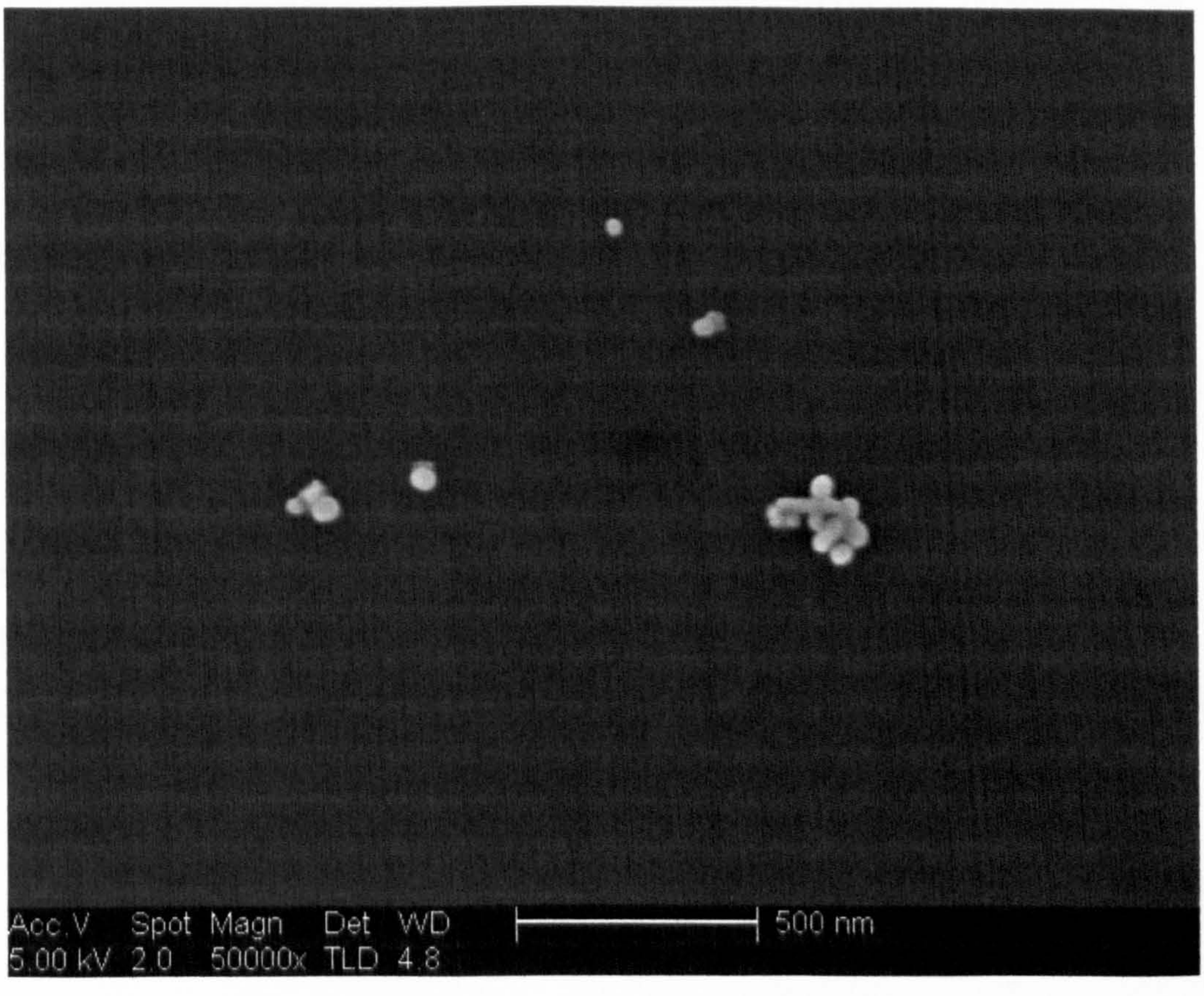

FIGURE 3.1. Scanning electron micrograph of the citrate reduced silver nanoparticles. The average diameter was found to be approximately 40 nm. Rod like particles up to 200 nm in the longest direction were also found.

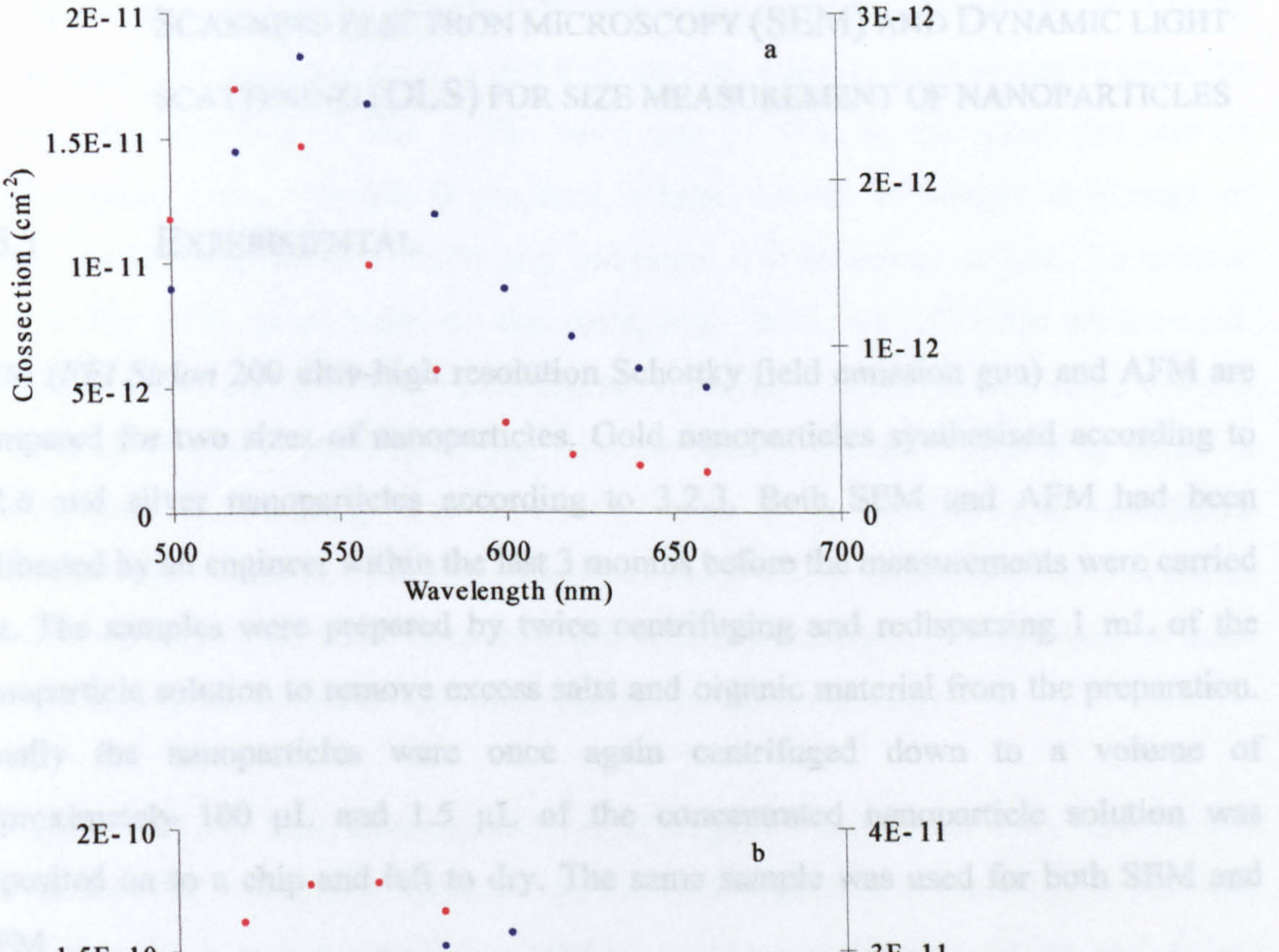

FIGURE 3.17. Scattering (blue markers, right hand scale) and absorption (red markers, left hand scale) cross sections for gold nanoparticle of 37 nm (a) and 59 nm (b). The corresponding extinction spectra can be seen in figure 3.10, page 48.

3.5 COMPARISON BETWEEN ATOMIC FORCE MICROSCOPY (AFM), SCANNING ELECTRON MICROSCOPY (SEM) AND DYNAMIC LIGHT SCATTERING (DLS) FOR SIZE MEASUREMENT OF NANOPARTICLES

3.5.1 EXPERIMENTAL

SEM (*FEI Sirion* 200 ultra-high resolution Schottky field emission gun) and AFM are compared for two sizes of nanoparticles. Gold nanoparticles synthesised according to 3.2.6 and silver nanoparticles according to 3.2.3. Both SEM and AFM had been calibrated by an engineer within the last 3 months before the measurements were carried out. The samples were prepared by twice centrifuging and redispersing 1 mL of the nanoparticle solution to remove excess salts and organic material from the preparation. Finally the nanoparticles were once again centrifuged down to a volume of approximately 100 μL and 1.5 μL of the concentrated nanoparticle solution was deposited on to a chip and left to dry. The same sample was used for both SEM and AFM.

In the last section three sizes of gold and silver nanoparticles, as determined by SEM, were measured using dynamic light scattering. The SEM micrographs were acquired as described in the previous section. DLS (HPPS Parkin Elmer) measurements were taken from the nanoparticle solution directly after synthesis without any further preparation from a 1 cm plastic cuvette. All nanoparticle solutions were prepared according to protocols described in chapter 3.2.

3.5.2. RESULTS AND DISCUSSION

COMPARISON OF AFM-SEM

Although scanning electron microscopy and atomic force microscopy are used on similar size scales, they have very different theories of operation. SEM detects electrons

scattering from the surface of the structure imaged, whereas AFM images through a physical interaction with the sample. This means that AFM has the advantage of being able to image a structure in the x, y and z dimension, whereas SEM primarily gives the physical dimensions in x and y. The advantage of SEM is the speed and cost of measurements. Once a sample is prepared, a large number of images, in a range of scales, can be obtained with hardly any additional cost in money or time. To achieve high quality AFM micrographs on this scale, high resolution AFM tips are required. These often have a very short lifetime and are relatively expensive. Less sharp tips can be used at the cost of resolution, and with the risk of structures appearing larger or smaller than they actually are. However, AFM is so far the more established nanometrology tool in the lower size range. Because it is desirable to be able to switch between the techniques freely in order to utilise their advantages, it is necessary to make sure the measurements are in very close agreement with each other.

In figures 3.18 and 3.19, scanning electron micrographs and atomic force micrographs are shown. The information between the both techniques is in close agreement with each other. Both give the particle diameters to be approximately 60 nm and 40 nm respectively as shown in table 3.5. Both techniques also show spherical or spheroidal particle shapes without any rods or pronounced sharp edges. In general the AFM micrographs are of lower quality. This could possibly be improved by optimising sample preparation and instrumentation.

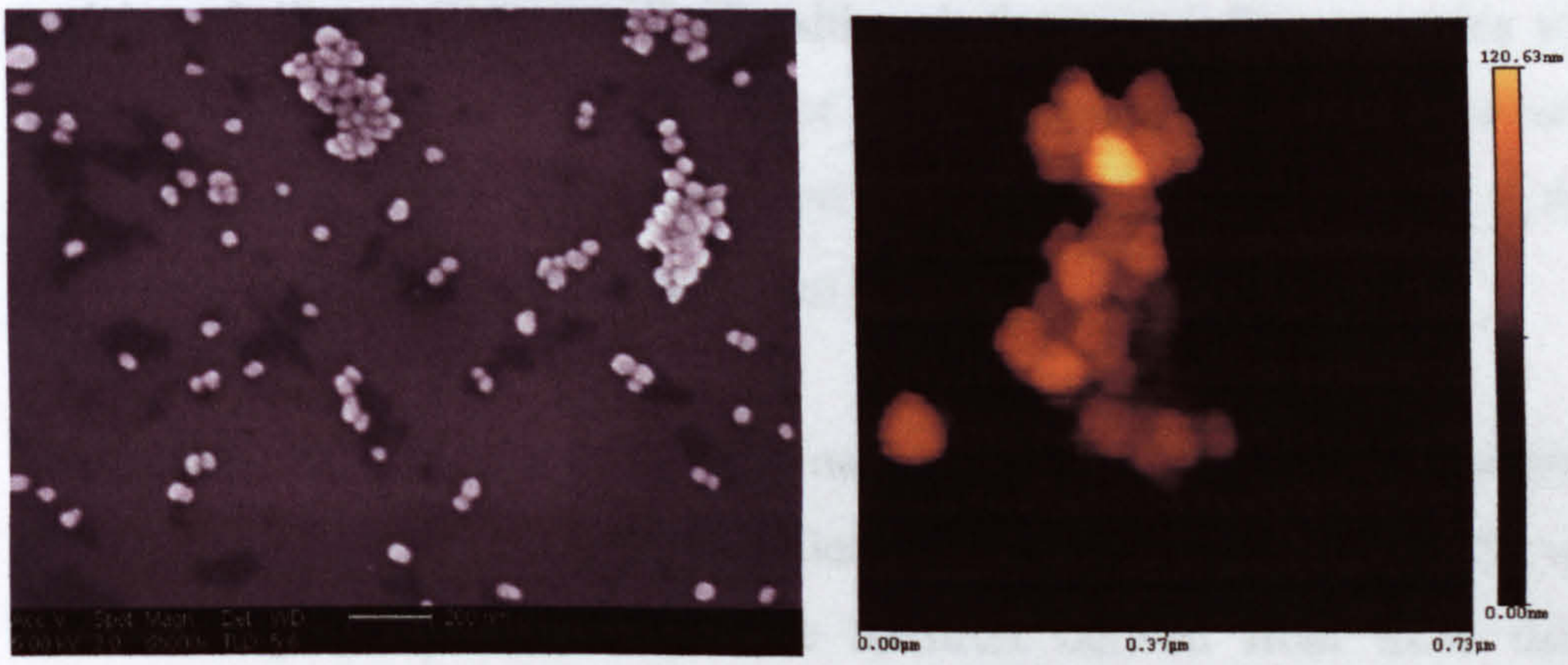

FIGURE 3.18. Comparison between SEM (left) and AFM (right) taken from a sample of silver nanoparticles. Both methods gave a particle diameter of just over 60 nm.

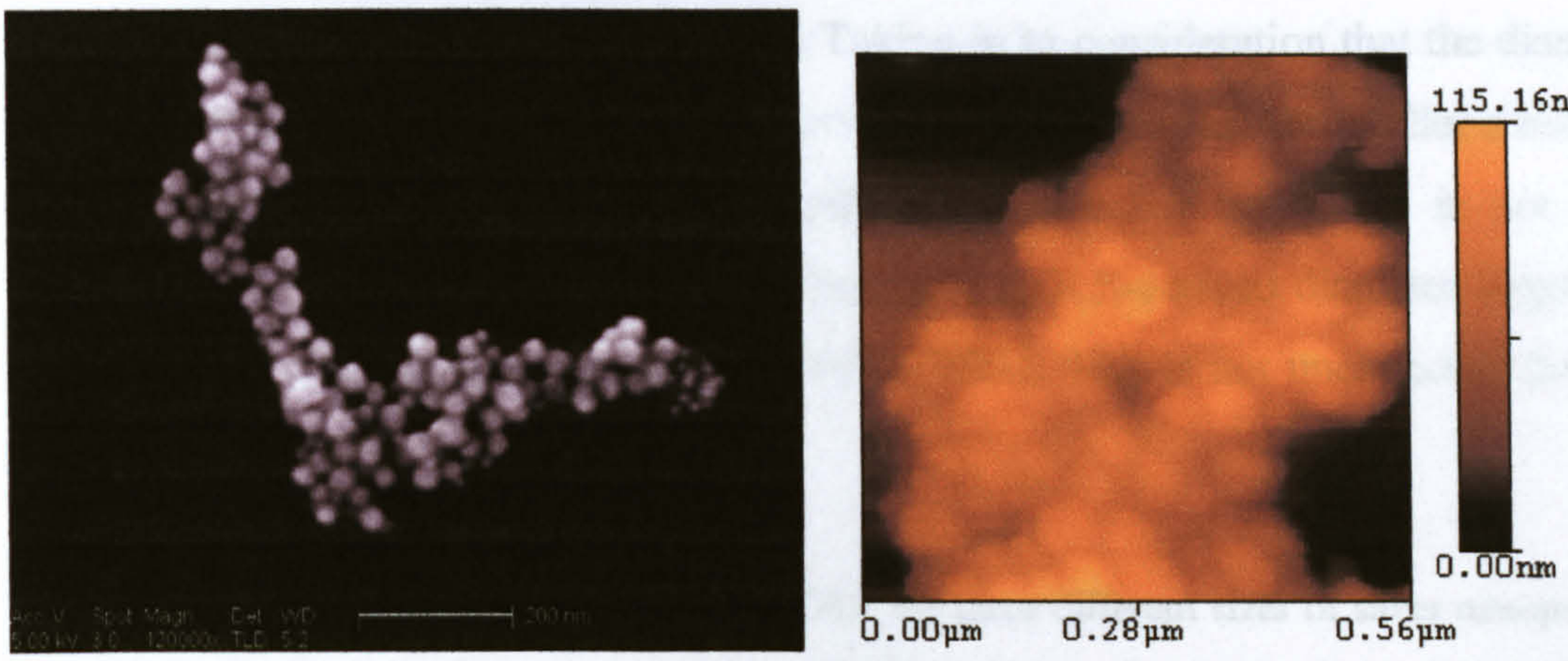

FIGURE 3.19. Comparison between SEM (left) and AFM (right) taken from a sample of silver nanoparticles. Both methods gave a particle diameter of just under 40 nm.

TABLE 3.5. Comparison between AFM and SEM for two different sizes of nanoparticles. At least 50 particles were counted for each size for each technique.

Batch	Average diameter (SEM)	Average diameter (AFM)
Silver	63 nm	62 nm
Gold	37 nm	38 nm

COMPARISON OF SEM-DYNAMIC LIGHT SCATTERING

Dynamic light scattering (DLS) is commonly used to determine the size of proteins and particles of silica or polymers[16, 17]. Although there are a few examples where it has been used also as an indicator of size of metal nanoparticles[18, 19], the accuracy of this measurements are sometimes questioned. The advantage of the method is the low cost and the ease at which a measurement can be made.

The primary data collected in the DLS measurement is the scattering intensity. Because larger particles scatter more than smaller particles, this means that if the nanoparticle solution is polydisperse, the particle diameter derived from these data may be significantly distorted in comparison to the average diameter based on the number of particles in the solution. The particle solutions measured here were all relatively

monodisperse as determined by SEM. The result from the comparisons between DLS and SEM are shown in tables 3.6 and 3.7. Taking in to consideration that the diameters according to DLS are given in discrete intervals (from 0.1 nm for the smaller sizes up to 10 nm intervals for 100 nm diameter particles), an exact agreement is not to be expected. Out of the six sizes examined, five give a DLS-derived diameter larger than the number average diameter as determined by SEM. This is not unexpected from the discussion above.

TABLE 3.6. Comparison between SEM and DLS for three different sizes of silver nanoparticles. The SEM value is a number average of the particles counted. The DLS value is for the highest intensity peak.

Batch	SEM average diameter (N)	DLS diameter (I)
1	36 nm	44 nm
2	51 nm	56 nm
3	72 nm	64 nm

TABLE 3.7. Comparison between SEM and DLS for three different sizes of gold nanoparticles. The SEM value is a number average of the particles counted. The DLS value is taken as the highest intensity peak.

Batch	SEM average diameter (N)	DLS diameter (I)
1	23 nm	26 nm
2	40 nm	49 nm
3	60 nm	72 nm

Figure 3.20 shows the intensity distribution over size for the DLS and the AFM measurement of 59 nm gold nanoparticles. The AFM data has been entered in the same size intervals as the DLS data is presented in. The tail towards smaller sizes in the DLS data is probably due to rotational diffusion[20] of the particles, and possibly some smaller particles that not were discovered in the AFM. The effect is however much more pronounced in particle batches with elongated species, and especially in silver

nanoparticle batches. Since the optical response of silver is more sensitive to shape than gold this suggests that it may be due to rotational diffusion rather than a true particle size fraction. To draw this conclusion however, the general quality of the nanoparticle solution has to be known.

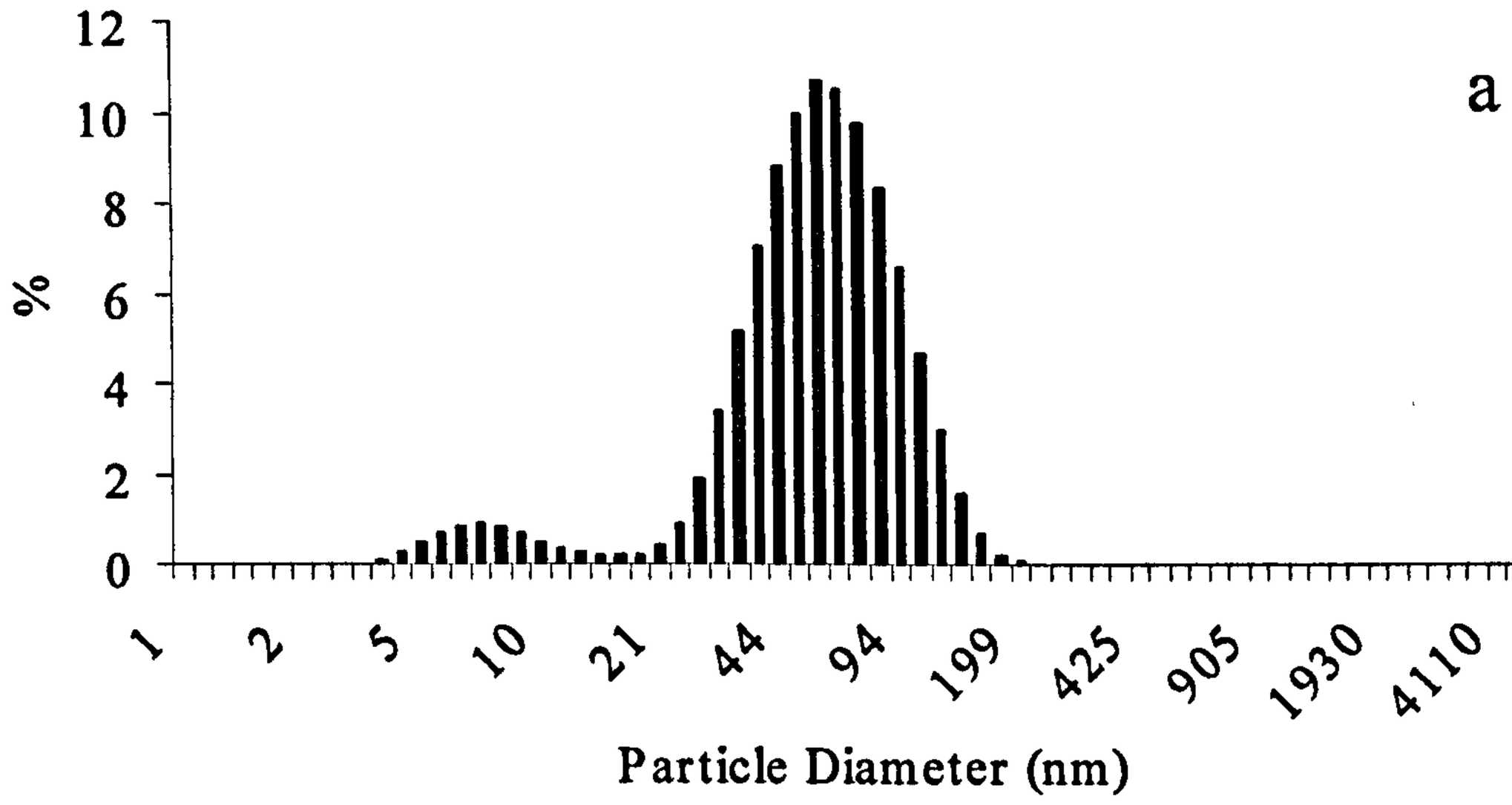

FIGURE 3.20. Size distribution of gold of 59 nm in diameter. a) shows the distribution according to DLS measurements. b) shows the size distribution as determined from AFM measurements of 50 particles from the same sample.

Figure 3.21 shows once again a comparison between SEM and DLS data, this time in the same graph. It is clear that both profiles peak at the same value, but the DLS-data is broader and has a tail towards smaller particle sizes. The broadening could be assigned to the fact that the DLS data is derived from an algorithm fitted to the intensity correlation data. Any imperfections in the plastic cuvette, gas bubbles or dust contaminations in the sample may show up as larger particles, as they are often invariant with time, which also may affect the result.

Another uncertainty factor in the experimental setup is the determination of the dielectric constants. The surface of the metal nanoparticles will be covered by an organic layer from the synthesis. In these measurements the values used are those for the elemental metal in water.

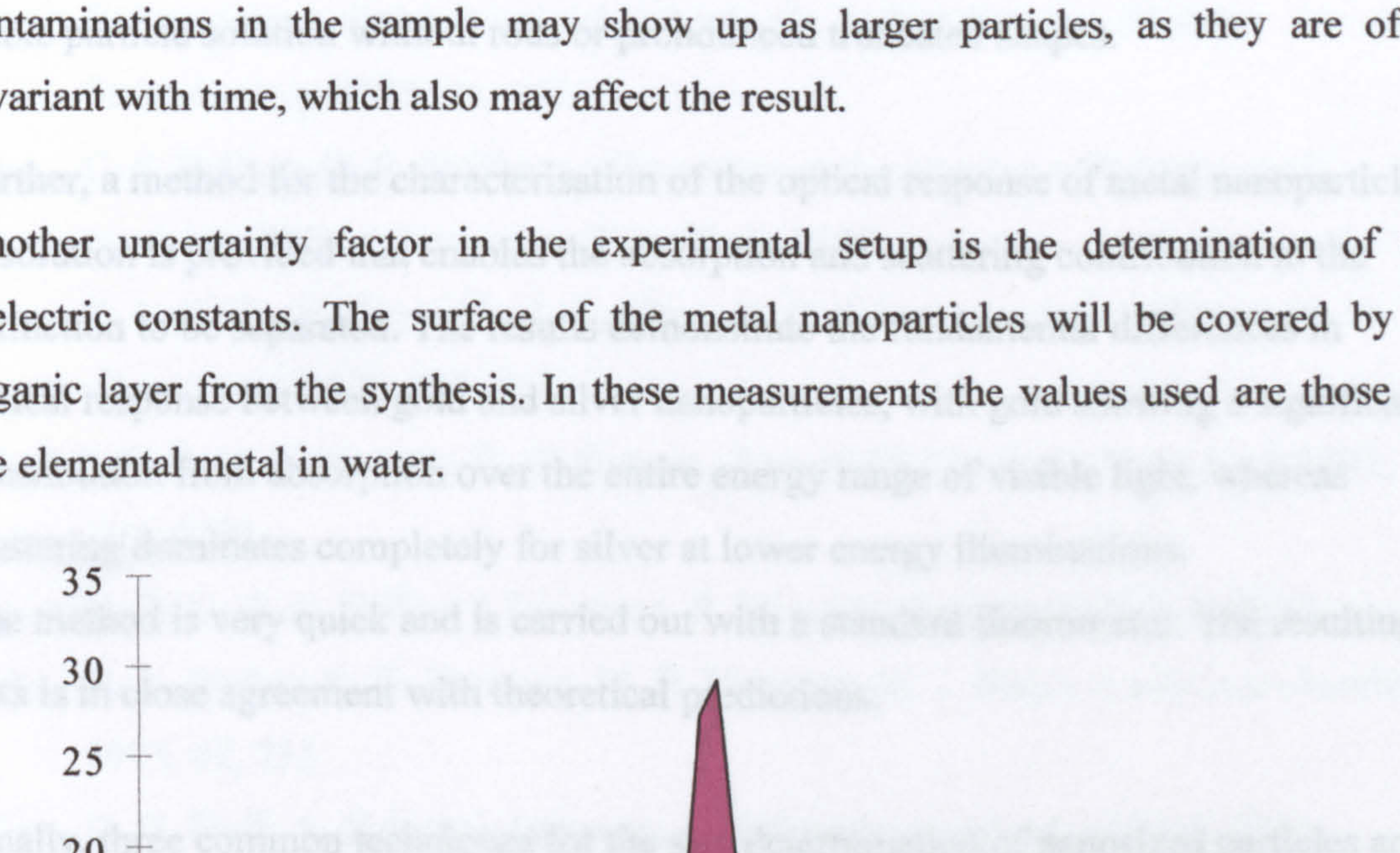

FIGURE 3.21. Size distribution according to DLS measurement (blue piles), and SEM (red graph, 150 particles counted).

3.6 CONCLUSIONS

In this chapter, several methods for the controlled synthesis of gold and silver nanoparticles in the size range 20-100 nm in diameter are demonstrated. This is the size range in which spherical nanoparticles show the strongest interaction with electromagnetic radiation with energies in the visible spectrum. Most methods provide a stable particle solution without rods or pronounced truncated shapes.

Further, a method for the characterisation of the optical response of metal nanoparticles in solution is provided that enables the absorption and scattering contribution to the extinction to be separated. The results demonstrate the fundamental differences in optical response between gold and silver nanoparticles, with gold showing a significant contribution from absorption over the entire energy range of visible light, whereas scattering dominates completely for silver at lower energy illuminations.
The method is very quick and is carried out with a standard fluorometer. The resulting data is in close agreement with theoretical predictions.

Finally, three common techniques for the size determination of nanosized particles are compared. Scanning electron microscopy and atomic force microsocpy are shown to be in agreement with each other. Dynamic light scattering is demonstrated as a useful technique for a very quick and cost efficient characterisation of a nanoparticle solution, provided the sample is known to be relatively monodisperse.

In short, this chapter provides a toolbox for the synthesis and characterisation of gold and silver nanoparticles in the size range where a large number of applications are found in the area of nanometrology.

[1] J. R. Cole, N. J. Halas, *Applied Physics Letters* **2006**, *89*, 153120.

[2] J. Yguerabide, E. Yguerabide, *Analytical Biochemistry* **1998**, *262*, 137.

[3] J. Yguerabide, E. Yguerabide, *Analytical Biochemistry* **1998**, *262*, 157.

[4] H. Xu, J. Aizpurua, M. Kall, P. Apell, *Phys. Rev. E* **2000**, *62*, 4318.

[5] C. Sonnichsen, B. M. Reinhard, J. Liphardt, A. P. Alivisatos, *Nature Biotechnology* **2005**, *23*, 741.

[6] C. F. Bohren, D. R. Huffman, *Absorption and scattering of light by small particles*, Wiley-Interscience, New York, **1998**.

[7] K. L. Kelly, E. Coronado, L. L. Zhao, G. C. Schatz, *Journal Of Physical Chemistry B* **2003**, *107*, 668.

[8] I. O. Sosa, C. Noguez, R. G. Barrera, *Journal Of Physical Chemistry B* **2003**, *107*, 6269.

[9] D. G. Duff, A. Baiker, I. Gameson, P. Edwards, *Langmuir* **1993**, *9*, 2310.

[10] K. C. Grabar, R. G. Freeman, M. B. Hommer, M. J. Natan, *Analytical chemistry* **1995**, *67*, 735.

[11] D. G. Duff, A. Baiker, I. Gameson, P. Edwards, *Langmuir* **1993**, *9*, 2301.

[12] P. C. Lee, D. Meisel, *Journal Of Physical Chemistry* **1982**, *86*, 3391.

[13] J. A. Creighton, C. G. Blatchford, M. G. Albrecht, *Journal Of The Chemical Society-Faraday Transactions Ii* **1979**, *75*, 790.

[14] S. M. Heard, F. Grieser, C. G. Barraclough, J. V. Sanders, *Journal of Colloid And Interface Science* **1983**, *93*, 545.

[15] D. Cunningham, R. E. Littleford, W. E. Smith, P. J. Lundahl, I. Khan, D. W. McComb, D. Graham, N. Laforest, *Faraday Discussions* **2006**, *132*, 135.

[16] R. Piazza, V. Degiorgio, M. Corti, J. Stavans, *Physical Review B* **1990**, *42*, 4885.

[17] R. Pecora, *Die Makromolekulare Chemie* **2003**, *2*, 73.

[18] J. J. Storhoff, A. A. Lazarides, R. C. Mucic, C. A. Mirkin, R. L. Letsinger, G. C. Schatz, *Journal Of The American Chemical Society* **2000**, *122*, 4640.

[19] S. Y. Park, J. S. Lee, D. Georganopoulou, C. A. Mirkin, G. C. Schatz, *Journal Of Physical Chemistry B* **2006**, *110*, 12673.

[20] J. Rodriguez-Fernandez, J. Perez-Juste, L. M. Liz-Marzan, P. R. Lang, *Journal of Physical Chemistry C* **2007**, *111*, 5020.

CHAPTER 4

OPTIMISATION OF AGGREGATING CONDITIONS FOR SURFACE ENHANCED RAMAN SCATTERING FROM NANOPARTICLE SOLUTIONS

TABLE OF CONTENTS

CHAPTER PAGE

4.1 INTRODUCTION

Metal particles can interact with light by excitation of a surface plasmon. The formation of a surface plasmon is accompanied by an enhanced electromagnetic field localised to the surface of the particle[1-4]. Bringing two such particles close together brings on additional enhancement effects by localising the potential drop between the two surfaces[5, 6]. The scattering from a molecule trapped between two such surfaces may be enhanced by a factor of 10^{11}, and possibly even enable single molecule detection. [6, 7]

The two most commonly used metals utilised in SERS are gold and silver. Though they share a number of physical properties, there are differences that will affect their suitability as SERS substrates at different excitation wavelengths. Among these are the resonance frequencies of the plasmon of nano sized gold and silver particles[1, 6, 8]. The gold plasmon is excited at lower excitation frequencies and also has lower threshold energy for interband absorption of the energy. This could have an impact on metal of choice in a certain experimental setup.

In many applications of SERS, it is desirable to utilise the increase in enhancement achieved from aggregation of the nanoparticles[9-11]. Although the aggregation is often considered a process that is difficult to control, the optical properties of the nanoparticle aggregates are expected to be strongly correlated with the individual nanoparticles making up the cluster, as well as on the aggregation conditions used[12]. Nodlander et al.[13] has shown theoretically, that for the least complex structure, when two particles interact via plasmon coupling as a dimer, there are two resonances that can be seen in the extinction profile. One corresponds to the plasmons of the individual particles moving out of phase (anti bonding), and one corresponding to the plasmons moving in phase (bonding). The latter resonance is red shifted compared to the single plasmon resonance. This red shift increases with decreasing particle separation, in contrast to the anti bonding mode which is fairly constant at the single particle plasmon resonance frequency. For calculations dealing with the optical properties of larger aggregates we turn to Schatz et al.[14] In agreement with Nordlander, he predicts the appearance of a second plasmon resonance that is red shifted with decreasing interparticle distance.

Further, it is predicted that this resonance will be further red shifted with increasing size of the particles making up the aggregate, as well as with increasing number of particles in the aggregate. However, this red shift will also depend on what type of cluster is formed. A compact cluster is predicted to be more sensitive to these factors than a fractal like cluster.

The calculations in the above mentioned articles deal with specific systems and the conclusions will primarily apply to these systems. In this chapter we aim to investigate how these parameters work in a commonly used SERS setup, with mercaptophenol-functionalised gold and silver nanoparticles of various sizes. It is shown that it is possible to manipulate the electronic response of an aggregated nanoparticle solution by varying particle size and particle concentration. The time dependence of the aggregation process is also investigated. Furthermore, we investigate the correlation between the electronic response of the aggregated nanoparticle solution and its properties as a substrate for surface enhancement of the Raman signal of an analyte adsorbed on to the nanoparticle surface. In these experiments we have chosen mercaptophenol as the analyte since it is an efficient Raman scatterer and does not benefit from any molecular resonance at any excitation wavelengths used here. We find that the effect of self extinction of the Raman scattered in many systems overshadows any increase in Raman scattering that an increased electronic response may bring. With the term self extinction we here refer to the process (that follows from Beer-Lamberts law) where Raman scattered light is reabsorbed or rescattered by the sample solution on its way from the analyte to the detector. Even data corrected for self extinction show little or no correlation between the collective electronic response of the aggregated nanoparticle solution, and the Raman scattering intensity of the analyte. This is in agreement with the results predicted theoretically by Le Ru et al[15], where it is shown that the enhancement fields inside the aggregates are only loosely connected to its extinction spectra.

4.2 EXPERIMENTAL

The aggregation study was carried out with 1800 μL of nanoparticle functionalised with 200 μL 10^{-6} mol/dm^3 of mercaptophenol, and aggregation was induced by addition of 200 μL of 1 mol/dm^{-3} of sodium chloride. The electronic spectra were recorded with a Parkin Elmer Instruments, Lambda 35 from a 1 cm path length disposable cuvette from VWR. Spectra were taken 30 seconds after aggregation started, unless otherwise stated.

The 633 nm and 785 nm data were collected using a Renishaw Ramascope system at 180° collection angle. The 532 nm data were collected with an Avalon Instruments Raman Station R3 focusing in a plastic cuvette, collecting at 180° degrees. The intensity of the 1080 cm^{-1} peak in the mercaptophenol spectra was taken as the SERS intensity and was normalized against a cyclohexane standard as described in chapter 2. All spectra were collected as 3 or 5 accumulations of 5 seconds each, and all data points were averages of 5 replicates.

The gold nanoparticles used were prepared according to the method described by Grabar et al. (22 nm diameter) and a modified method of Duff et al (59 nm). The silver nanoparticles used were prepared from reduction by EDTA (36 nm diameter), and a recently developed method for seeded growth of silver nanoparticles (63 nm). All batches were characterized by AFM, SEM, and electronic spectra (chapter 3).

Samples for SERS measurements were prepared by mixing nanoparticle (900 μL) and 10^{-6} mol/dm^3 of mercaptophenol (100 μL). To aggregate the nanoparticles 100 μL of 1 mol/dm^3 sodium chloride solution was added to the sample to cause it to aggregate completely. SERS-spectrum and molecular structure of mercaptophenol is shown in figure 4.1.

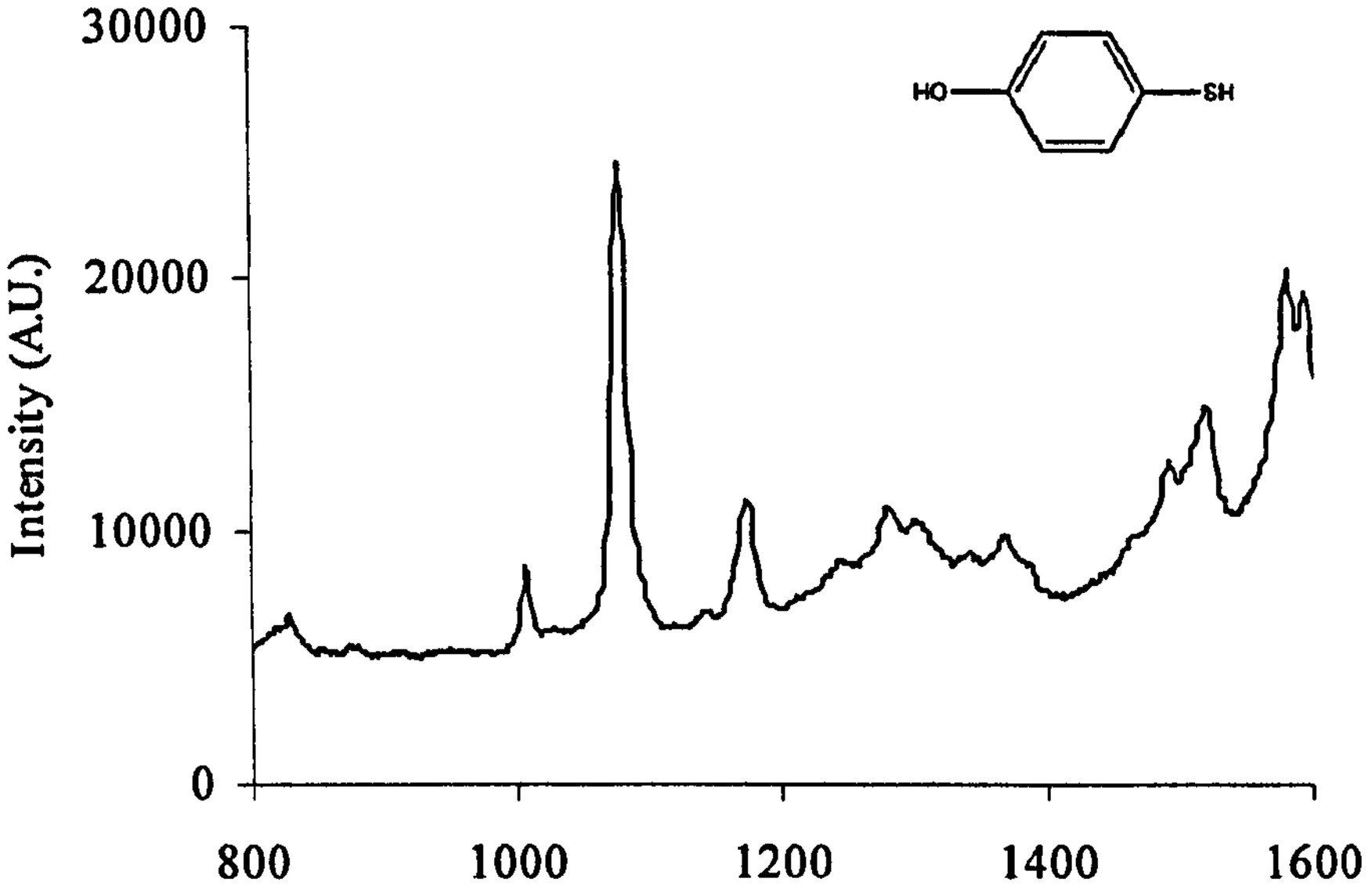

FIGURE 4.1. The molecular structure and the SERS-spectrum of mercaptophenol on aggregated silver nanoparticles at 633 nm excitation, 3x5s accumulation.

4.3 RESULTS AND DISCUSSION

As aggregation is a dynamic effect, there will be time dependence in the electronic response of the aggregated nanoparticle solution. Upon addition of sodium chloride, the particle solution changes colour within a few seconds from red to blue (gold) or from yellow to green/grey (silver). It is not practically possible to record an electronic spectrum that quickly with the instrument used here. The data in figure 4.2 show aggregation data for goldparticles of 22 nm diameter at $2.5x10^{13}$ particles/L. The results show that after this first rapid process, the aggregation continues with time, albeit at a significantly slower rate. The difference is most pronounced from 700 nm and onwards, suggesting that the change is correlated with the growth of larger clusters, expected to be resonant at longer wavelengths[14] , possibly in combination with a process where large and compact clusters grow by ripening of smaller clusters[16]. This shows that careful consideration should be given to the time factor when using aggregated nanoparticle solutions in experiments.

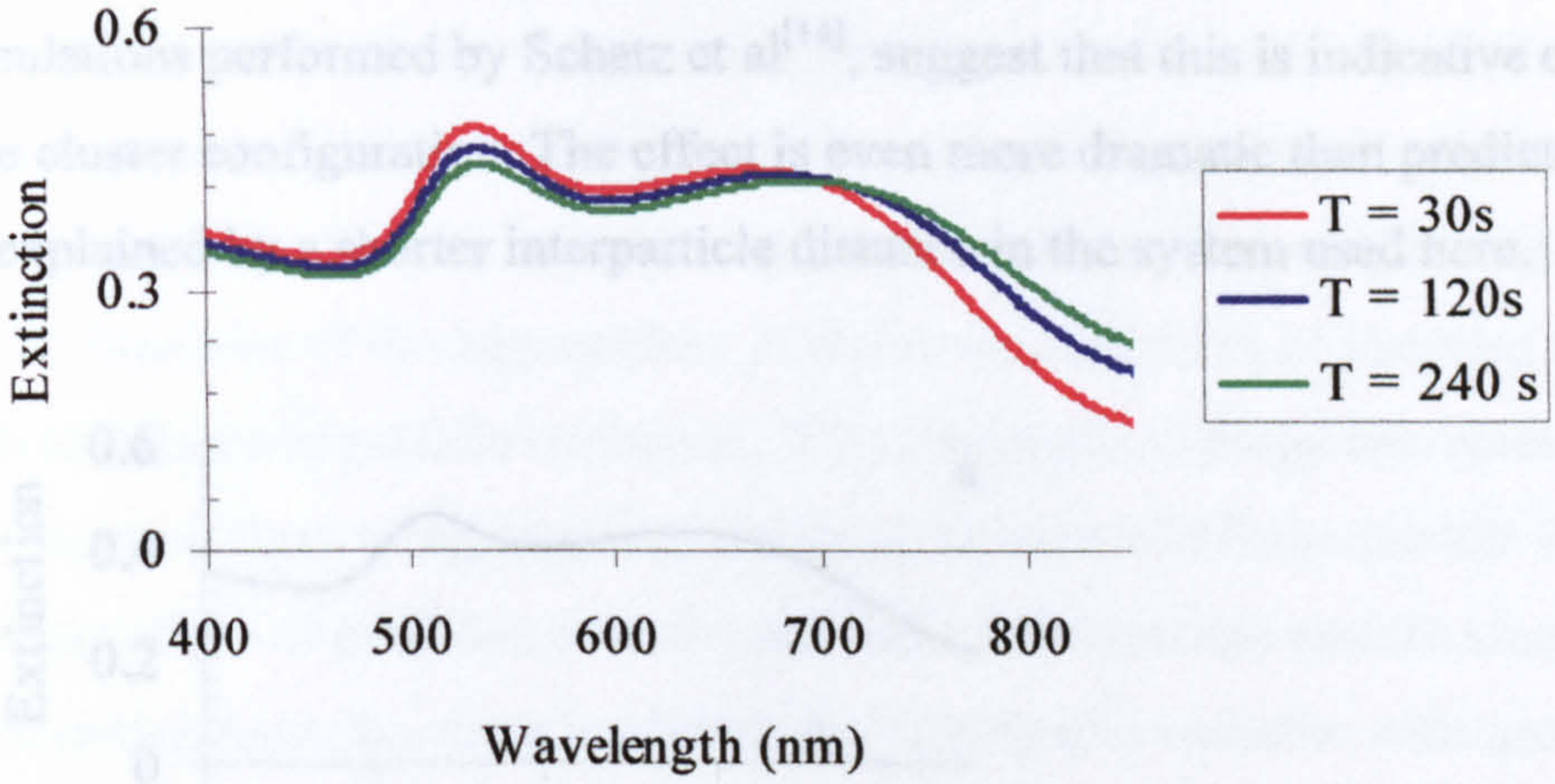

FIGURE 4.2. The change in the electronic spectra of aggregated gold nanoparticles of 22 nm diameter with time. It is clear that there is an increase with time of the extinction at longer wavelengths that is correlated with a decrease at 520 nm, which is the single particle resonance wavelength of the gold particles. The particle concentration is 2.5×10^{13} particles/L.

Figure 4.3 demonstrates the dependence on size of the aggregated nanoparticle, of the electronic response of an aggregated gold nanoparticle solution. In figure 4.3 a) (22 nm diameter) and 4.3.b) (37 nm diameter) the nanoparticle concentration is 5×10^{13} particles/L in both cases. The peak extinction of the lower energy maxima shifts from around 680 nm to almost 800 nm. In figure 4.3.c) the particle diameter is 59 nm, but the particle concentration is down to ¼ compared to the two smaller sizes. The lowering of particle concentration is expected to bring a smaller cluster size. At higher concentrations, the low energy peak of the aggregated solution is shifted out of the range of the spectrometer, and even for the lower concentration used here, it is shifted to around 830 nm. The experiment shows that the effect of increasing the size of the particle making up the aggregate has a dramatic effect on the red shift of the lower energy peak, and is an effective way of manipulating the electronic response of the nanoparticle clusters.It is expected that the particle plasmon resonance frequency of a nanoparticle is shifted towards lower frequencies (longer wavelengths) as the size increases, in this case from approximately 520 nm for the smallest size to 530 nm for the 37 nm particles to 540 nm for the 59 nm[17, 18] size. The results presented in figure 4.3 indicate that the corresponding shift for the second maxima of the aggregated species is much larger, with a shift from 670 nm to 760 nm for the 22 nm particles and

37 nm particles respectively, and further still for the largest size. The numerical calculations performed by Schatz et al[14], suggest that this is indicative of a compact type cluster configuration. The effect is even more dramatic than predicted, which could be explained by a shorter interparticle distance in the system used here.

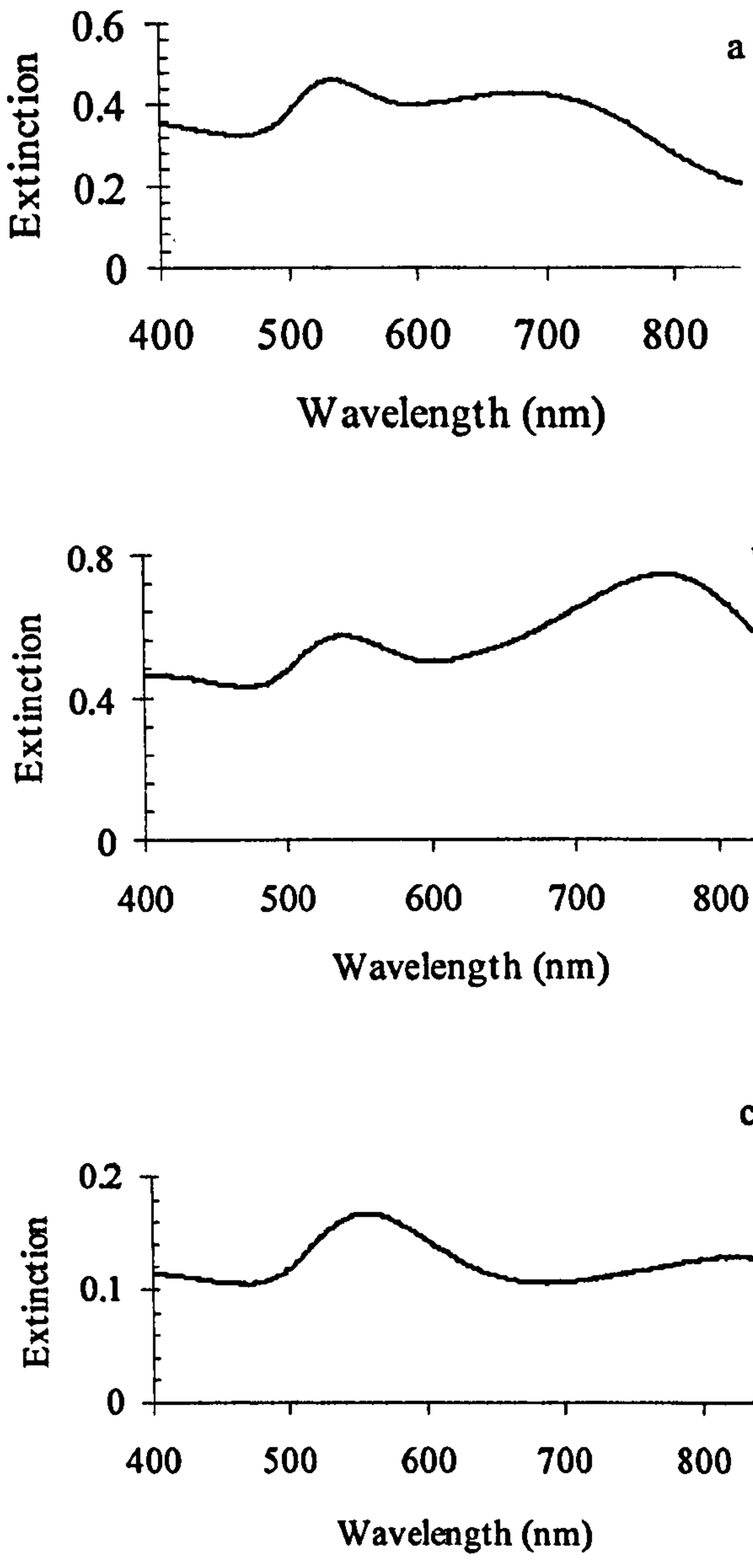

FIGURE 4.3. Dependence of electronic spectra of the aggregates on the size of the aggregated nanoparticle. a) show the extinction spectra of aggregated 22 nm diameter gold particles, $5x10^{13}$ particles/L b) 37 nm, $5x10^{13}$ particles/L and c) 59 nm diameter, $1.25x10^{13}$ particles/L All spectra are taken 30 s after aggregation was initiated.

Figure 4.4 shows the particle concentration dependence of the aggregation process for 22 nm gold nanoparticles. A general increase in extinction, the trend of a redshift of the second maxima, and an increase in relative extinction compared to the high energy maxima between the four samples can be clearly seen. This can once again be explained by the dynamics of the aggregation. A higher concentration of particles will mean a high likelihood of particle collisions. When the surface charge decreases, many collisions can lead to aggregation, and large clusters will form quickly. At the lowest concentrations of particles, even though there is not enough surface charge to repel surrounding particles, there is a lower probability of a collision with another particle. This also means that there may be a difference in the structure of the aggregates formed, which may contribute to the difference.

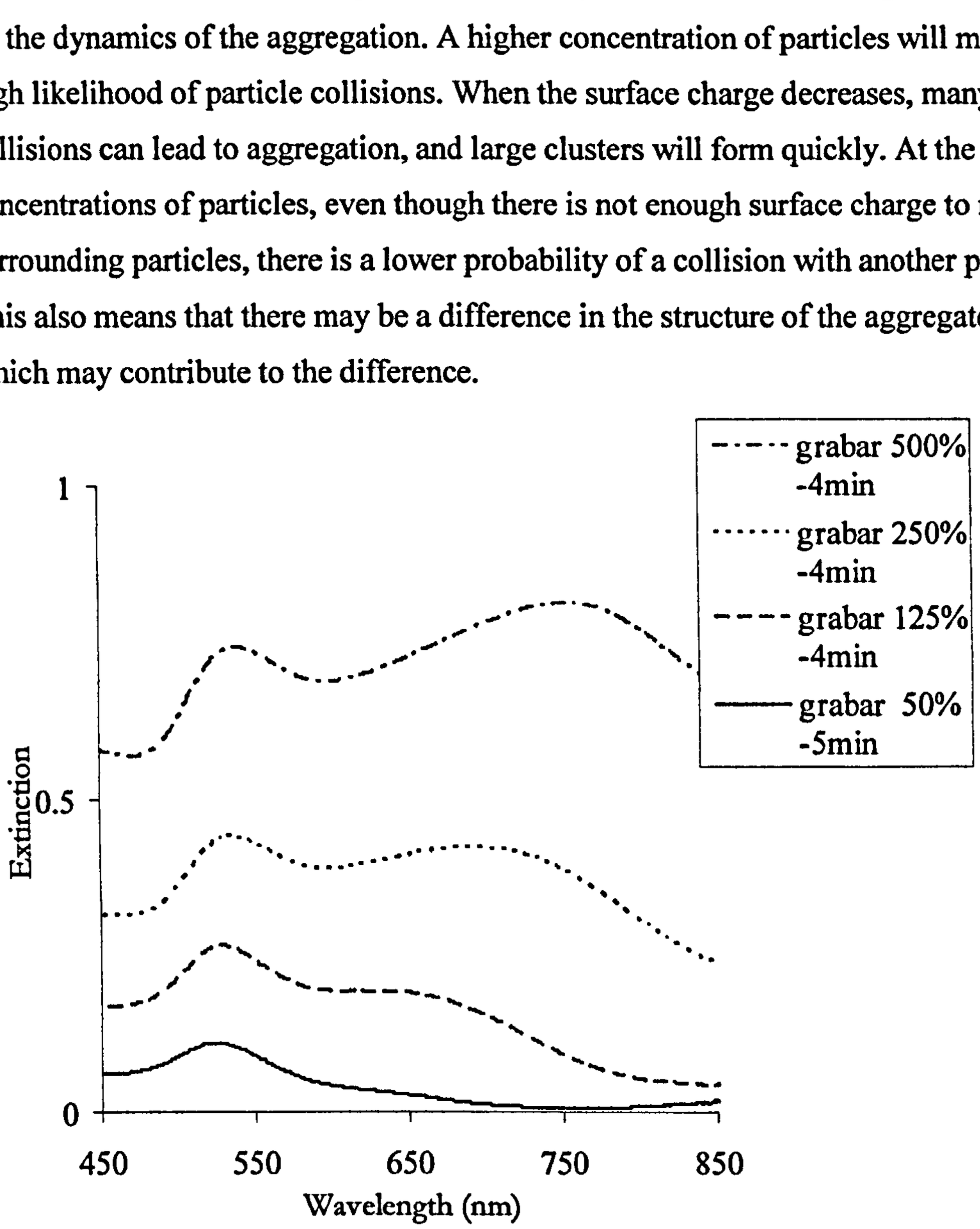

FIGURE 4.4. The concentration dependence on aggregation of 22 nm gold nanoparticle solution. 100 % concentration equals 2.5×10^{14} particles/L. All spectra were acquired 30 s after aggregation was initiated. There is a clear red shift of the lower energy maxima as the particle concentration increases. This is mainly attributed to the formation of larger clusters at higher particle concentrations.

In figure 4.5 the same effect is demonstrated for 36 nm silver nanoparticles and the same trends are observed.

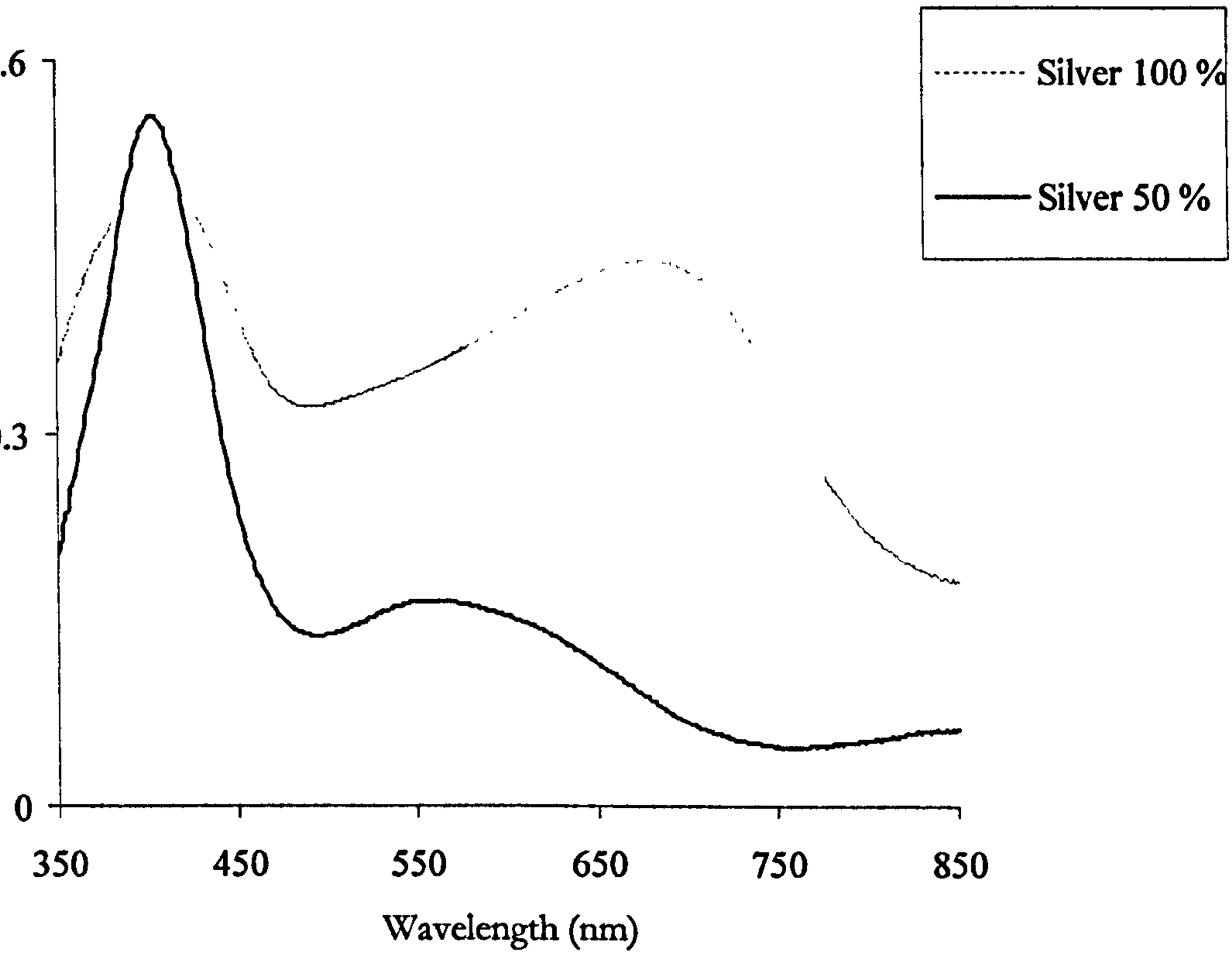

FIGURE 4.5. The dependence of aggregation on silver nanoparticle (36 nm diameter) concentration. 100 % concentration equals 10^{14} particles/L. All spectra were acquired 30 s after aggregation was initiated. There is a clear red shift of the lower energy maxima as the particle concentration increases. This is mainly attributed to the formation of larger clusters at higher particle concentrations.

Having established the means available to manipulate the optical response of an aggregated nanoparticle solution, we now examine the connection between this response and their properties as SERS substrates. We begin by noting that in setting up a SERS experiment involving nanoparticle solutions, the effect of self extinction of scattered light from the analyte by the nanoparticle solution is a major factor to take in consideration. From the Beer-Lambert law (equation 4.1) it follows that the further in to the solution the laser focus penetrates, the more important this effect becomes. A is the extinction, ε is the molar extinction coefficient of the nanoparticles and C the particle concentration.

$$A = l \cdot \varepsilon \cdot C \qquad (4.1)$$

In table 4.1 the results for the normalised SERS intensity of the 500% (1.25×10^{15} particles/L) and the 125 % gold nanoparticle solutions in figure 4.4 and the silver nanoparticle solutions in figure 4.5 at 633 nm and 785 nm are shown. In figure 4.6 the excitation frequency and the emission wavelength of the Raman peak used for measurement of the intensity are illustrated. From these data it is evident that the effect of self absorption of Raman scattered light by the nanoparticle solution has a major impact on the SERS intensity at the Raman band emission point. It is most apparent for the 633 nm data, where the highly concentrated nanoparticle solutions are very poor SERS substrates.

TABLE 4.1. Normalised SERS intensity obtained from the aggregated nanoparticle solutions in figures 4.4 and 4.5 at 633 nm and 785 nm excitation. The excitation points and Raman spectra of the mercaptophenol in relation to the extinction spectra of the nanoparticle solution is further demonstrated in figures 4.6 and 4.7.

Excitation Wavelength	Normalised SERS Intensity			
	Ag –36 nm 100%	Ag-36nm 50%	Au-22nm 500%	Au-22nm 125%
633 nm	0.32	0.61	0.09	0.24
785 nm	0.29	0.22	0.38	0.39

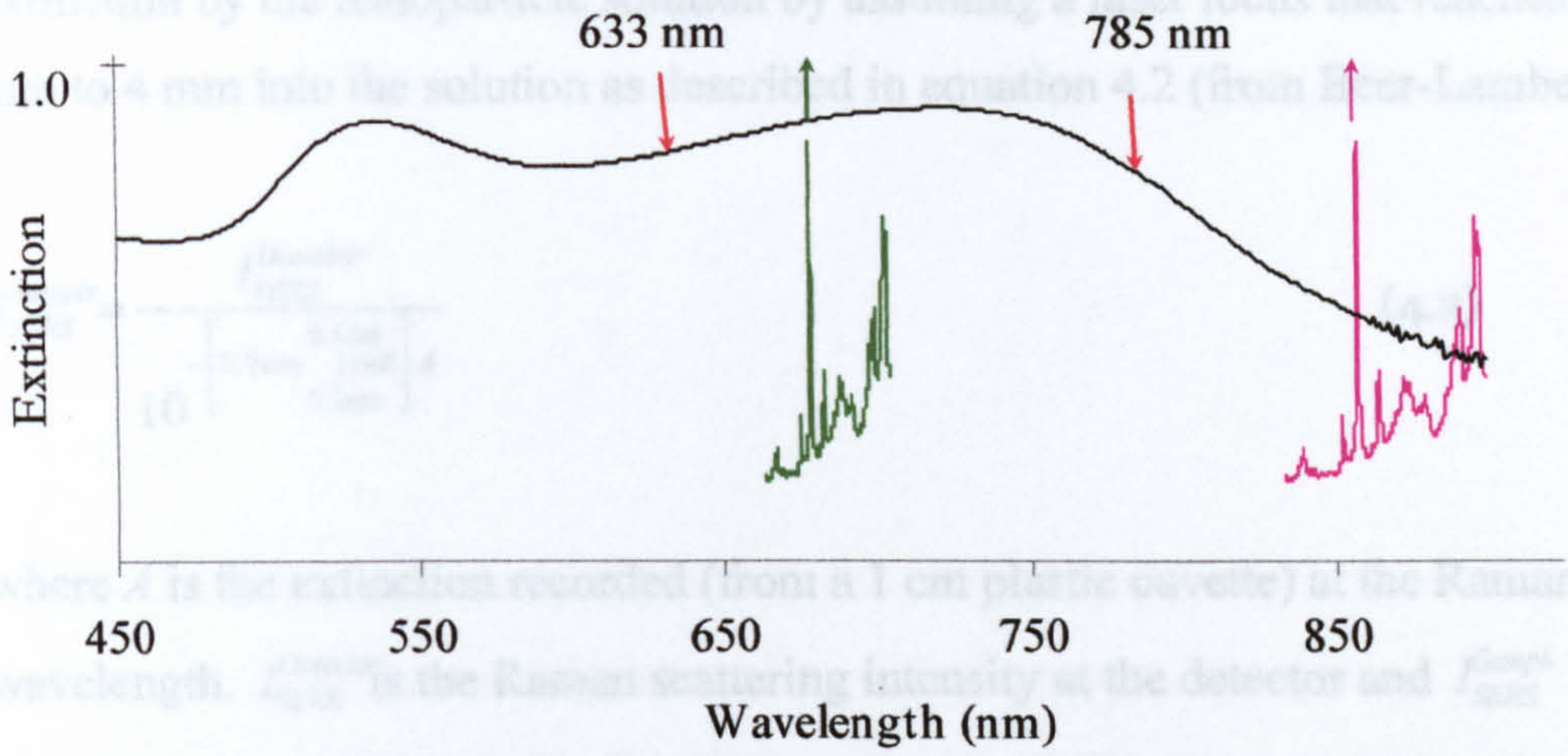

FIGURE 4.6. Illustration of the electronic response of the aggregated 22 nm 500 % gold nanoparticle solution at the excitation point (red downwards arrow) and the photon collection point (arrows pointing upwards). The green and red spectra show the position of the Raman spectra in comparison to the extinction spectra of the nanoparticle solution.

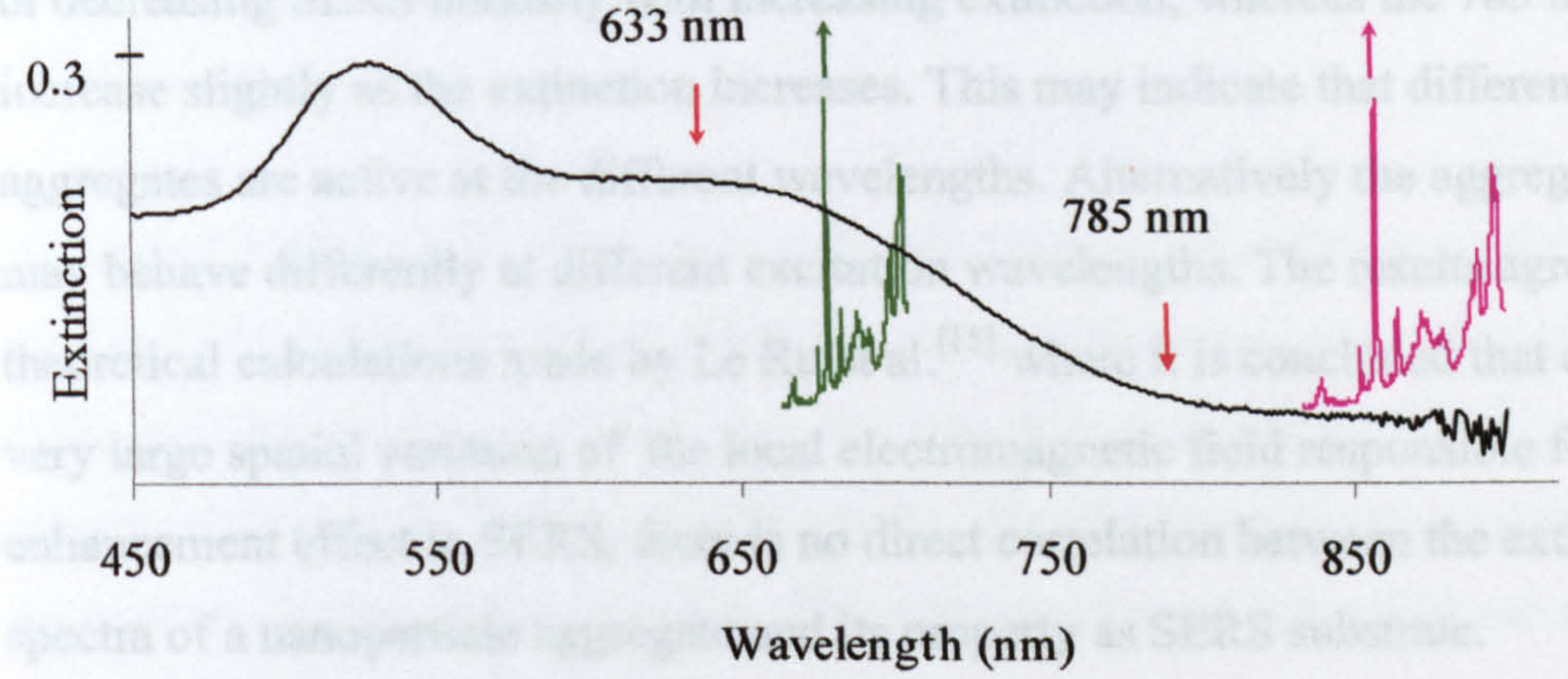

FIGURE 4.7. Illustration of the electronic response of the aggregated 22 nm 125 % gold nanoparticle solution at the excitation point (red downwards arrow) and the photon collection point (arrows pointing upwards). The green and red spectra show the position of the Raman spectra in comparison to the extinction spectra of the nanoparticle solution.

The effect of the plasmon response at the excitation wavelength is more difficult to discern. In figure 4.8 the SERS intensity has been plotted against the extinction at the excitation wavelength. The SERS intensity has been compensated for the effect of self

extinction by the nanoparticle solution by assuming a laser focus that reaches from 2 mm to 4 mm into the solution as described in equation 4.2 (from Beer-Lamberts law)

$$I_{SERS}^{Sample} = \frac{I_{SERS}^{Detector}}{10^{-\left[\int_{0.2cm}^{0.4cm} LdL\right]\cdot A}} \qquad (4.2)$$

where A is the extinction recorded (from a 1 cm plastic cuvette) at the Raman emission wavelength. $I_{SERS}^{Detecto}$ is the Raman scattering intensity at the detector and I_{SERS}^{Sampl} is the Raman scattering intensity in the volume of excitation in the sample. In this setup, the effect of self extinction takes away between 5% for the most dilute samples, up to 50% for the most concentrated samples.

The data does not show any clear trends. There is a difference between the data recorded with 633 nm and the 785 nm laser lines, where the 633 nm data show a trend of decreasing SERS intensity with increasing extinction, whereas the 785 nm data increase slightly as the extinction increases. This may indicate that different types of aggregates are active at the different wavelengths. Alternatively the aggregates formed may behave differently at different excitation wavelengths. The results agree with the theoretical calculations made by Le Ru et al.[15] where it is concluded that due to the very large spatial variation of the local electromagnetic field responsible for the enhancement effect in SERS, there is no direct correlation between the extinction spectra of a nanoparticle aggregate and its property as SERS substrate.

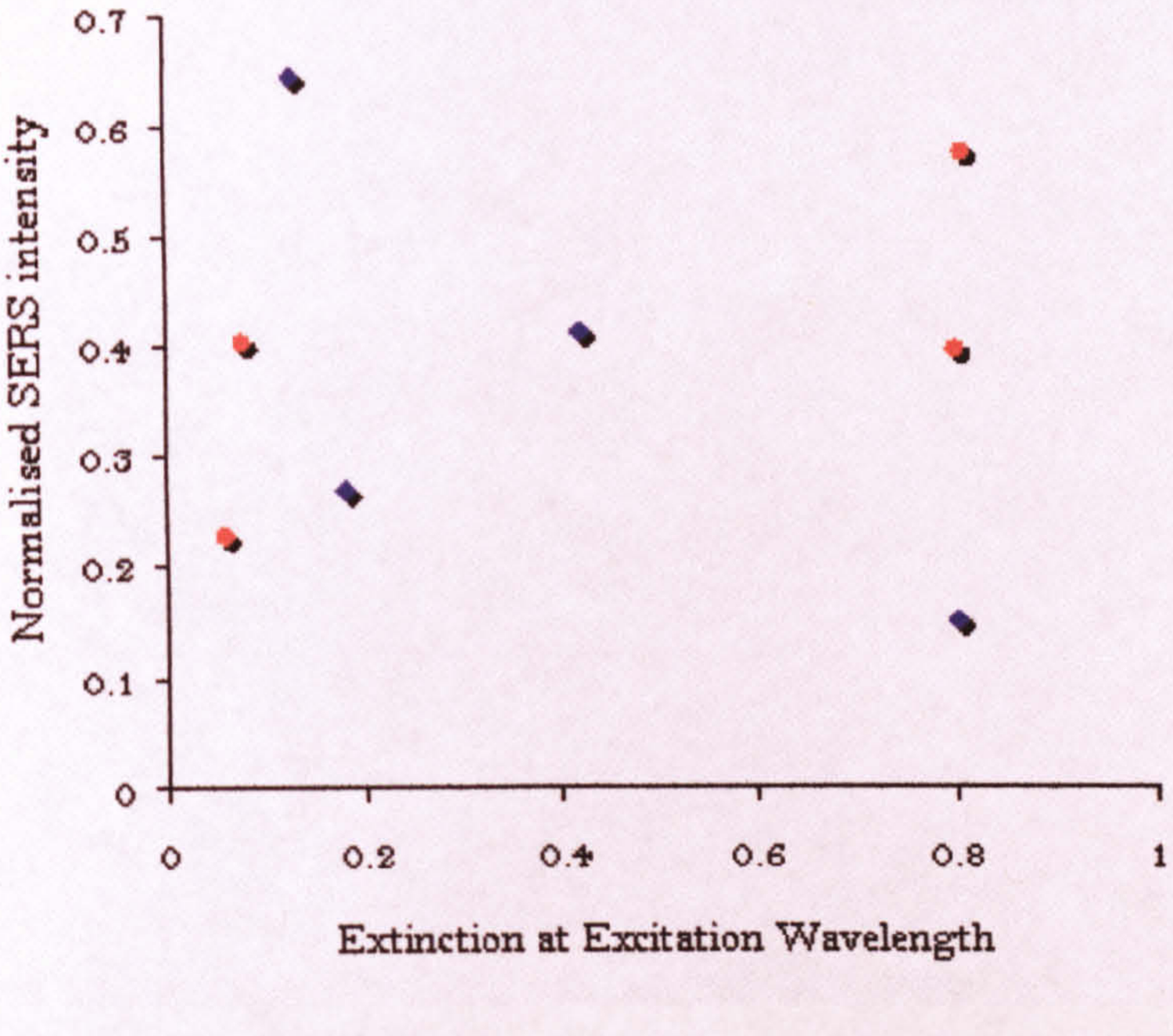

FIGURE 4.8. The SERS intensity data from table 4.1 plotted against extinction at the excitation wavelength. The markers represent data from both gold and silver nanoparticle solutions of different sizes. The SERS intensity has been corrected for self extinction. Blue markers show the Raman intensity from 633 nm excitation data, and orange markers show the Raman intensity from 785 nm excitation data.

In figure 4.9 the SERS intensities from figure 4.8 have instead been plotted against the diameter of the nanoparticle of which the cluster is made up from. Once again it is difficult to draw any conclusions from the data. It is clear that the larger nanoparticles give the strongest SERS intensity. Of course, this could also be due to the fact that that they are made from different metals. The other conclusion is that 785 nm on average give a higher intensity for both types of particles.

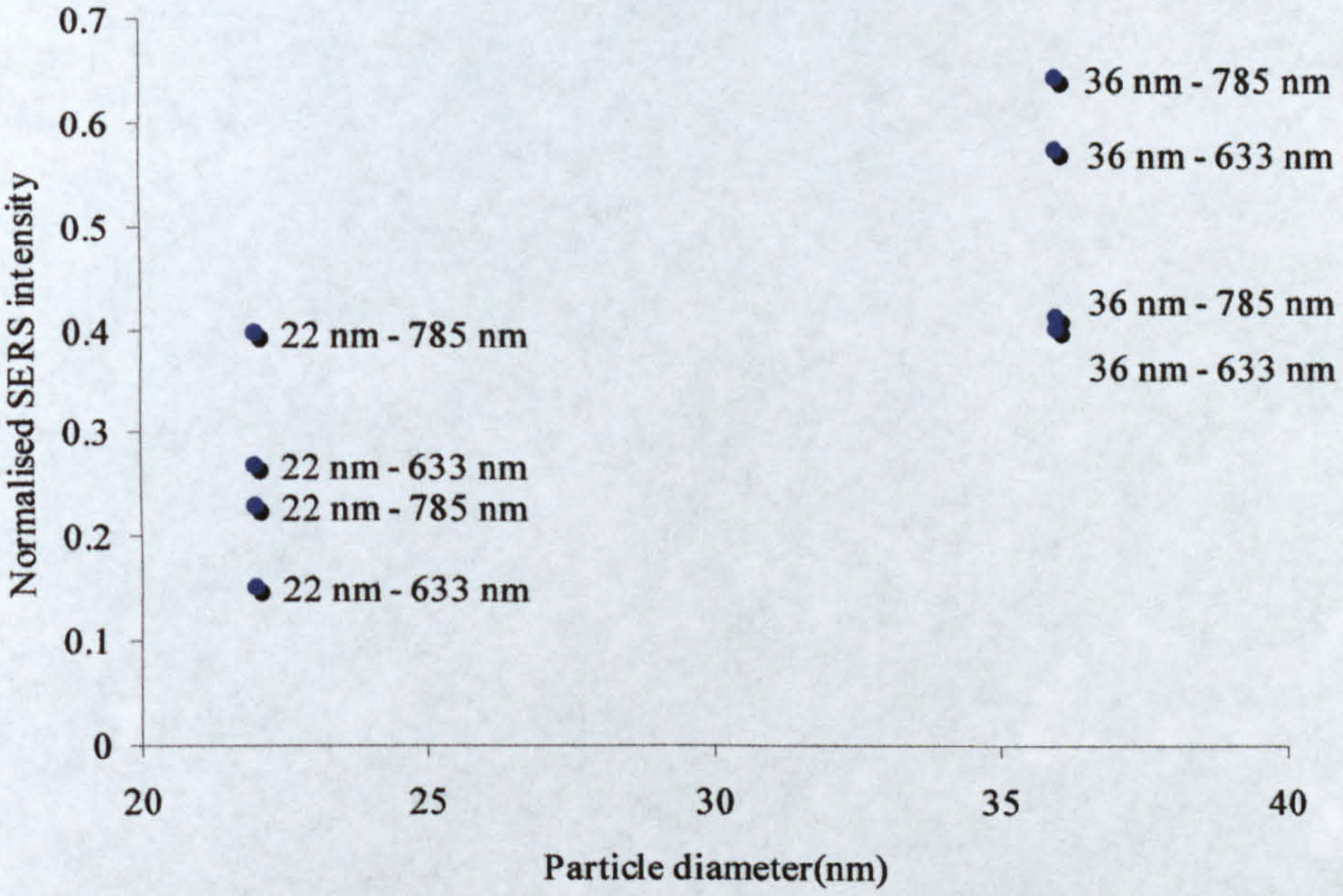

FIGURE 4.9. The SERS intensity data from table 4.1 plotted against particle diameter. The SERS intensity has been corrected for self extinction. All 22 nm data points are from gold particles and all 36 nm data points are from silver particles.

To investigate the impact of choice of metal on SERS intensity, an experiment was carried out where two batches of nanoparticles were synthesised, one of gold and one of silver. The two particle batches were closely correlated in size and shape, as shown in figure 4.10, and diluted to the same concentration. The electronic responses of the two aggregated particle solutions are displayed in figure 4.11. Although there may be small differences between the two batches, they are similar enough to make a comparison valid. There are also close resemblances in the electronic response between the two solutions.

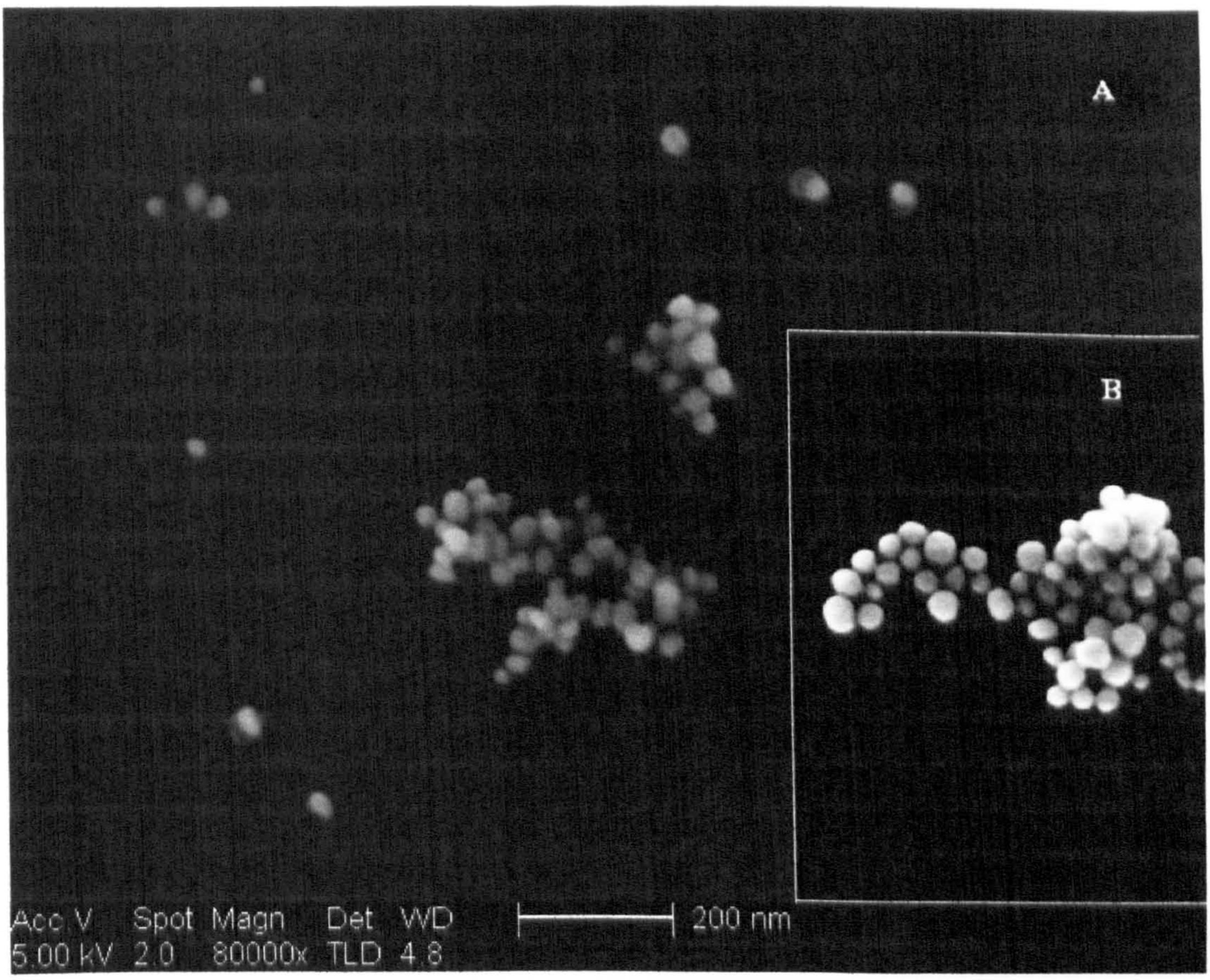

FIGURE 4.10. SEM images of the36 nm diameter silver (A) and 37 nm diameter gold (B, inset, same scale as A) nanoparticles used.

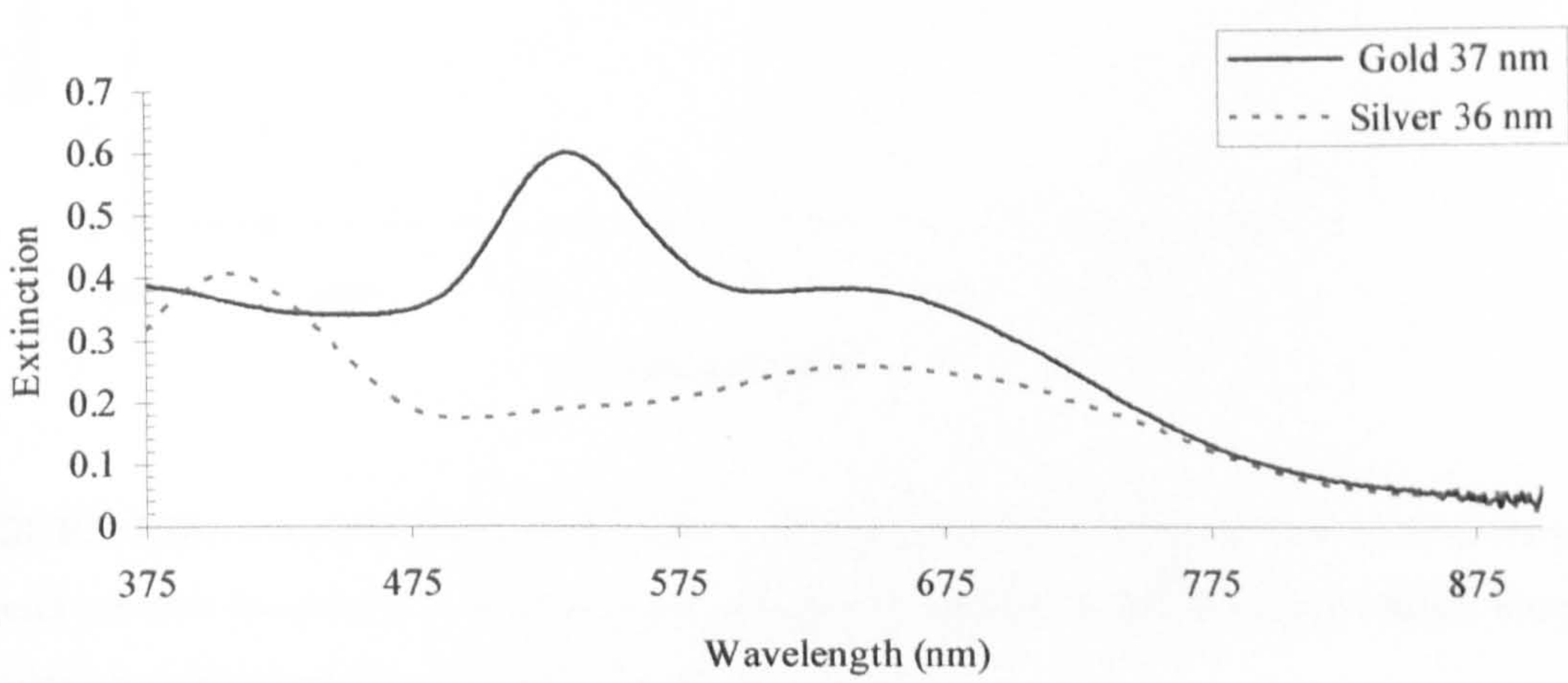

FIGURE 4.11. Electronic spectra of the aggregated gold and silver nanoparticle solutions.

In figure 4.12 the resulting normalised SERS intensity (at the detector) is plotted against the excitation wavelength. At the 532 nm excitation line, the intensity from the gold

particle solution is expected to be severely quenched by self absorption of the scattered light. Also, the particles surface plasmons are expected to be heavily dampened by absorption of the laser light by the particle, transforming photons to heat. At 633 nm there is little difference in intensity between silver and gold and at 785 nm gold appears to be the more efficient SERS substrate. The reason for the rapid improvement of gold as a SERS substrate may be assigned to the decreasing contribution of interband transitions to the plasmon damping at longer wavelength, to a point at 785 nm where gold is expected to, like silver, behave as a Drude model free-electron metal. At 785 nm excitation, the electronic responses of the aggregated gold and silver nanoparticles are almost identical. Despite this, the gold particle solution yields a significantly higher SERS intensity as the silver particle solution.

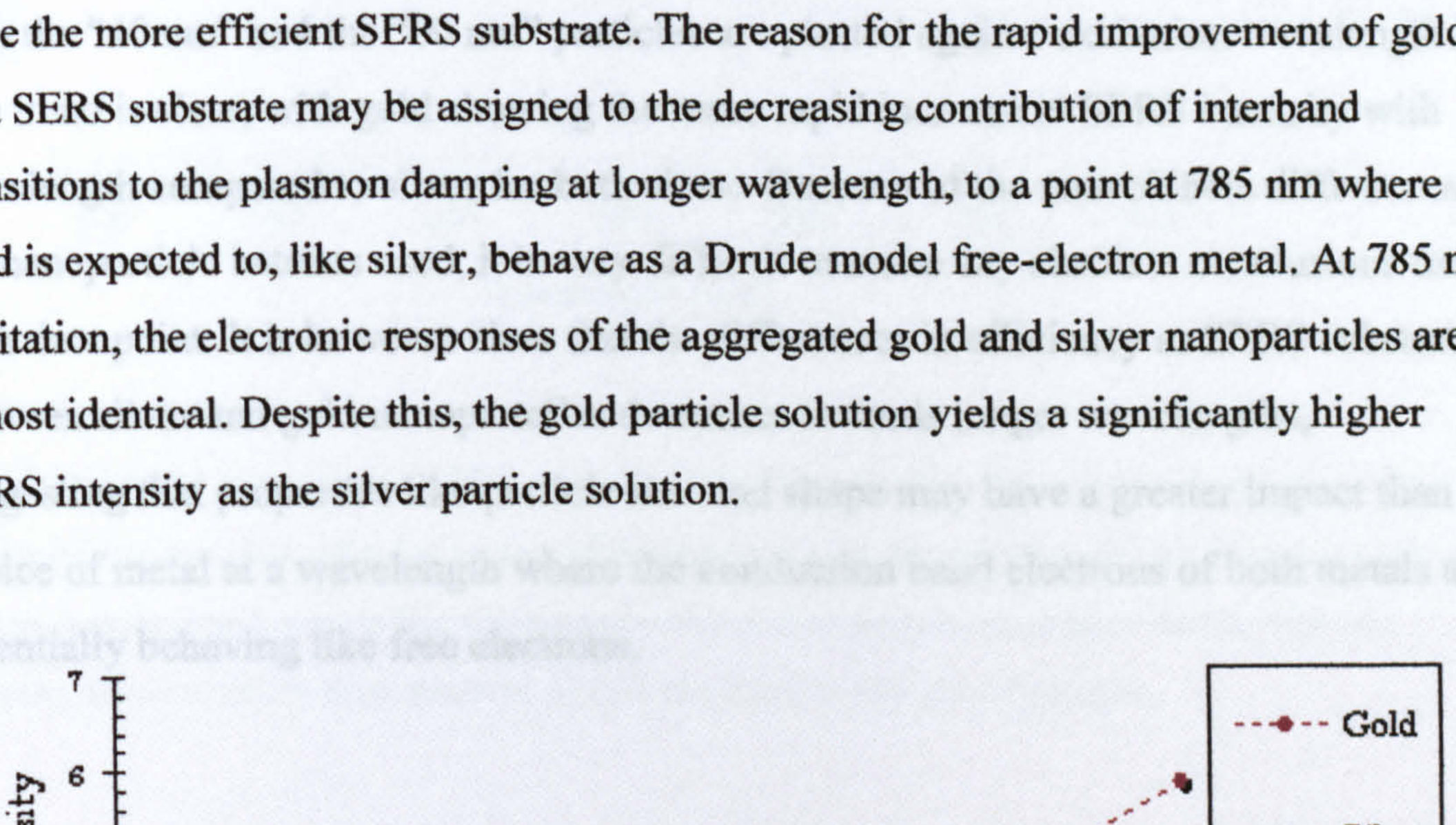

FIGURE 4.12. Comparison of gold and silver, 30 nm diameter, as SERS substrates from the green spectra towards the infra red. All points are averages of 5 replicates and the relative SERS intensity standard deviations are less than 10 % for all data points.

The experiment was repeated with approximately 60 nm diameter particles. The differences between the particle batches were more significant for this experiment, especially the variation in size within the particle solutions. Still, some similarities in the resulting data can be seen (figure 4.13). Gold nanoparticles are still very inefficient

with 532 nm excitation. However, even though silver gives the highest SERS intensity at 785 nm, gold show a more rapid increase in SERS intensity than silver towards lower excitation energies. This is also illustrated in figure 4.14 where the intensity ratios for gold nanoparticles SERS intensity divided by the silver nanoparticle SERS intensity for both the "40 nm" and the "60 nm" particles are plotted against excitation wavelength. The trend is clear, with gold showing the more rapid increase in SERS intensity with wavelength compared to silver for both sizes. Because of the unavoidable differences in the nanoparticle batches used, it is very difficult to make any absolute conclusions from each data point. It is however clear that the differences in efficiency as SERS substrate between silver and gold nanopartciles decreases towards longer wavelengths, suggesting that properties like particle size and shape may have a greater impact than choice of metal at a wavelength where the conduction band electrons of both metals are essentially behaving like free electrons.

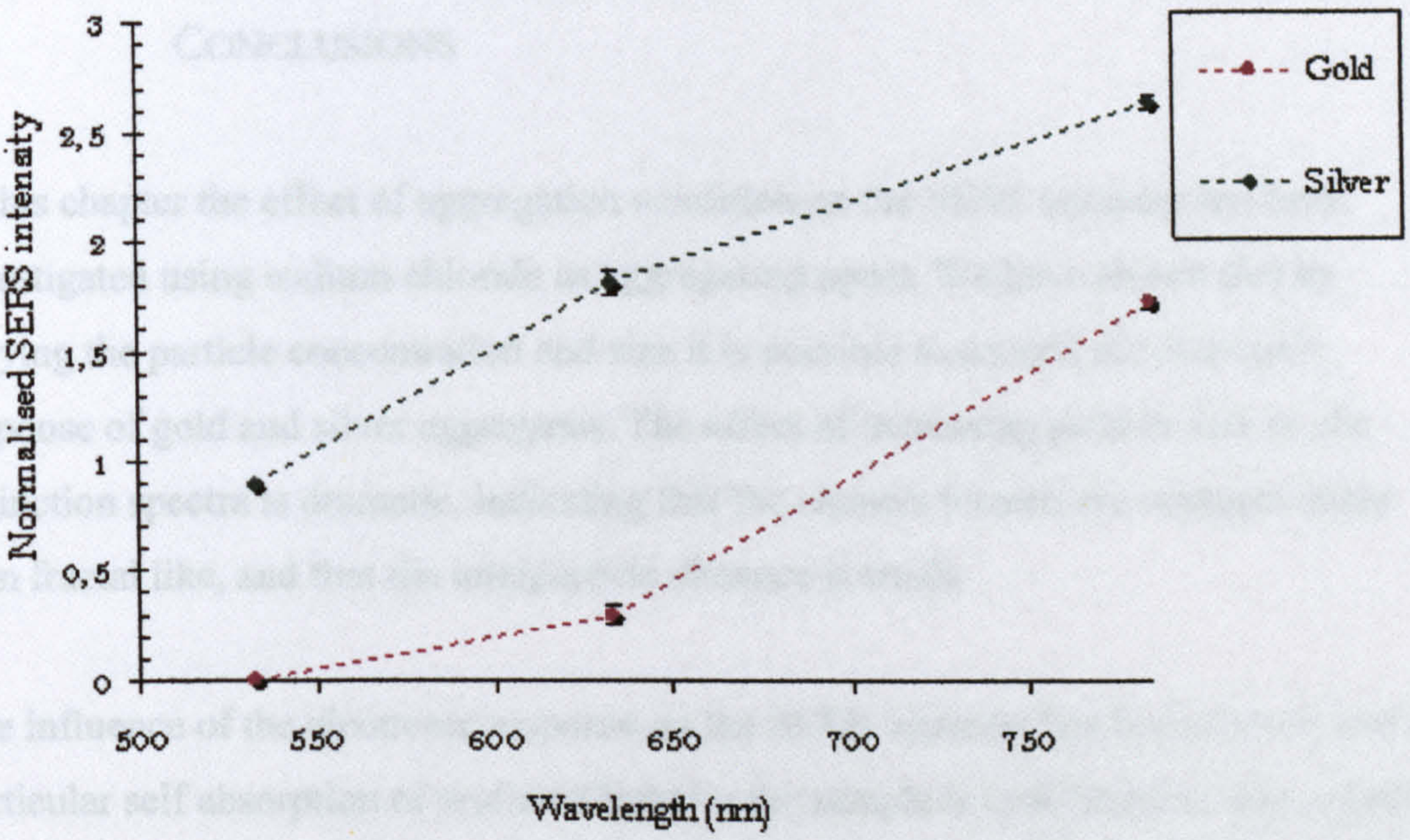

FIGURE 4.13. Comparison of gold and silver, 60 nm diameter, as SERS substrates from the green spectra towards the infrared. All points are averages of 5 replicates and the relative SERS intensity standard deviations are less than 10 % for all data points.

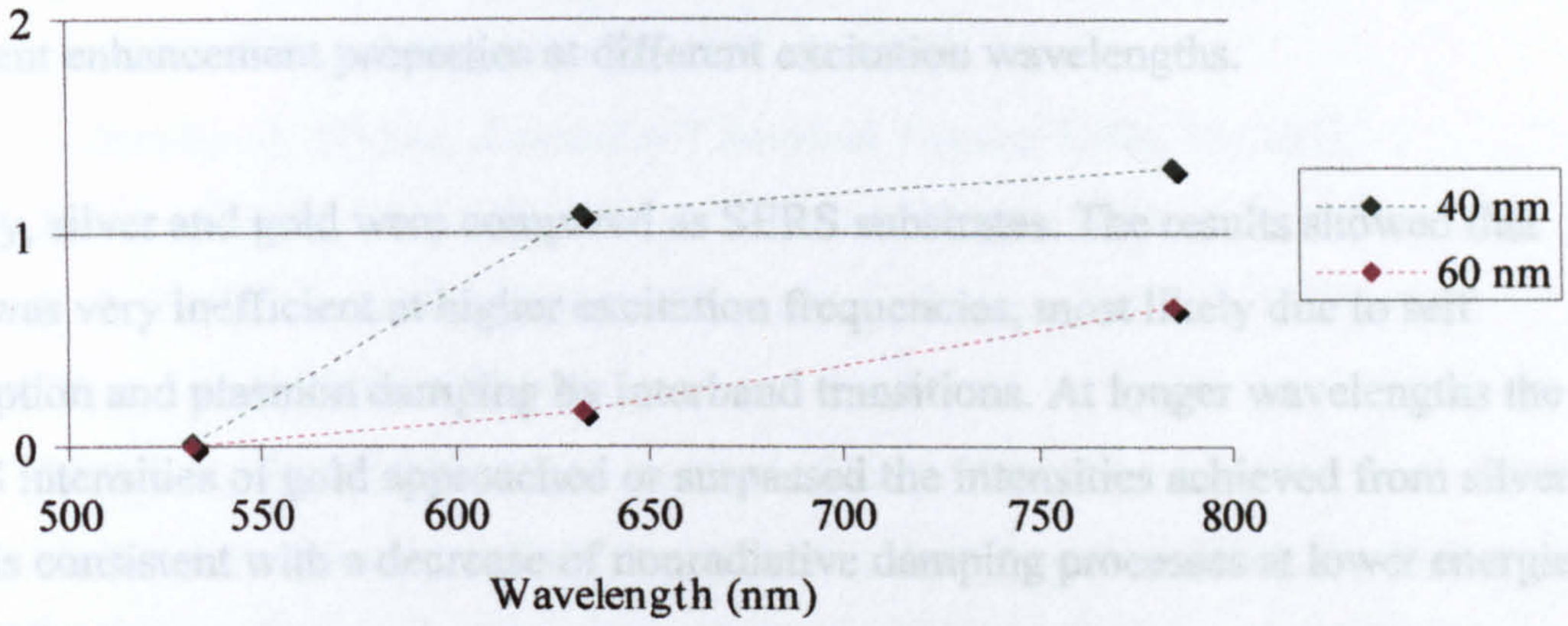

FIGURE 4.14. SERS intensity ratio between 40 nm and 60 nm gold and silver nanoparticle for 532, 633 and 785 nm excitation. The normalised SERS intensities from figures 4.12 and 4.13 for gold particles have been divided by the SERS intensities for the silver particles of the same size. Hence, a ratio over 1 means that the intensity acquired from gold particles is higher than the intensity acquired from silver particles at that wavelength and size of particle.

4.4 CONCLUSIONS

In this chapter the effect of aggregation condition on the SERS intensity has been investigated using sodium chloride as aggregating agent. We have shown that by varying the particle concentration and size it is possible to control the electronic response of gold and silver aggregates. The effect of increasing particle size on the extinction spectra is dramatic, indicating that the clusters formed are compact rather than fractal like, and that the interparticle distance is small.

The influence of the electronic response on the SERS intensity has been shown, and in particular self absorption of scattered light by the sample is concluded to have a major impact. Two different trends were identified at 633 nm and 785 nm excitation. At 633 nm, the trend was a decrease of SERS intensity with increasing extinction at the excitation wavelength. At 785 nm the trend was the opposite. This may suggest different type of clusters (such as fractal or compact) being resonant at the different

wavelengths with different properties, alternatively that the same type of cluster have different enhancement properties at different excitation wavelengths.

Finally, silver and gold were compared as SERS substrates. The results showed that gold was very inefficient at higher excitation frequencies, most likely due to self absorption and plasmon damping by interband transitions. At longer wavelengths the SERS intensities of gold approached or surpassed the intensities achieved from silver. This is consistent with a decrease of nonradiative damping processes at lower energies for gold.

[1] C. F. Bohren, D. R. Huffman, *Absorption and scattering of light by small particles*, Wiley-Interscience, New York, **1998**.

[2] J. Gersten, A. Nitzan, *Journal of Chemical Physics* **1980**, *73*, 3023.

[3] E. Hao, Schatz, G. C., *Journal of Chemical Physics* **2004**, *120*, 357.

[4] K. L. Kelly, E. Coronado, L. L. Zhao, G. C. Schatz, *Journal Of Physical Chemistry B* **2003**, *107*, 668.

[5] M. Moskovits, *103 Topics in Applied Physics* **2006**, 1.

[6] H. Xu, J. Aizpurua, M. Kall, P. Apell, *Physical Review E* **2000**, *62*, 4318.

[7] H. Xu, X. Wang, M. P. Persson, H. Q. Xu, M. Kall, P. Johansson, *Physical Review Letters* **2004**, *93*, in print.

[8] Y. Sun, Y. Xia, *Analyst* **2003**, *128*, 686.

[9] K. Faulds, R. P. Barbagallo, J. T. Keer, W. E. Smith, D. Graham, *Analyst* **2004**, *129*, 567.

[10] K. Faulds, R. E. Littleford, D. Graham, G. Dent, W. E. Smith, *Analytical Chemistry* **2004**, *76*, 592.

[11] C. G. Blatchford, J. R. Campbell, J. A. Creighton, *Surface Science* **1982**, *120*, 435.

[12] M. Sladkova, B. Vlckova, P. Mojzes, M. Slouf, C. Naudin, G. Le Bourdon, *Faraday Discussions* **2006**, *132*, 121.

[13] P. Nordlander, C. Oubre, E. Prodan, K. Li, I. Stockman, *Nano Letters* **2004**, *4*, 899.

[14] S. Y. Park, J. S. Lee, D. Georganopoulou, C. A. Mirkin, G. C. Schatz, *Journal Of Physical Chemistry B* **2006**, *110*, 12673.

[15] E. C. Le Ru, C. Galloway, P. G. Etchegoin, *Physical chemistry chemical physics* **2006**, *8*, 3083.

[16] J. J. Storhoff, A. A. Lazarides, R. C. Mucic, C. A. Mirkin, R. L. Letsinger, G. C. Schatz, *Journal Of The American Chemical Society* **2000**, *122*, 4640.

[17] J. Yguerabide, E. Yguerabide, *Analytical Biochemistry* **1998**, *262*, 157.

[18] J. Yguerabide, E. Yguerabide, *Analytical Biochemistry* **1998**, *262*, 137.

CHAPTER 5

DEPENDENCE ON NANOPARTICLE SIZE AND EXCITATION WAVELENGTH OF SURFACE ENHANCED RAMAN SCATTERING FROM NANOPARTICLE SOLUTIONS

Table of Contents

5.1 INTRODUCTION

Light can interact with metal particles small compared to the wavelength of the light through the excitation of a surface plasmon, a collective oscillation of the conduction electrons of the particle. This is accompanied by a large increase in light absorption, light scattering and local field enhancement[1-4]. This local field enhancement is the major surface enhancement contribution to single particle surface enhanced Raman scattering[5-9]. The strength of the optical coupling depends on the polarizability of the particle. This means that type of metal and size and shape of the particle will be crucial to its optical response[1, 4, 5, 7, 9, 10]. Bringing two such particles together, for example by aggregation as in the case of a nanoparticle solution, brings additional effects, such as confining the potential drop of the electromagnetic field outside the particle between two surfaces. This brings potentially huge signal enhancements of a Raman scatterer trapped between the two particles, making detection of extremely low concentrations of a targeted substance possible[11, 12].

In many techniques, such as surface enhanced Raman scattering, a slow decay of the particle plasmon is desired. In particular, damping through nonradiative processes, leading to the loss of a photon and heating of the sample, should be minimized[13]. The plasmon will decay due to a number of damping processes depending on particle size and shape. The plasmon damping can be due to either radiative or nonradiative processes. The nonradiative processes are due to interband or intraband absorption of the energy of the oscillating electron of the metal[1, 14, 15]. The radiative processes are accompanied by the creation of a photon, i.e. scattering. Damping via radiative processes is strongly correlated with size. At small sizes, electron scattering can occur from collisions with the particle surface, and at larger sizes because of retardation effects[13, 14, 16-20] The effects of plasmon damping can to some extent be traced in a broadening of the resonance peak of the nanoparticle[15, 21]. In addition, the direction of the plasmon oscillation and the localized electromagnetic field will affect the level of polarization of the Raman scattering molecule[5, 22].

There are a number of excellent publications dealing with the theoretical and numerical predictions of these processes. However, there are fewer experimental investigations of the implications of these parameters, in particular applied to metal nanoparticles in solution. In this manuscript, silver nanoparticles of different sizes as SERS substrates are investigated and correlated against their optical response. In investigation of single particle systems, an analyte with a chromophore resonant at the excitation frequencies used is chosen as a probe of the Raman enhancement in order to enable detection of the Raman spectra. It is found that there is a clear correlation between the enhancement of the Raman signal, and the relation between particle volume and excitation wavelength. This relation has been derived by Wokoun[20] to be V/λ^3, and this is in agreement with our findings. We also find that this correlation remains even as the nanoparticles are aggregated, using the non resonant molecule mercaptophenol as the analyte. We do not believe that this has been shown elsewhere. It is also concluded that it is possible to correlate the near field enhancement of the Raman signal in a single particle system, to the far field scattering efficiency derived from the technique described in chapter 3.

5.2 EXPERIMENTAL

The benzotriazole azo dye used (3,5-dimethoxy-4-(6'-azobenzotriazolyl)phenol) for the unaggregated samples was synthesized in house. It has previously been reported as a non aggregating SERRS dye[23, 24] (figure 5.1). All other chemicals used were acquired from Sigma-Aldrich.

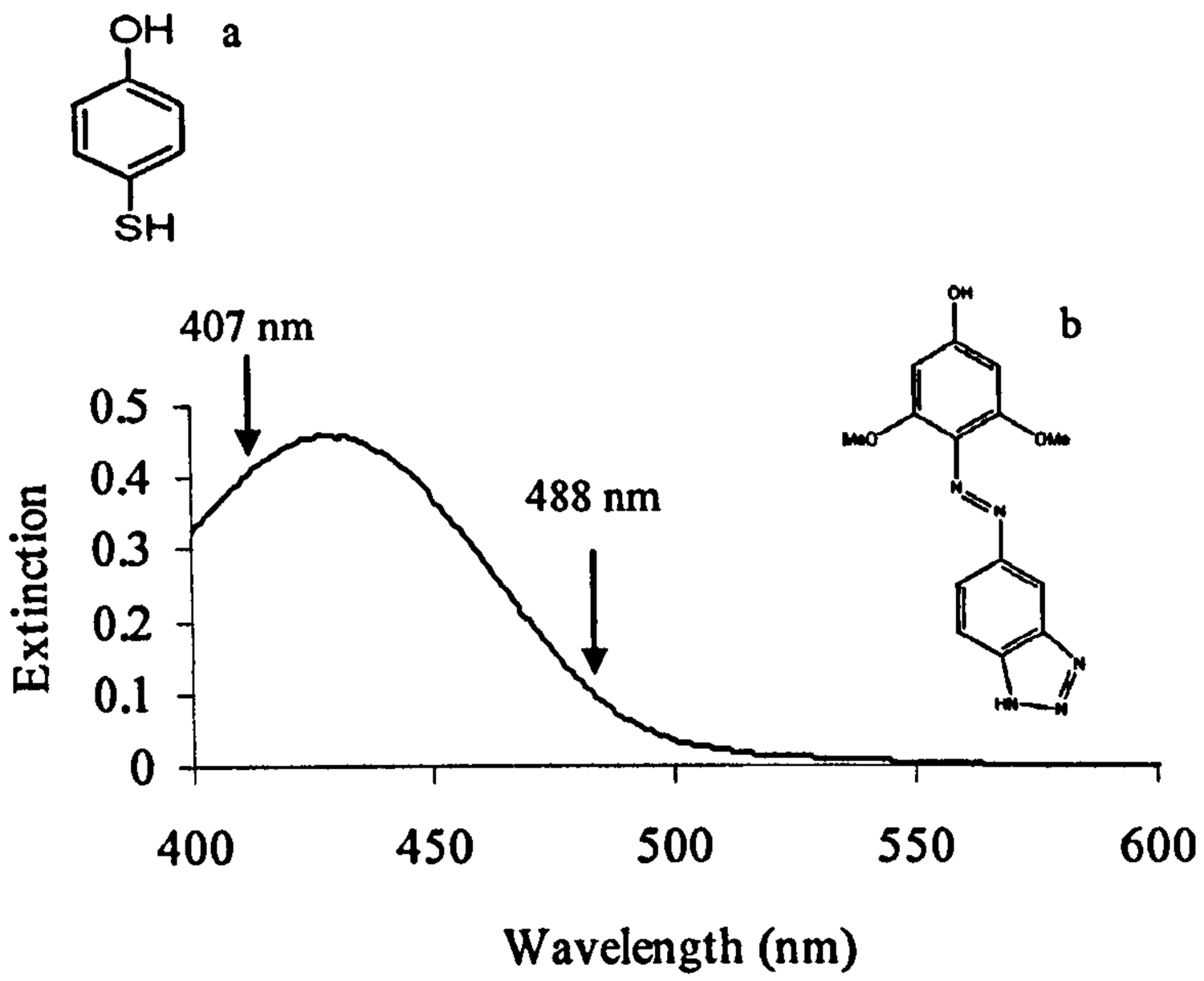

FIGURE 5.1. a) Molecular structure of mercaptophenol. It does not have any molecular resonance in the visible end of the spectra b) Electronic spectra and molecular structure of 3,5-dimethoxy-4-(6'-azobenzotriazolyl)phenol. The absorption profile of a dye may blue shift slightly in close vicinity to the excited particle surface plasmon[8]. There is however still enough molecular resonance contribution to enable detection of the SERRS spectra in these experiments.

A SpectraPro 300i Monochromator from Acton Research Corporation was used to acquire the data for the 407 nm laser line (Ar^+-ion laser) and the 488 nm laser line (He-Ne-ion laser) excitation sources (see chapter 2 for details). The scattered light was collected at 90° angle. The 633 nm and 785 nm data were collected using a Renishaw Ramascope system at 180° collection angle. All spectra were normalized against a cyclohexane standard. The nanoparticles used were synthesized according to a recently developed method, and thoroughly characterized using AFM, SEM and electronic spectra (see chapter 3).

Unaggregated samples were prepared by mixing nanoparticles (900 μL) and 10^{-6} mol/dm^3 of the benzotriazole azo dye solution (100 μL). Electronic spectra and dynamic light scattering data were taken before and after addition of dye solution to monitor any change in aggregation. For aggregated samples, the same procedure was carried out, only mercaptophenol was used instead of the azo dye. The reason for this is the poor

SERS-scattering from the azo dye outside its absorption band. 100 μL of 1 mol/dm^3 sodium chloride solution was added to the sample to cause it to aggregate completely. All spectra were collected as 3 or 5 accumulations of 5 seconds each, and all data points were averages of 5 replicates.

5.3 Results and Discussion

Five sizes of well characterized spherical silver nanoparticles of 36 (RSD = 22.1 %), 51 (RSD = 12.0 %), 63 (RSD = 11.2 %), 72 (RSD = 12.1 %) and 81 nm (RSD = 11.2 %) diameter were investigated for efficiency as SERS substrates. The particles were characterized with SEM (x-y dimensions) and AFM (x-y-z dimensions). At least 150 particles were measured for each fraction, except for the 36 nm size, where 75 particles were measured. None of the batches showed any rods and very few particles with sharp edges or pronounced surface features (see chapter 3 for details). In chapter 3 the optical response was probed for the 36 nm, the 63 nm and the 81 nm sizes. This data is reproduced here in figure 5.2 for convenience.

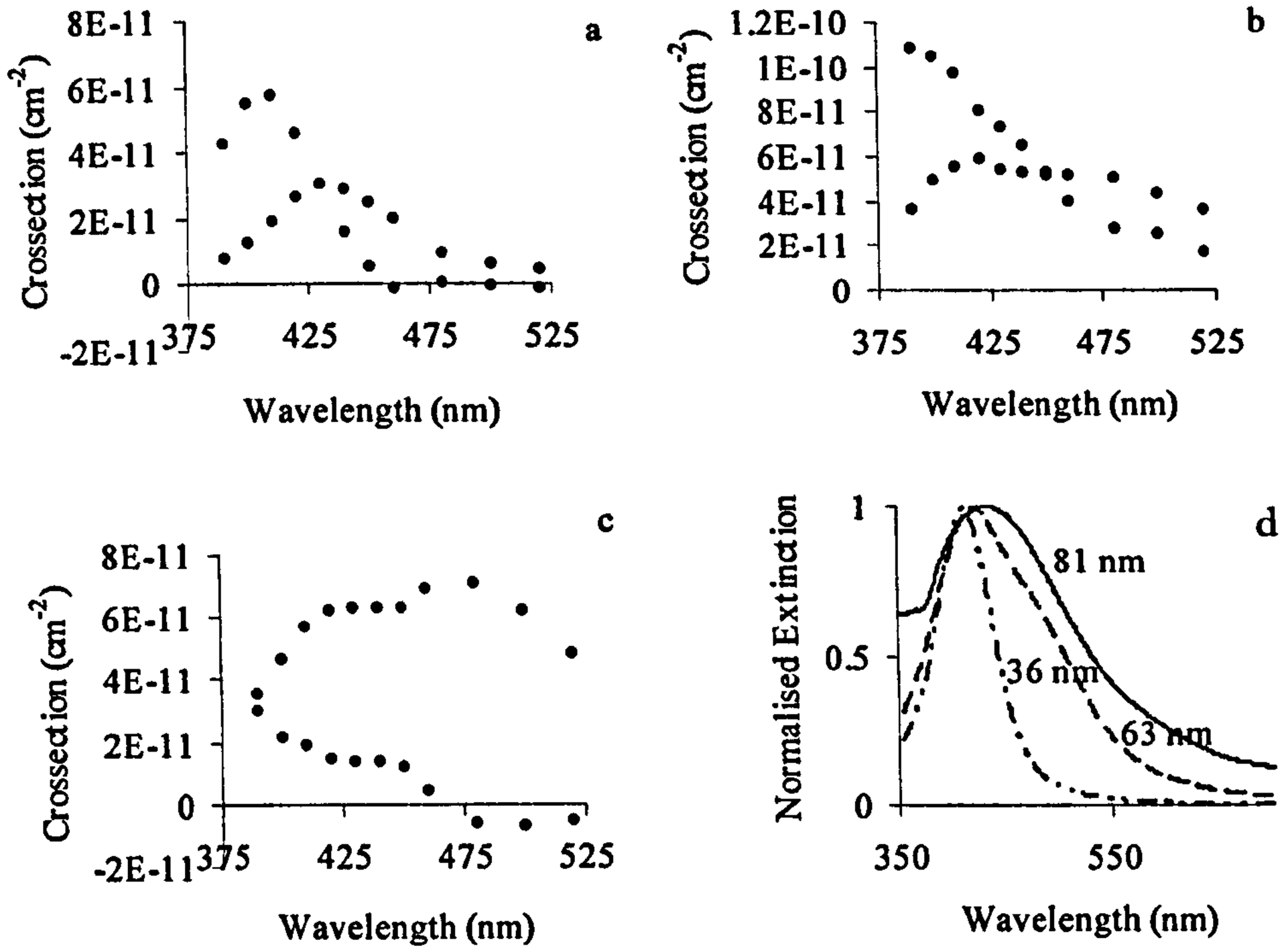

FIGURE 5.2. a) to c) shows scattering (blue) and absorption (red) cross sections for a) 36 nm, b) 63 nm and c) 81 nm silver particles. d) shows the extinction spectra of the nanoparticle solutions.

There are a number of noteworthy features in these spectra, that can be explained from the calculations made by Schatz et al.[22] and Sosa et al.[25] The scattering at the dipole position increases and is blue shifted with particle size. The indication of a splitting into two peaks is accompanied by a blue shift in the absorption profile. We ascribe this to the formation of higher order oscillations as the particle diameter approaches the wavelength of the excitation source. In all graphs, the absorption decreases rapidly towards 450 nm. This means that the nanoparticles will behave more like Drude-model free electron metals towards the red spectrum, where the dipole oscillation occurs, and be more dampened by absorption in the blue region, at the position of the quadrupole. The extinction spectra (the sum of scattering and absorption) are also broadened for larger particles. This is sometimes used to probe the damping of the plasmon oscillation[15, 17], but may not be a straight forward method for systems where there is a significant contribution of higher order oscillations.

To acquire SERS spectra from the unaggregated samples, a molecule with a resonance peak at 428 nm and strong affinity to the silver surface was used. There were two

reasons for this. Firstly, SERS from unaggregated particles without a resonance contribution from a molecular chromophore is very difficult to record, whereas surface enhanced resonance Raman from single particles has been recorded previously[26, 27]. This is possible because of the additional enhancement of surface enhanced resonance Raman scattering over SERS[28-30]. Secondly, the molecule used here has been reported not to aggregate nanoparticles in solution, even at high surface coverage[24].

For every sample, the nanoparticle concentration was optimized to achieve the strongest possible Raman signal. It was determined both experimentally and theoretically that all analyte molecules were allowed to attach directly onto the surface of the nanoparticles as first layer. Experimentally this was done by carrying out an isotherm. To do this the analyte is added to the nanoparticle solution, either until the increase in Raman intensity tails of when further added analyte is no longer able to attach as first layer, or increases rapidly, in the case where the dye aggregates the nanoparticle solution. Theoretically it was done by comparing available surface area for each added molecule to the surface area determined by Dougan et al[31] and Mirkin et al[32] for other thiol molecules binding to silver and gold nanoparticle surfaces. In figure 5.3 the SERS intensity data against nanoparticle diameter for 488 nm excitation frequency is plotted. From the scattering spectra it can be seen that this is close to the dipole resonance frequency for all but the 36 nm diameter nanoparticle. The results show a dramatic increase of SERS intensity with size up to 63 nm diameter, and a rapid decrease at larger sizes. This decrease indicates that the surface enhancement is reduced as a result of damping of the plasmon oscillation with size.

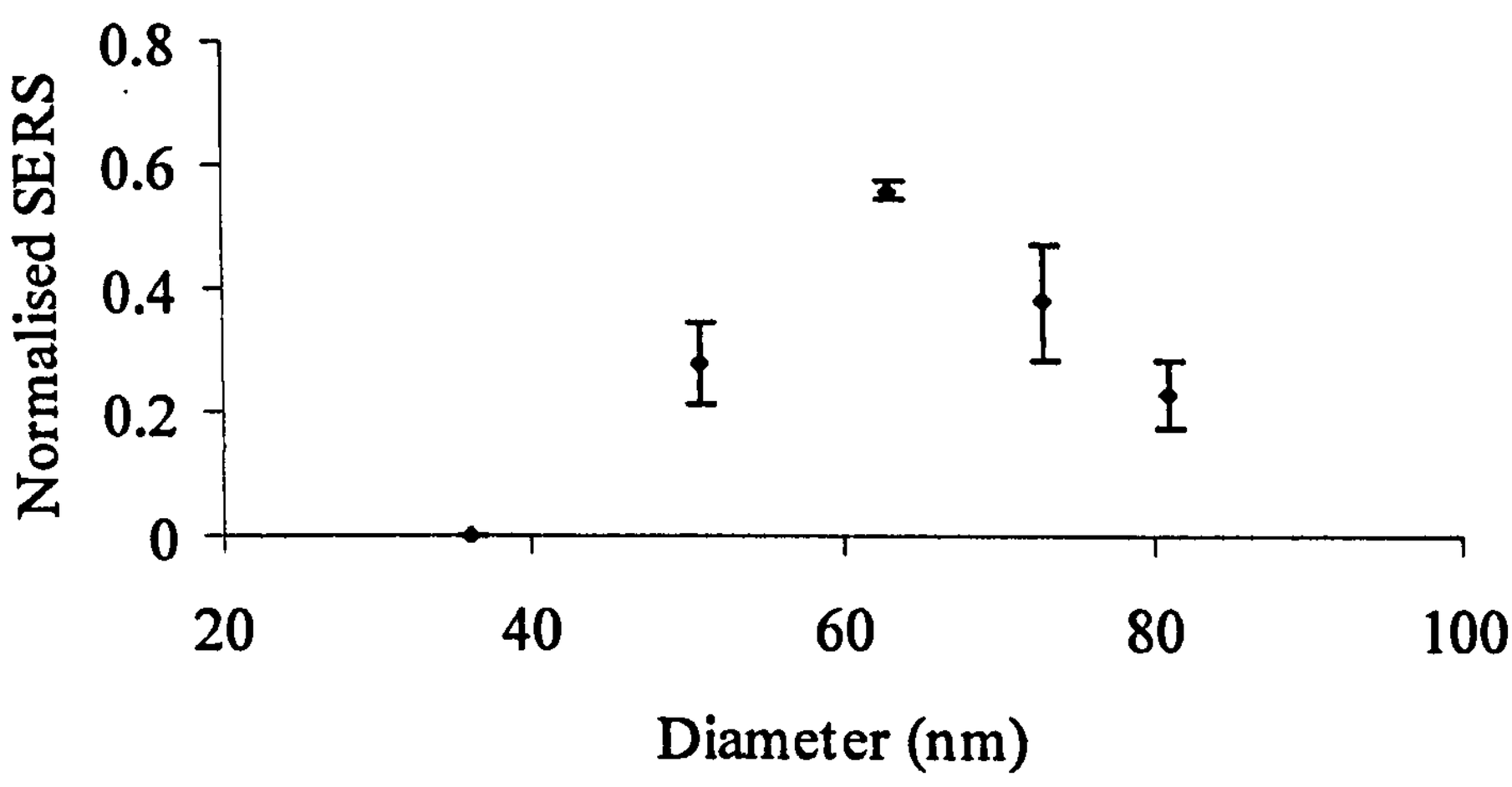

FIGURE 5.3. Normalised SERRS intensity of the 3,5-dimethoxy-4-(6'-azobenzotriazolyl)phenol adsorbed onto silver nanoparticle against size of nanopartice. The excitation wavelength is 488 nm and the spectra were taken as 3 accumulations of 5 seconds each. All points are averages of 5 replicates.

Figure 5.4 shows the attained normalized SERS intensity when exciting at 407 nm. For all but the 36 nm diameter nanoparticle, at this frequency, the plasmon should have a large quadropole contribution. The intensity profile against diameter is less sharp and the 51 nm, 63 nm and 72 nm data points are within the error bars of each other, so it is difficult to see any peak in the profile. This may be due to the mix of different order oscillations making up the plasmon being less efficient in polarising the Raman scatterer.

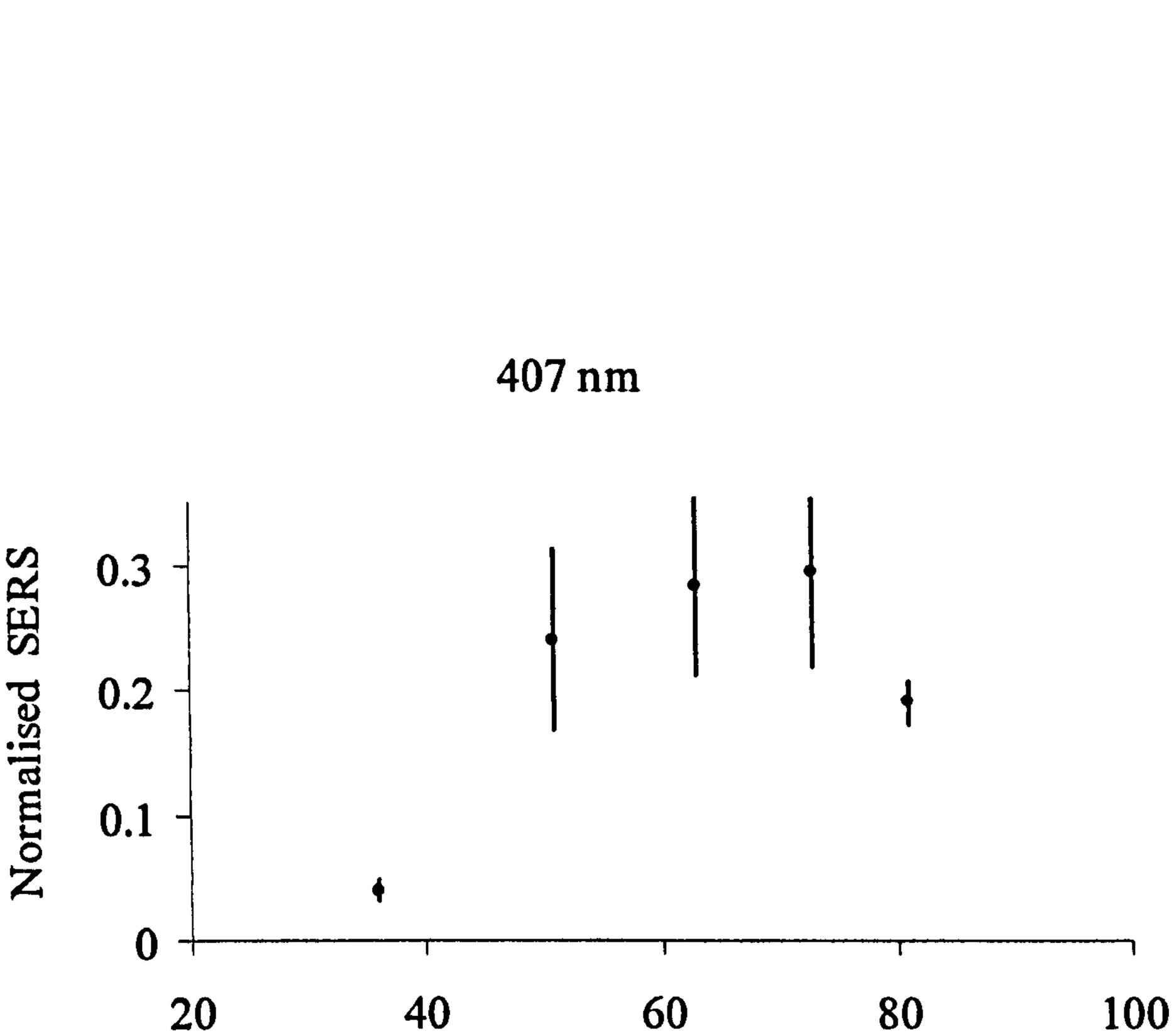

FIGURE 5.4. Normalised SERRS intensity of the 3,5-dimethoxy-4-(6'-azobenzotriazolyl)phenol adsorbed onto silver nanoparticle against size of nanopartice. The excitation wavelength is 407 nm and the spectra were taken as 3 accumulations of 5 seconds each. All points are averages of 5 replicates.

The 36 nm diameter particle data serves as a useful reference point in these measurements. The fact that no signal was attained at 488 nm (figure 5.3) for this size confirms that the results are not due to any aggregation, as this would show up for this data point also. It is also interesting to see that for all other points, the intensity increases from the 407 nm data point (figure 5.4) to the 488 nm point, even though the 407 nm excitation is closer to the peak resonance of the chromophore of the azo dye (figure 5.1.b.). This indicates that the dipole oscillation is the more efficient process in polarizing the Raman scatterer.

In figure 5.5 the SERRS intensities for the 36 nm, 63 nm and 81 nm particles in figure 5.3 and 5.4 are plotted against the scattering efficiencies, $Q=C_{sca}/\pi r^2$ derived from figure 5.2. This means that the scattering cross section is normalised against the geometrical cross sectional area of the particle, taking into account the strength of the plasma oscillation. In the case of a purely dipolar oscillation, the far field scattering efficiency should be close to proportional to the near-field scattering efficiency[21]. It appears from

this that for the 488 nm excitation data, there is a direct correlation between the scattering efficiency of the nanoparticle and its suitability as SERS substrate. For the 407 nm excitation however, the 36 nm particle data goes completely opposite to the expected. This could partially be explained by the 407 nm data being a mix between different orders of oscillations, bringing other factors, such as the direction of the electromagnetic field, in to play. Of the six data points, the 36 nm particle at 407 nm excitation is the only outlier.

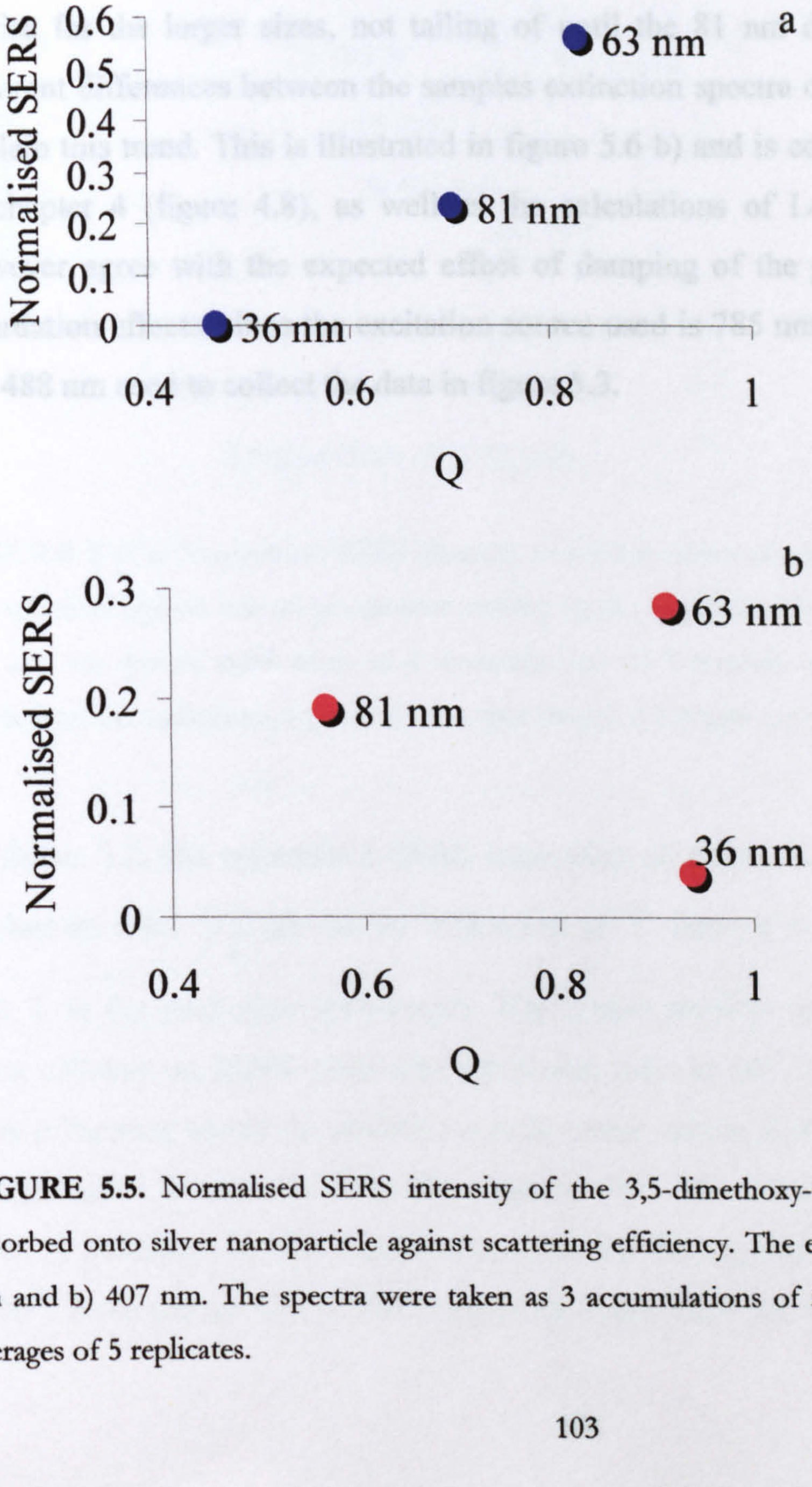

FIGURE 5.5. Normalised SERS intensity of the 3,5-dimethoxy-4-(6'-azobenzotriazolyl)phenol adsorbed onto silver nanoparticle against scattering efficiency. The excitation wavelength is a) 488 nm and b) 407 nm. The spectra were taken as 3 accumulations of 5 seconds each. All points are averages of 5 replicates.

To record data for aggregated samples mercaptophenol was used as reporter because it binds strongly to the surface and lowers the surface charge, thus ensuring complete aggregation, and is an efficient Raman scatterer. To ensure that the samples were completely aggregated, sodium chloride (100 μL, 1 M) was added. When the solution is aggregated, it is important to bear in mind that it becomes crucial to control the aggregation conditions to achieve optimal conditions for SERS. The data is shown in figure 5.6 a). Although the general trend remains, with the larger size nanoparticles providing the best SERS substrate, the intensity no longer peaks at 63 nm, but continues to rise for the larger sizes, not tailing of until the 81 nm diameter nanoparticle. No apparent differences between the samples extinction spectra could be found that would explain this trend. This is illustrated in figure 5.6 b) and is consistent with the findings in chapter 4 (figure 4.8), as well as the calculations of Le Ru[33]. The data would however agree with the expected effect of damping of the plasmon with size due to retardation effects, since the excitation source used is 785 nm, significantly longer than the 488 nm used to collect the data in figure 5.3.

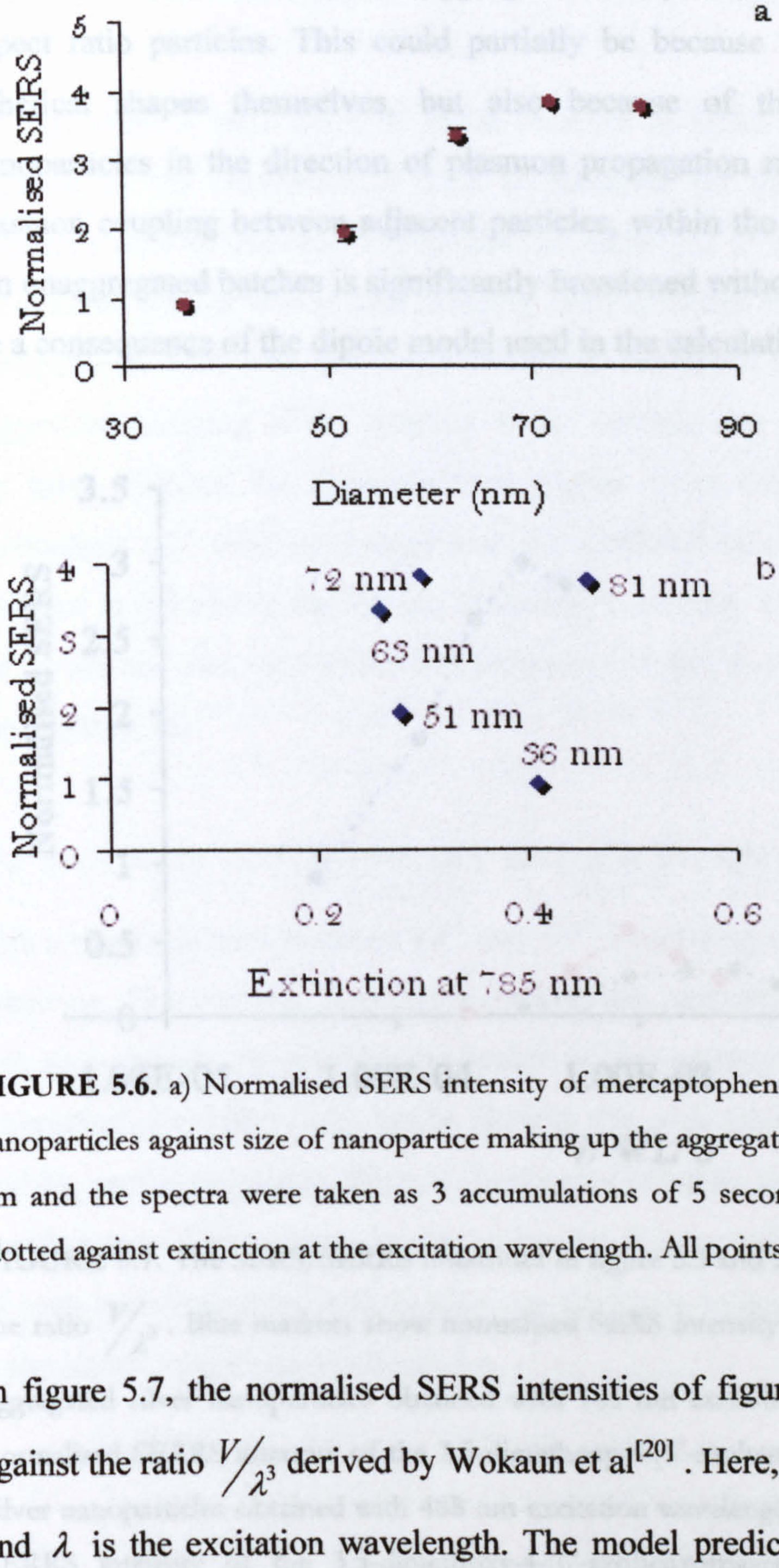

FIGURE 5.6. a) Normalised SERS intensity of mercaptophenol adsorbed onto aggregated silver nanoparticles against size of nanopartice making up the aggregate. The excitation wavelength is 785 nm and the spectra were taken as 3 accumulations of 5 seconds each. b) The SERS data in a) plotted against extinction at the excitation wavelength. All points are averages of 5 replicates.

In figure 5.7, the normalised SERS intensities of figure 5.2, 5.3 and 5.5 are plotted against the ratio V/λ^3 derived by Wokaun et al[20] . Here, V is the volume of the particle, and λ is the excitation wavelength. The model predicts spherical particles to be the most efficient as SERS substrates when this ratio is 10^{-3}. For elongated particles the peak efficiency would be shifted towards lower values. It is seen that for the 488 nm unaggregated batches the intensity peaks at 10^{-3}. This hence is in close agreement to what is predicted by the model. The data for the aggregated samples peaks around $5x10^{-4}$. Even though this is still close to the value expected for a spherical particle, it is

not unrealistic to assume that aggregated nanoparticles will behave more like high aspect ratio particles. This could partially be because the cluster may take on non spherical shapes themselves, but also because of the dipole-dipole coupling of nanoparticles in the direction of plasmon propagation rather than retardation induced plasmon coupling between adjacent particles, within the cluster[34]. The data from 407 nm unaggregated batches is significantly broadened without any distinct peak. This may be a consequence of the dipole model used in the calculation becoming invalid.

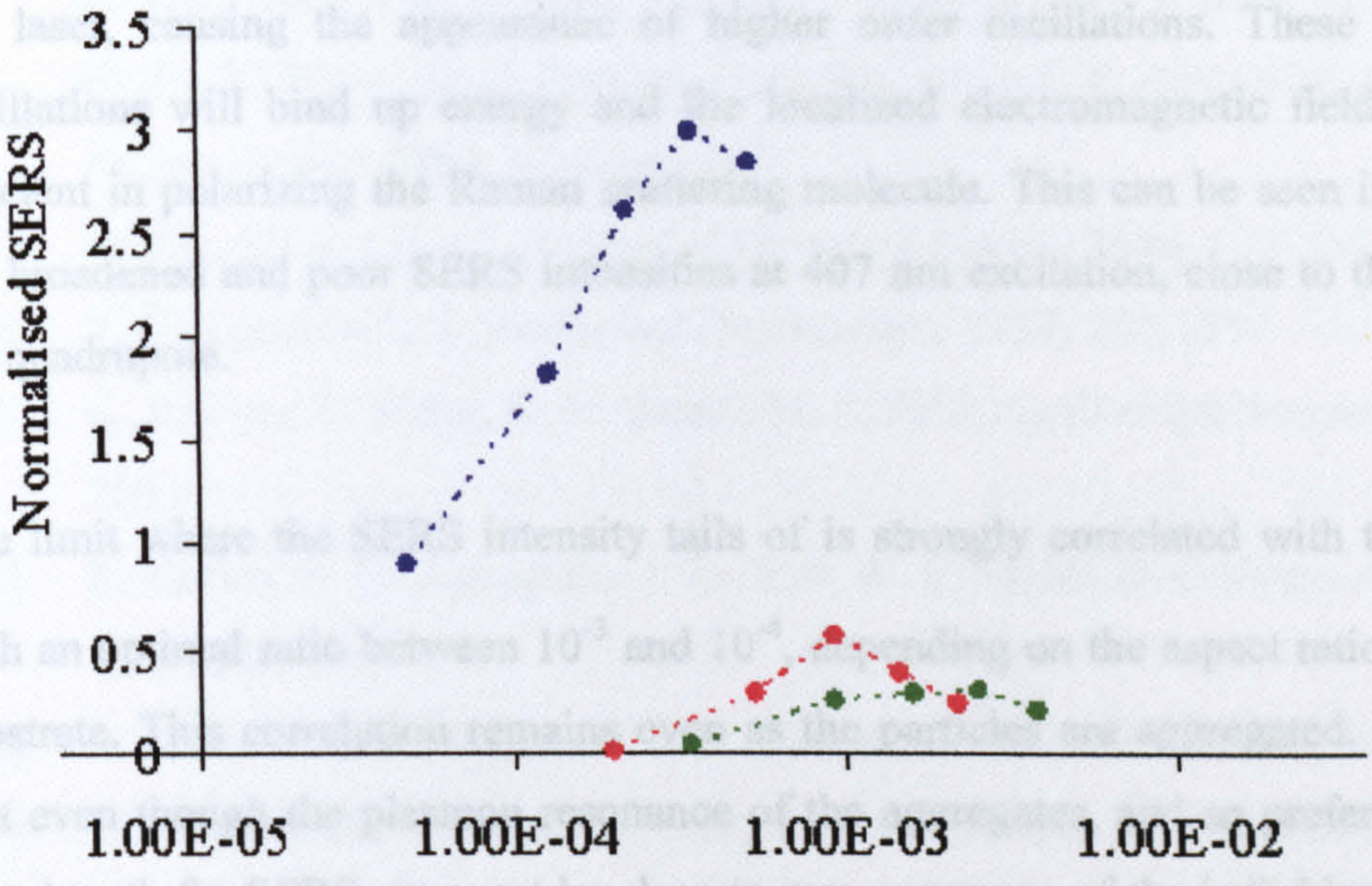

FIGURE 5.7. The SERS/SERRS intensities in figure 5.3 and 5.4 and 5.6 has been plotted against the ratio V/λ^3. Blue markers show normalised SERS intensity of mercaptophenol adsorbed onto aggregated silver nanoparticles obtained with 785 nm excitation wavelength. Red markers show normalised SERRS intensity of the 3,5-dimethoxy-4-(6'-azobenzotriazolyl)phenol on unaggregated silver nanoparticles obtained with 488 nm excitation wavelength. Green markers show normalised SERRS intensity of the 3,5-dimethoxy-4-(6'-azobenzotriazolyl)phenol on unaggregated silver nanoparticles obtained with 407 nm excitation wavelength. All spectra were taken as 3 accumulations of 5 seconds each. All points are averages of 5 replicates.

5.4 CONCLUSIONS

All data show a clear trend of initial increase in SERS enhancement with increasing diameter of the nanoparticles used as substrate for the surface enhancement. This correlates with an increase in polarization leading to an increase in optical response of the nanoparticle, as well as less damping from electrons colliding with the surface of the nanoparticle. However, for larger diameters, the SERS intensity tails off or decreases, suggesting damping of the plasmon as the particle size approaches the wavelength of the laser, causing the appearance of higher order oscillations. These higher order oscillations will bind up energy and the localized electromagnetic field will be less efficient in polarizing the Raman scattering molecule. This can be seen in figure 4, as the broadened and poor SERS intensities at 407 nm excitation, close to the position of the quadrupole.

The limit where the SERS intensity tails of is strongly correlated with the ratio V/λ^3, with an optimal ratio between 10^{-3} and 10^{-4}, depending on the aspect ratio of the SERS substrate. This correlation remains even as the particles are aggregated. This suggests that even though the plasmon resonance of the aggregates, and so preferred excitation wavelength for SERS, may not be close to any resonance of the individual nanoparticle making up the aggregate, the ratio between excitation wavelength and particle diameter is still a crucial parameter to achieve the strongest possible SERS signal. Some features of each individual nanoparticle plasmon are hence preserved upon aggregation, and has a significant impact on its properties.

[1] C. F. Bohren, D. R. Huffman, *Absorption and scattering of light by small particles*, Wiley-Interscience, New York, **1998**.

[2] J. Yguerabide, E. Yguerabide, *Analytical Biochemistry* **1998**, *262*, 137.

[3] J. Yguerabide, E. Yguerabide, *Analytical Biochemistry* **1998**, *262*, 157.

[4] C. Sonnichsen, B. M. Reinhard, J. Liphardt, A. P. Alivisatos, *Nature Biotechnology* **2005**, *23*, 741.

[5] M. Moskovits, *103 Topics in Applied Physics* **2006**, 1.

[6] J. Gersten, A. Nitzan, *Journal Of Chemical Physics* **1980**, *73*, 3023.

[7] H. Xu, J. Aizpurua, M. Kall, P. Apell, *Physical Review E* **2000**, *62*, 4318.

[8] H. Xu, X. Wang, M. P. Persson, H. Q. Xu, M. Kall, P. Johansson, *Physical Review. Letters* **2004**, *93*, in print.

[9] E. Hao, Schatz, G. C., *Journal of Chemical Physics* **2004**, *120*, 357.

[10] Y. E. Yguerabide J., *Analytical Biochemistry* **1998**, *262*, 157.

[11] K. Kneipp, Y. Wang, R. R. Dasari, M. S. Feld, *Applied Spectroscopy* **1995**, *49*, 780.

[12] K. Faulds, R. P. Barbagallo, J. T. Keer, W. E. Smith, D. Graham, *Analyst* **2004**, *129*, 567.

[13] S. Link, M. A. El-Sayed, *Journal of physical Chemistry B* **1999**, *103*, 8410.

[14] C. Sönnichsen, T. Franzl, T. Wilk, G. von Plessen, J. Feldmann, *Physical review letters* **2002**, *88*, 077402.

[15] C. Sönnichsen, S. Geier, N. E. T. Hecker, G. von Plessen, J. Feldmann, H. Ditlbacher, B. Lamprecht, J. R. Krenn, F. R. Aussenegg, V. Z.-H. Chan, J. P. Spatz, M. Möller, *Applied Physics Letters* **2000**, *77*, 2949.

[16] F. Stietz, J. Bosbach, T. Wenzel, T. Vartanyan, A. Goldmann, F. Träger, *Physical Review Letters* **2000**, *84*, 5644.

[17] S. E. Kooij, B. Poelsema, *Physical chemistry chemical physics* **2006**, *8*, 3349.

[18] Y.-H. Liau, A. N. Unterreiner, Q. Chang, N. F. Scherer, *Journal of physical Chemistry B* **2001**, *105*, 2135.

[19] M. Perner, P. Bost, U. Lemmer, G. von Plessen, J. Feldman, U. Becker, M. Mennig, M. Schmitt, H. Schmidt, *Physical Review Letters* **1997**, *78*, 2192.

[20] A. G. Wokaun, J.P.; Liao, *Physical Review Letters* **1982**, *48*, 957.

[21] T. Klar, M. Perner, S. Grosse, G. von Plessen, W. Spirkl, J. Feldman, *Physical Review Letters* **1998**, *80*, 4249.

[22] K. L. Kelly, E. Coronado, L. L. Zhao, G. C. Schatz, *Journal Of Physical Chemistry B* **2003**, *107*, 668.

[23] R. Brown, Smith, E.W., Graham, D., *Tetrahedron Letters* **2002**, *44*, 1339.

[24] K. Faulds, R. E. Littleford, D. Graham, G. Dent, W. E. Smith, *Analytical Chemistry* **2004**, *76*, 592.

[25] I. O. Sosa, C. Noguez, R. G. Barrera, *Journal Of Physical Chemistry B* **2003**, *107*, 6269.

[26] I. Khan, D. Cunningham, R. E. Littleford, D. Graham, W. E. Smith, D. W. McComb, *Analytical Chemistry* **2006**, *78*, 224.

[27] I. Khan, E. Polwart, D. W. McComb, W. E. Smith, *Analyst* **2004**, *129*, 950.

[28] A. M. Stacy, R. P. Van Duyne, *Chemical Physics Letter* **1983**, *102*, 365.

[29] P. Hildebrandt, M. Stockburger, *Journal Of Physical Chemistry* **1984**, *88*, 5935.

[30] S. Habuchi, M. Cotlet, R. Gronheid, G. Dirix, J. Michiels, J. Vanderleyden, F. C. De Schryver, J. Hofkens, *Journal of the American Chemical Society* **2003**, *125(28)*, 8446.

[31] J. A. Dougan, C. Karlsson, W. E. Smith, D. Graham, *Nucleic Acids Research* **2007**, *35*, 3668.

[32] E.-Y. Kim, J. Stanton, R. A. Vega, K. J. Kunstman, C. A. Mirkin, S. M. Wolinsky, *Nucleic Acids Research* **2006**, *34*, e54.

[33] E. C. Le Ru, C. Galloway, P. G. Etchegoin, *Physical chemistry chemical physics* **2006**, *8*, 3083.

[34] J. P. Kottman, J. F. O. Martin, *Optics Letters* **2001**, *26*, 1096.

CHAPTER 6

THE WAVELENGTH DEPENDENCE OF THE INTENSITY OF SURFACE ENHANCED RAMAN SCATTERING AND SURFACE ENHANCED RESONANCE RAMAN SCATTERING

TABLE OF CONTENTS

*In collaboration with Dale Cunningham

6.1 INTRODUCTION

Surface enhanced Raman scattering (SERS) and surface enhanced resonance Raman scattering (SERRS) can provide molecularly specific information on a molecule at low concentrations on a suitable surface[1-3]. Single molecule detection and characterisation have been reported[4, 5]. These studies demonstrate that SERS/SERRS is suitable for use as a sensitive and informative detection technique in the development of novel analytical methodologies[6-8]. However, the design of new and effective methods requires an understanding of many factors and a key one is the choice of excitation wavelength which can have a very significant effect on the magnitude of the enhancement. Wavelength dependence is characterised in this paper for visible excitation using selected analytes with different properties and citrate nanoparticle as substrate. It is expected that, although the actual magnitude of the enhancements may vary, the general conclusions will be applicable to most commonly used substrates.

For SERS to occur, the analyte has to be in the close vicinity of a nanoscale roughened surface[9, 10]. Most common substrates are developed from silver or gold since the surfaces of these metals can be modified to give a good combination of plasmonic properties[11, 12] and chemical stability[13-15]. For efficient enhancement the excitation wavelength chosen to give Raman scattering should be close to that of the surface plasmon resonance frequency of the substrate and the molecule should be in direct contact with the surface[16]. SERRS has the additional requirement that the analyte must contain a chromophore and the excitation wavelength should be reasonably close in frequency to both the plasmon resonance and molecular resonance frequencies. Under these conditions SERRS has an additional enhancement over SERS through a contribution from molecular resonance[17, 18]. For analytes which give effective SERRS, very high scattering cross sections have been reported[19, 20]. This additional sensitivity reduces the possibility of interference from other species present in the assay since most will not have the correct combination of molecular and surface enhancement required for the chosen excitation frequency. Combined with the sharp peaks in the molecularly specific spectrum and the fluorescence quenching which occurs on the surface, this provides SERRS with a huge potential for sensitive *in situ* detection of multiple

analytes[21]. In practice this combination is not always easy to obtain and this study is designed to characterise the relative importance of the molecular and plasmonic enhancements in one commonly used approach. The advantage of this is that it will help to inform the choice of different parameters such as dye absorbance frequency, plasmon resonance frequency, particle size and aggregation state for any chosen excitation wavelength and so simplify the planning of new SERRS detection methods. Silver nanoparticles has proved to be effective in the development of quantitative assays and was chosen as the substrate[22, 23].

This chapter is made up by two separate experiments using similar techniques. They are kept as separate sections because, even though they are similar, there are some differences in experimental details and they are complementary to each other. In the first section, we show that the rate and concentration that the additions of analyte to the nanoparticle suspension is made at, is critical in order to avoid local aggregation. The effect of local aggregation is seen as a significant effect. The molecular chromophore enhancement effect in a SERS/SERRS system using gold and silver nanoparticle suspensions is demonstrated in the first and second section. This is done by comparing the Raman scattering from a nonresonant analyte adsorbed onto the metal surface, mercaptophenol, to analytes with chrompohores in the blue and in the red end of the spectra. The effect is shown for both aggregated and unaggregated suspensions. An important finding is the dramatic increase gained from molecular resonance in Raman scattering intensity when exciting close to the resonance frequency of single nanoparticles for unaggregated nanoparticle suspensions.

6.2 SERS/SERRS FROM UNAGGREGATED NANOPARTICLE SUSPENSION

6.2.1 EXPERIMENTAL

Silver nitrate and trisodium citrate were obtained from Sigma-Aldrich. 4.5 mL disposable cuvetes used in the UV-Vis and particle sizing experiments where obtained from VWR International. Victoria Blue was obtained from Sigma Aldrich, as was

Mitoxantrone. The dye 3,5-dimethoxy-4-6(6'-azobenzotriazolyl)phenylamine (ABT-DMOPA) was synthesized in-house and has previously been reported to be suitable as a SERRS- analyte on silver nanoparticles[22]. All these dyes will cause the nanoparticles to aggregate once adsorbed on the surface in sufficient numbers.

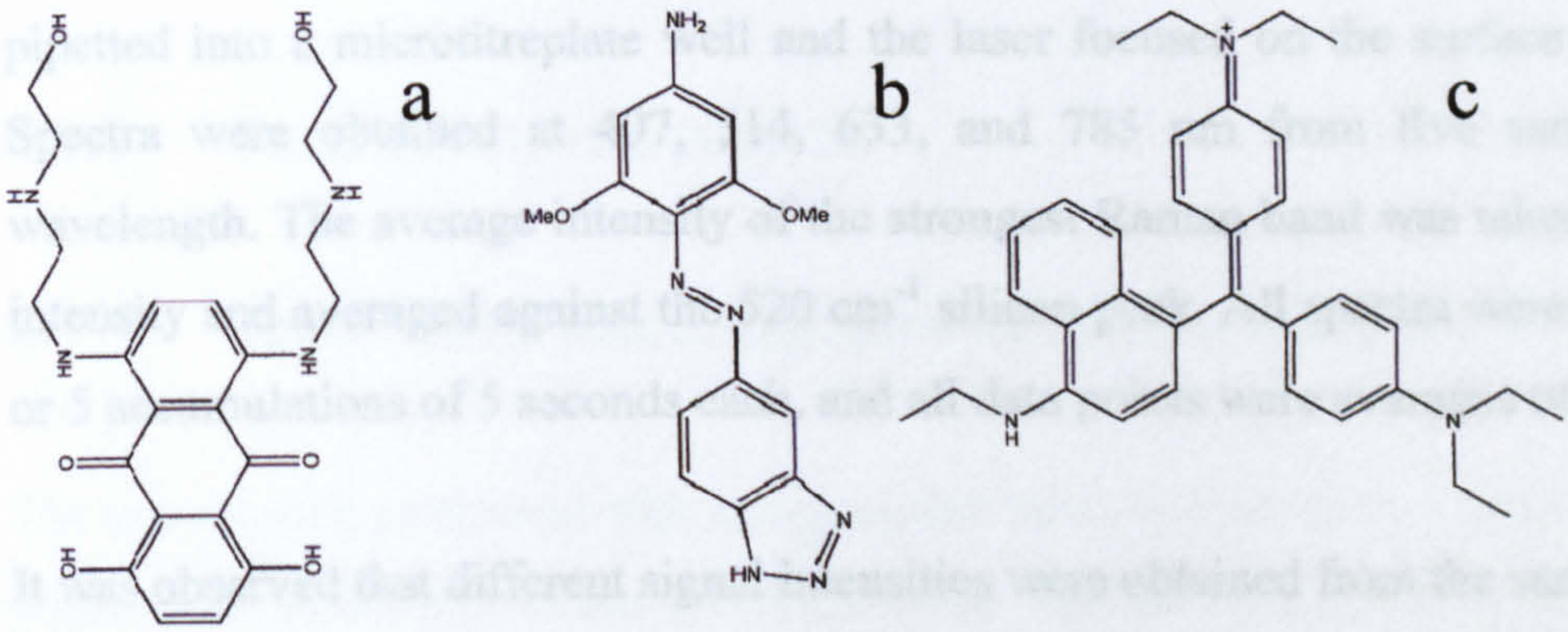

FIGURE 6.1. Molecular structure of a) Mitoxantrone b) ABT-DMOPA and c) Victoria Blue.

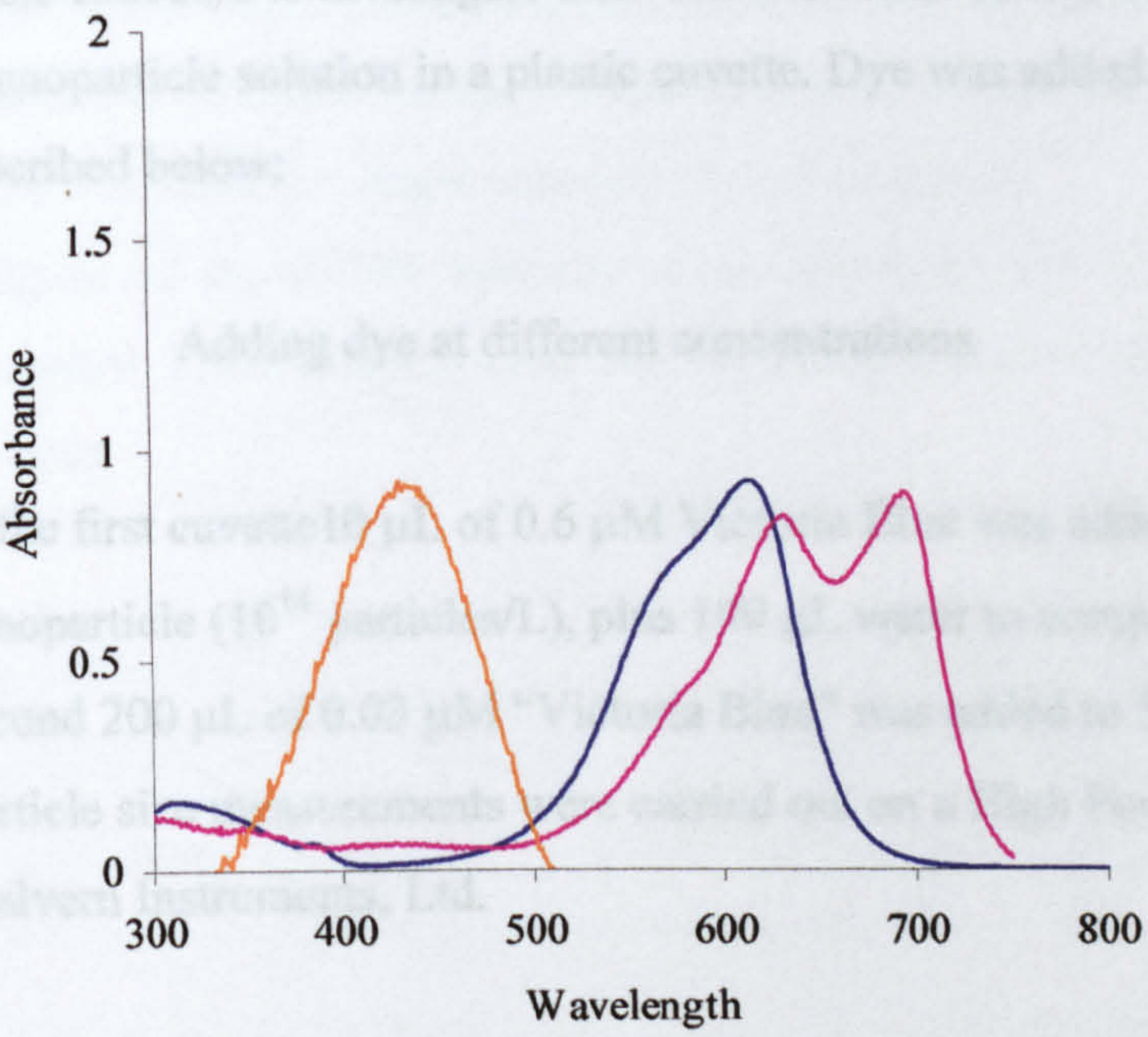

FIGURE 6.2. Electronic spectra of the molecules used in the experiments.

Silver nanoparticles were synthesized according to Lee and Meisel[14] . The exact protocol is given in chapter 3.2.4.

a) SERS/SERRS from unaggregated nanoparticle suspensions

100 μL of 10^{-6} M dye was added to 1000 μL of nanoparticles (10^{14} particles/L), resulting in a final concentration of 10^{-7} M at which the nanoparticles are considered to be largely unaggregated. This was confirmed by electronic spectra. The sample was pipetted into a microtitreplate well and the laser focused on the surface of the liquid. Spectra were obtained at 407, 514, 633, and 785 nm from five samples at each wavelength. The average intensity of the strongest Raman band was taken as the signal intensity and averaged against the 520 cm^{-1} silicon peak. All spectra were collected as 3 or 5 accumulations of 5 seconds each, and all data points were averages of 5 replicates.

It was observed that different signal intensities were obtained from the same final concentrations of dye in a nanoparticle solution, depending on at which rate and what concentration the dye was added. This was seen as an indication of local aggregation upon addition of analyte to nanoparticle solution. Therefore a number of experiments where executed to investigate this. The excitation source was a 514 nm laser focused in a nanoparticle solution in a plastic cuvette. Dye was added under constant stirring as described below;

b) Adding dye at different concentrations

In the first cuvette10 μL of 0.6 μM Victoria Blue was added to a solution of 1000 μL nanoparticle (10^{14} particles/L), plus 190 μL water to compensate for dilution. In the second 200 μL of 0.03 μM "Victoria Blue" was added to 1000 μL nanoparticle solution. Particle size measurements were carried out on a High Performance Particle Sizer from Malvern Instruments, Ltd.

c) Further adding of dye to already dye coated nanoparticles

In the first cuvette 15 μL of 10 μM ABT-DMOPA was added to a solution of 1000 μl nanoparticle (10^{14} particles/L), plus 45 μL water to compensate for dilution. In the second 50 μL of 0.5 μM ABT-DMOPA was added to 1000 μL nanoparticle solution in

a first step. After a minute another 15 μL of 10 μM ABT-DMOPA was added. The intensity and Raman bands of the spectra where compared. Particle size measurements were carried out on a High Performance Particle Sizer from Malvern Instruments, Ltd and Zeta potential measurements were taken on a Malvern Zetasizer 2000.

6.2.2 RESULTS AND DISCUSSION

a) SERS/SERRS from unaggregated nanoparticle solutions

The experiments performed with unaggregated nanoparticles show a good correlation between the absorbance of the dye used and the SERRS-intensity. This would imply that when no or very few clusters are formed, the molecular resonance part of SERRS is dominating. The fact that Mitoxantrone gives virtually no detectable signal at 407 nm, which is close to the single nanoparticle absorbance frequency (410 nm), further suggests that single particle enhancement in itself in this system is very poor indeed. It should also be noted that there could be dimers present. Removing these could possibly further decrease the single nanoparticle enhancement.

In figure 6.2 the SERRS intensity of the dyes compared to their respective absorbance is illustrated. There is a very clear correlation between both intensity and shape between the both.

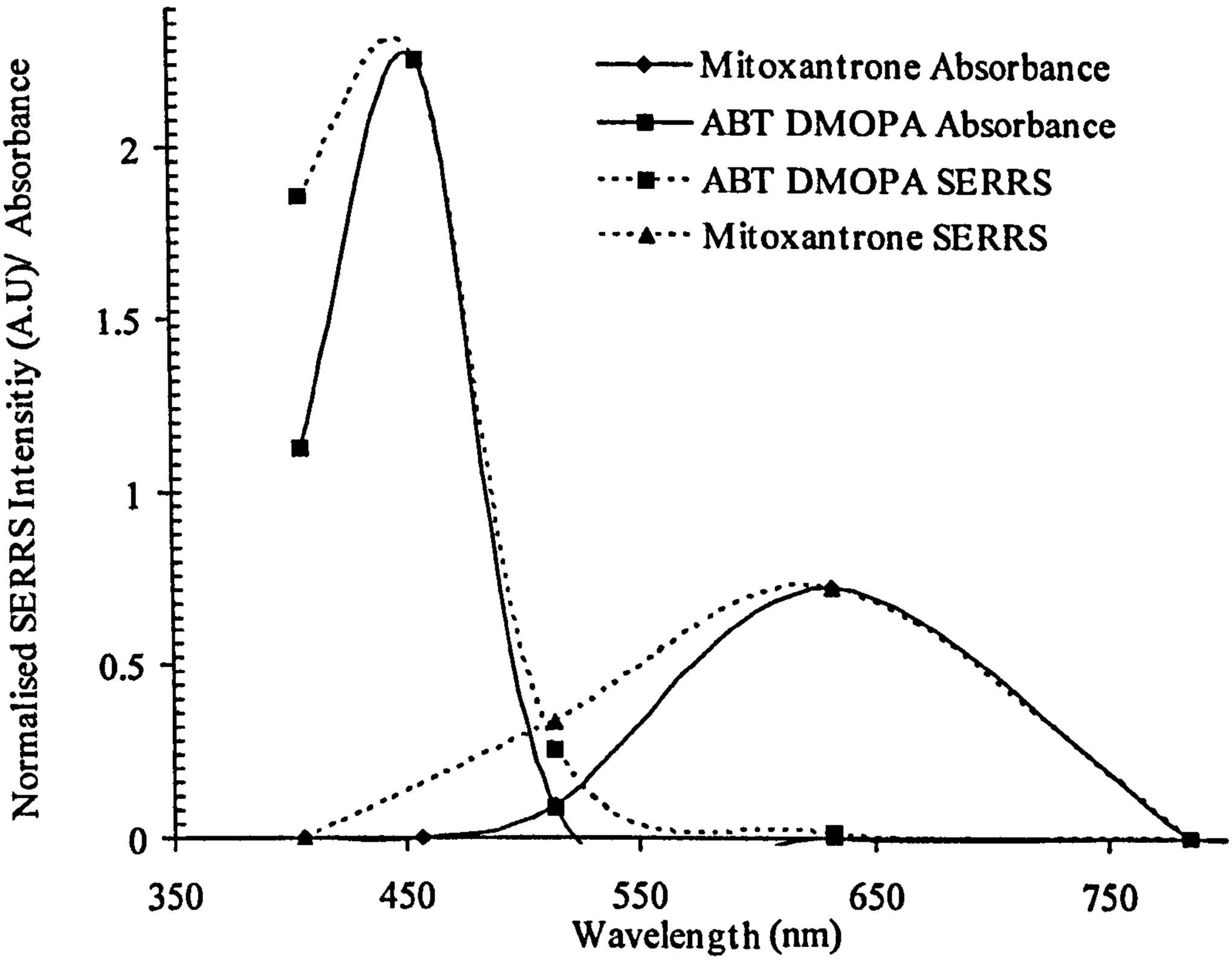

FIGURE 6.2. Comparison of SERRS from ABT-DMOPA and Mitoxantrone for unaggregated nanoparticles. Also included, relation between SERRS and absorption. The SERRS intensity has been normalised to coincide with the absorption maximum of the corresponding dye.

b) Adding dye at different concentrations

The experiment shows that it is crucial at what concentration the dye is added to the nanoparticle solution. The difference in SERRS intensity between the spectra in figure 6.3 clearly shows that even though both the solutions have the same final concentration and are considered unaggregated (both having Z-average well under -30mV, which means surface charges are strong enough for nanoparticles to repel each other), the enhancement attained from the different solutions can be of completely different order.

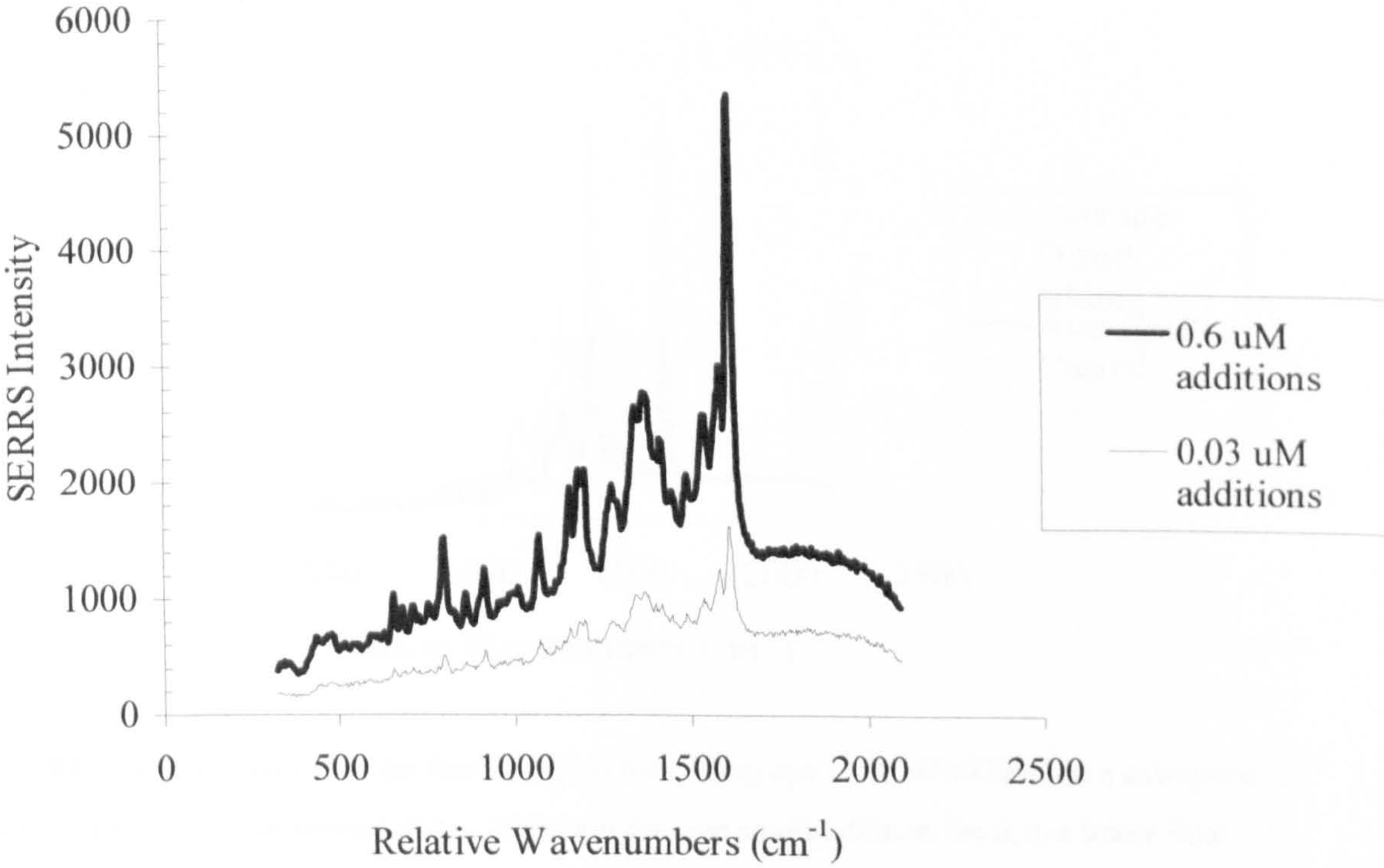

FIGURE 6.3. Comparison of the Raman signal for different methods of adding dye. The blue spectrum shows the Raman spectrum when adding a high concentration solution. The red spectrum show the spectrum acquired when adding the dye in a lower concentration. The final concentrations are the same.

c) Further adding of dye to already dye coated nanoparticles

The experiment seems to show that a layer of adsorbed molecules on the nanoparticles will in some way decrease the effect of an addition of dye to a nanoparticle solution. This could be an effect of less surface area available for the second addition of dye to attach to, leading to a more even distribution of the dye, and thus fewer aggregates. Once again Zeta-potential measurements as well as HPP size measurements and electronic spectra show that the nanoparticles are mainly unaggregated and the surface plasmon is unshifted. The spectra are averages of 5 separate experiments as the effect is not a stable one, and will also depend on concentrations used.

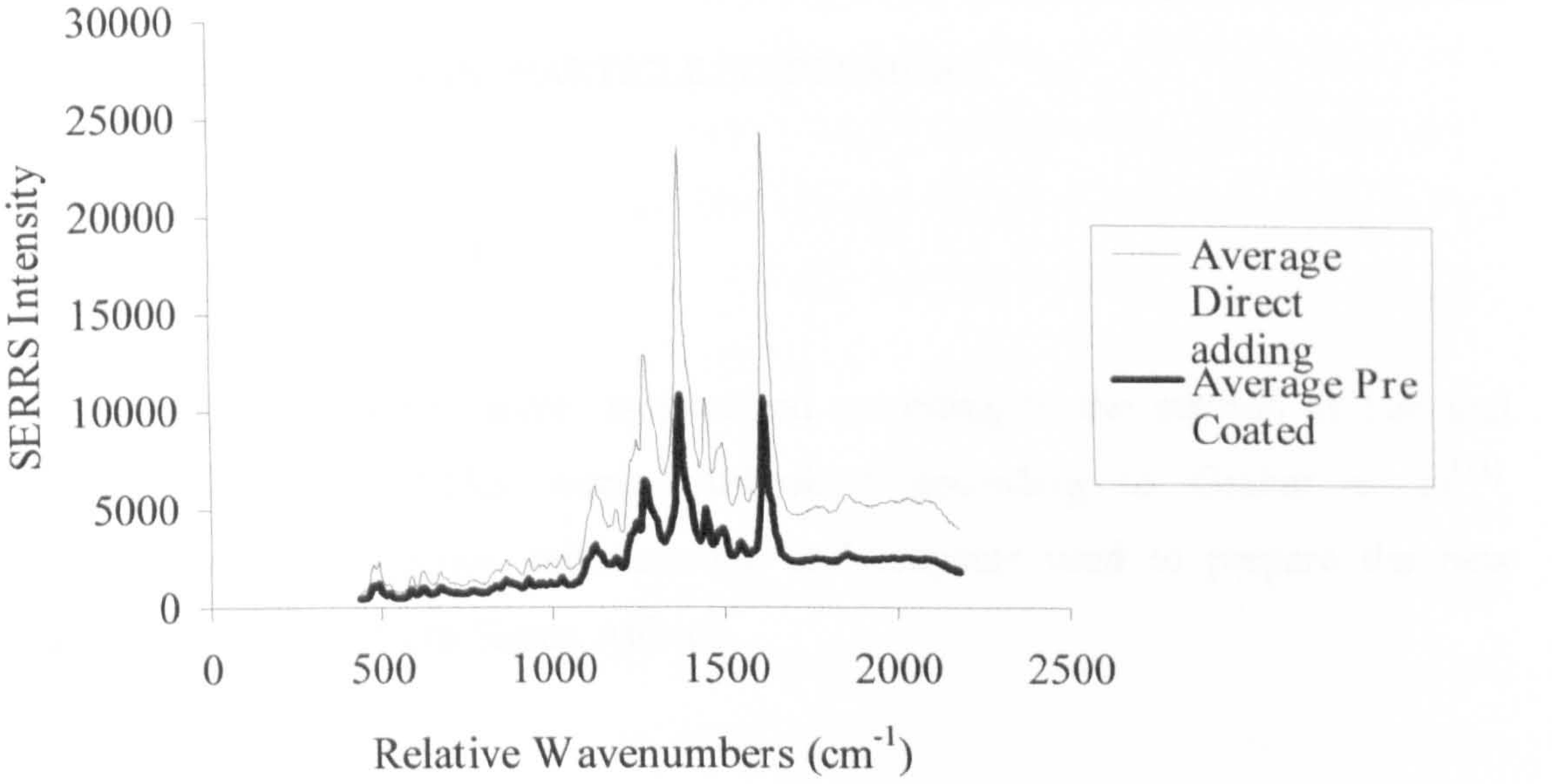

FIGURE 6.4. Comparison of the Raman signal for adding dye (ABT-DMOPA) to a nanoparticle solution directly, and in several doses. Although the one single addition leads to a lower final concentration, it gives the highest SERS intensity.

UV/ Vis

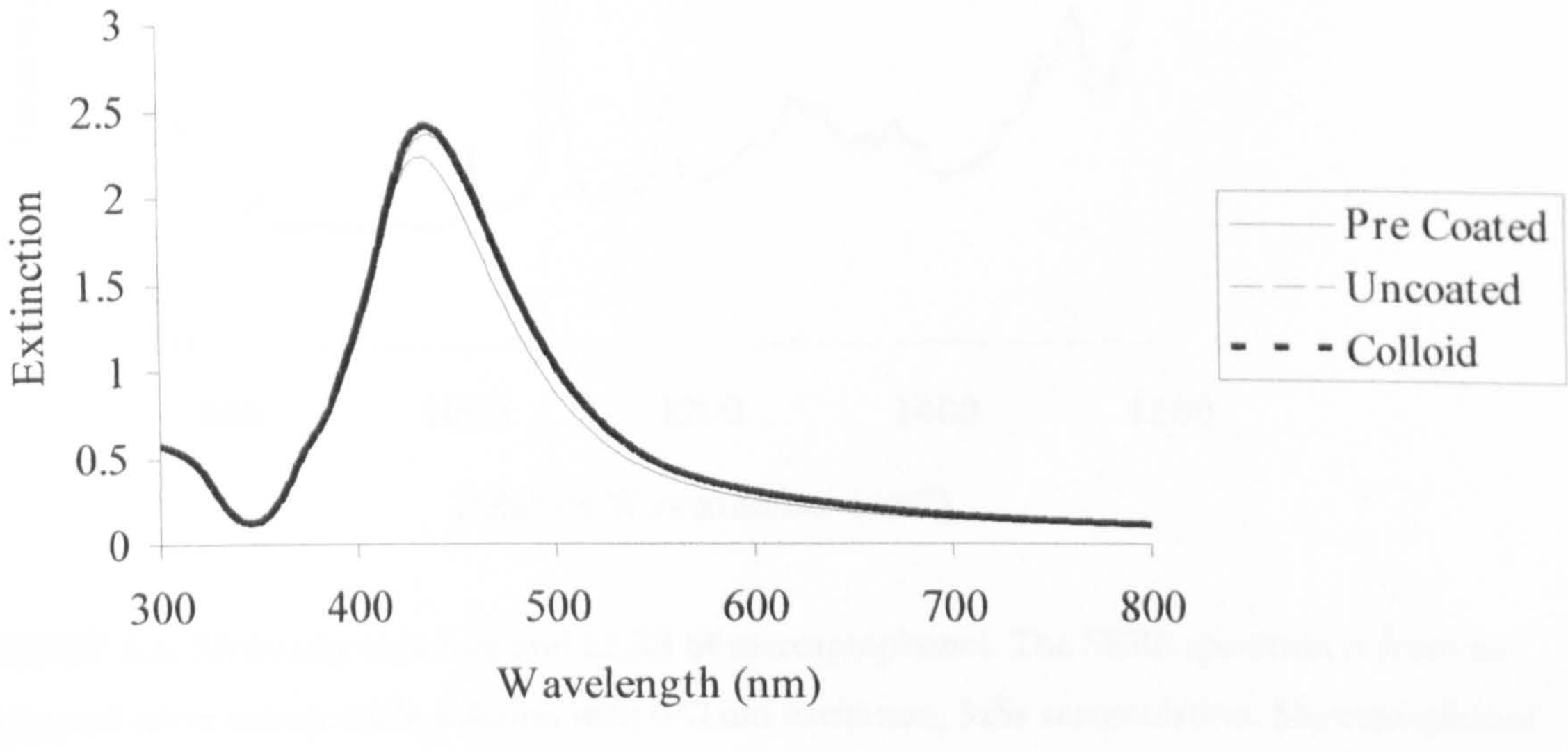

FIGURE 6.5. UV/Vis of the different samples. There are small differences, but all samples appear to be unaggregated.

6.3 SERS/SERRS FROM UNAGGREGATED AND AGGREGATED SILVER AND GOLD NANOPARTICLE SUSPENSIONS

6.3.1 EXPERIMENTAL

Silver nanoparticle solutions were synthesised according to the method of Lee and Meisel[14], gold nanoparticles were synthesised according to Grabar et al[13]. Cyclohexane, mercaptophenol, mitoxantrone and reagents used to prepare the new analyte were purchased from Sigma Aldrich.

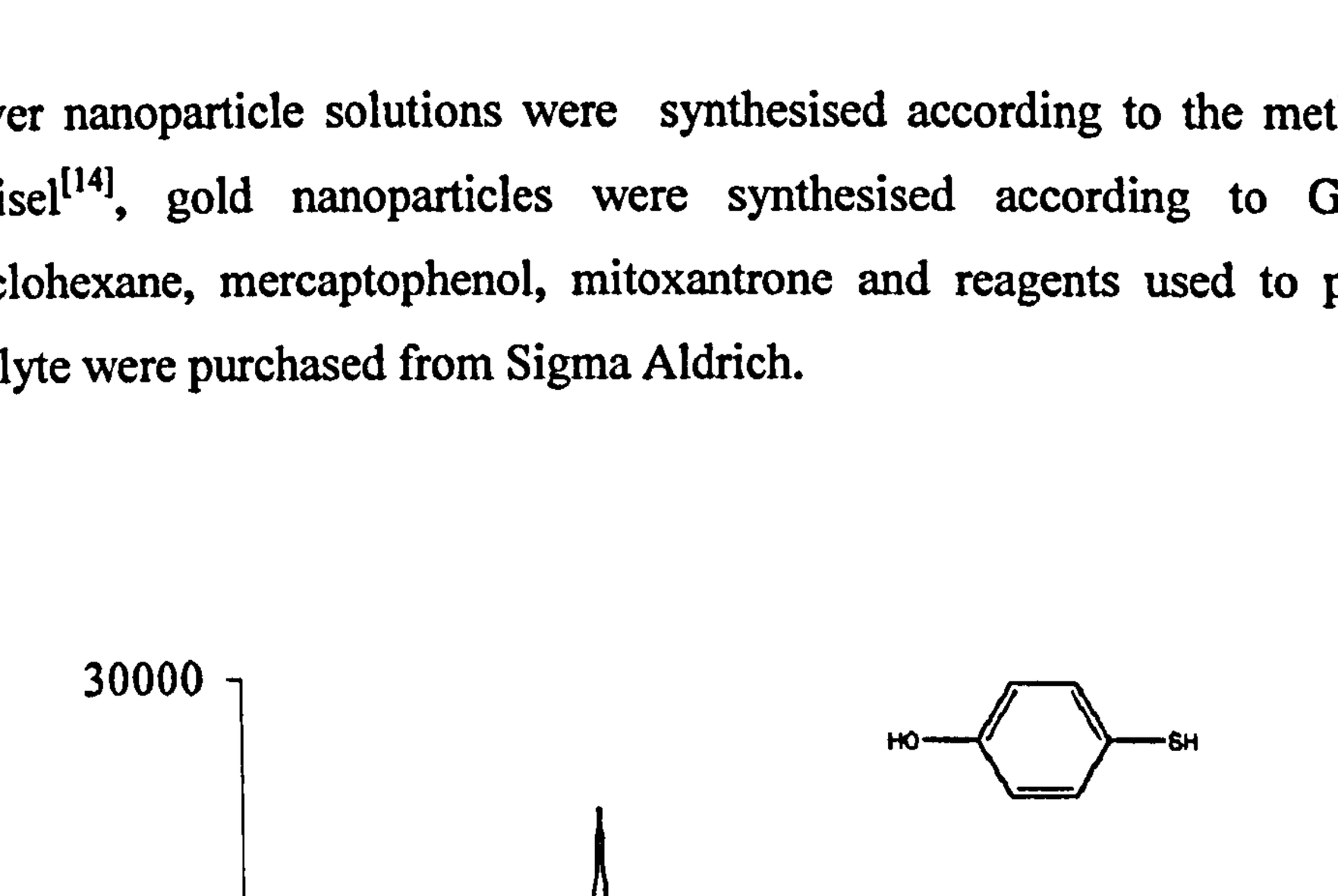

FIGURE 6.6. Molecular structure and SERS of mercaptophenol. The SERS spectrum is from an aggregated silver nanoparticle solution with 633 nm excitation, 3x5s accumulation. Mercaptophenol does not have any resonance in the visible region.

2-Allyl-6-(2-mercapto-ethylamino)-benzo[/de/]isoquinoline-1,3-dione ("Dye A", figure 6.8c) was synthesised as follows. 4-Bromo-1,8-naphthalic anhydride (2.20 g) was refluxed with allylamine (0.65 ml) for 2 h in 50 ml of ethanol. After cooling and

filtering, the solid was washed with ethanol and dried at 105 °C. A pale yellow product was obtained, mp 139-141 °C. The product was then refluxed for three hours with Cysteamine · HCl and an equivalent amount of Na_2CO_3 to neutralise the released HCl. The product was evaporated to dryness. Mp 128-130 °C MS^+: 313. HNMR: δ_H(400 MHz, DMSO) 1.3(1H, s, SH), 2.6(2H, t, CH_2), 3.3(2H, t, CH_2), 4.6(2H, d, CH_2), 5.1(2H, m, CH_2), 5.9(1H, m, CH), 7.9-8.8(5H, m, Ar)

Raman spectra were recorded using Renishaw Raman microscopes and excitation at 406 nm (Krypton laser), 633 nm (Helium Neon laser) and 785 nm (Diode laser). For these systems the laser was focused on the surface of the nanoparticleal suspension in a microtitre plate well and scattering collected at 180 degrees. An Avalon Instruments Raman Station R3 was used to obtain spectra with 532 nm (diode laser) excitation. Spectra were collected at 180 degrees from a 1 cm cuvette. An Acton Research Corporation Spectra Pro-300i spectrometer was use to obtain spectra with excitation at 457 nm and 488 nm (Argon laser). Spectra were collected at 90 degrees from a 1 cm cuvette. The distribution of the laser lines used are illustrated in figure 6.7.

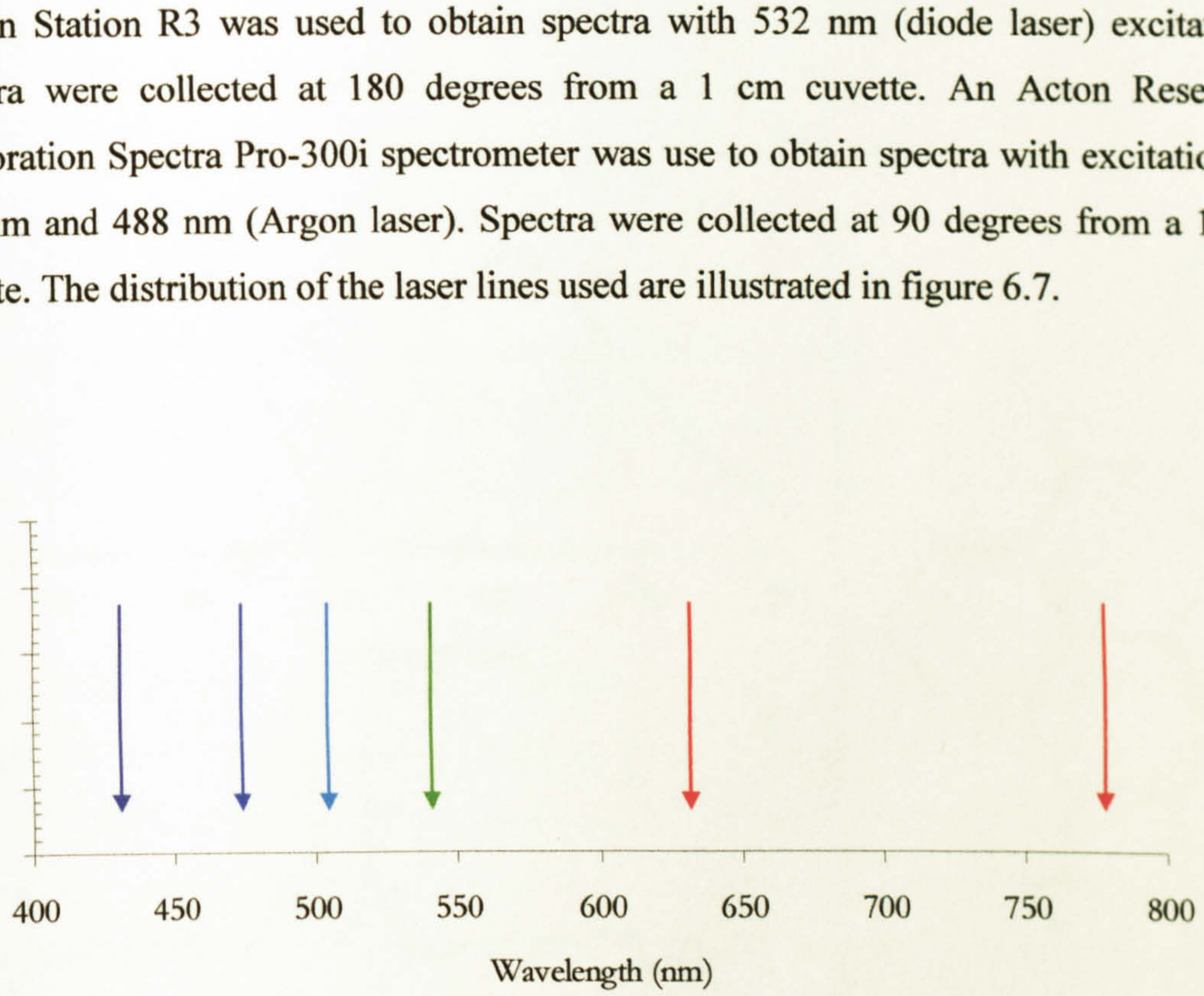

FIGURE 6.7. Distribution of the laser lines used in the study over the visible spectrum.

Samples were prepared by adding 100 μL of a $5x10^{-7}$ M solution of the analyte to 900 μL of nanoparticle solution (10^{14} particles/L for silver, $2.5 \cdot 10^{14}$ particles/L for gold). The concentrations were calculated as the concentration which would be present in the

final mixture before adsorption of the analyte to the nanoparticle. The solutions did not exhibit any detectable change in extinction spectra, zeta-potential or dynamic light scattering on adding the reagents at this concentration indicating little to no aggregation. Aggregation was caused by adding 100 μL of an aqueous solution of 1 M sodium chloride to the nanoparticle suspension. All spectra were collected as 3 or 5 accumulations of 5 seconds each, and all data points were averages of 5 replicates.

The aggregation state of the nanoparticle solutions were monitored by measuring the extinction spectra (Perkin Elmer Lambda 35), zeta potential (Malvern Zetasizer 2000) and particle size (Malvern High Performance Particle Sizer (HPPS)).

6.3.2 RESULTS AND DISCUSSION

The three analytes have been chosen to adhere efficiently to the surface and to provide contrasting molecular resonance contributions. Mercaptophenol has no chromophore in the visible region and will give SERS throughout. Mitoxantrone has a peak in the red region and can be used to separate SERS and SERRS in unaggregated nanoparticle for which the plasmon resonance frequency is in the blue region. Dye A was synthesised to provide a chromphore close to the plasmon resonance of unaggregated nanoparticle. It is fluorescent at shorter wavelengths (figure 6.8). When added to a silver nanoparticle suspension, the fluorescence was completely quenched and an intense SER(R)S spectrum appeared. This indicates that the molecule adsorbs effectively onto the surface.

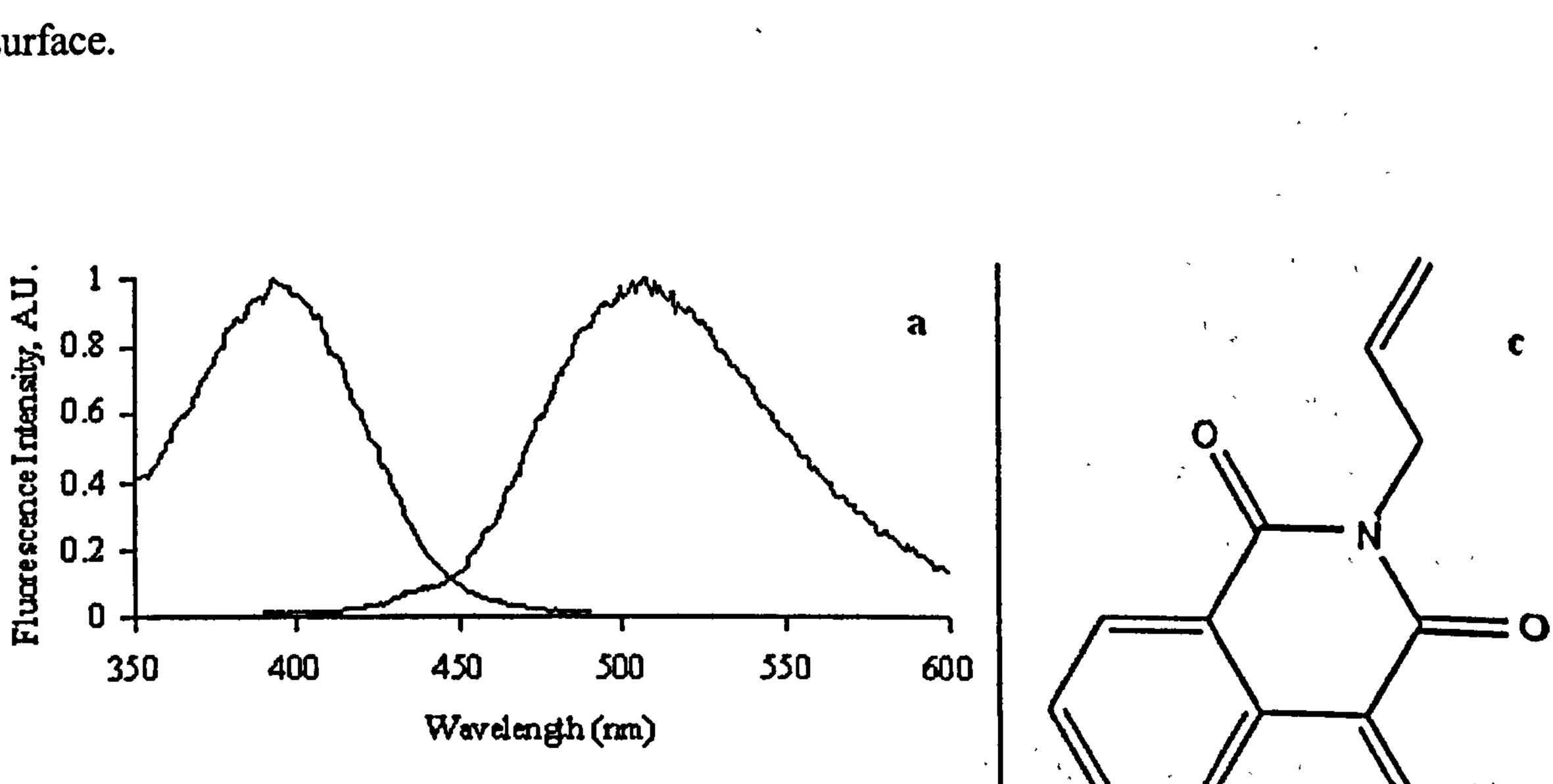

FIGURE 6.8. a) Fluorescence excitation and emission profiles of dye A in water, b) SERS spectrum of dye A adsorbed on aggregated silver nanoparticle using 633 nm excitation, 3x5s accumulation c) Structure of dye A.

Surface enhancement from nanoparticles is greatly increased in particle aggregates due to the high field intensities at the points where particles interact. In larger clusters, cooperative interactions create hot spots which give the greatest scattering [24, 25]. SERRS has been observed from single particles. For example, a study of a large number of single particles and small aggregates showed that 2% of single particles were SERRS active at the detection limit of the experiment[26, 27]. There is doubt as to whether SERS has been observed from single particles.

In the experiments carried out here, the amount of analyte added was chosen to ensure that very little aggregation occurred when added. Previous studies indicate that with the concentrations used, surface coverage will be considerably less than half a monolayer[28]. As a result, sufficient surface charge should be retained to ensure nanoparticle stability. Zeta-potential and particle size measurements verified that no appreciable aggregation had taken place. (Zeta potential before addition of mercaptophenol 50.7 mV +/- 1.4 mV and after addition 50.1 mV +/- 0.8 mV). It is still possible that a small number of clusters with plasmon resonance frequencies in the red are formed but, provided this is borne in mind, the data shows that a comparison can be made of SERS/SERRS from "unaggregated" nanoparticle and a nanoparticle efficiently aggregated with sodium chloride.

Figure 6.9 a) shows the extinction spectrum of unaggregated nanoparticles treated with mercaptophenol. The extinction coefficient of the nanoparticle is very high so that no absorption from any analyte is observed even with Mitoxantrone with a chromophore in the red end of the visible region away from the main plasmon resonance. If any aggregation occurs, the plasmon resonance is usually affected and longer wavelength absorption occurs. The spectrum is identical to that of the untreated nanoparticle confirming the conclusion from the zeta-potential and particle size measurements that no appreciable aggregation has occurred.

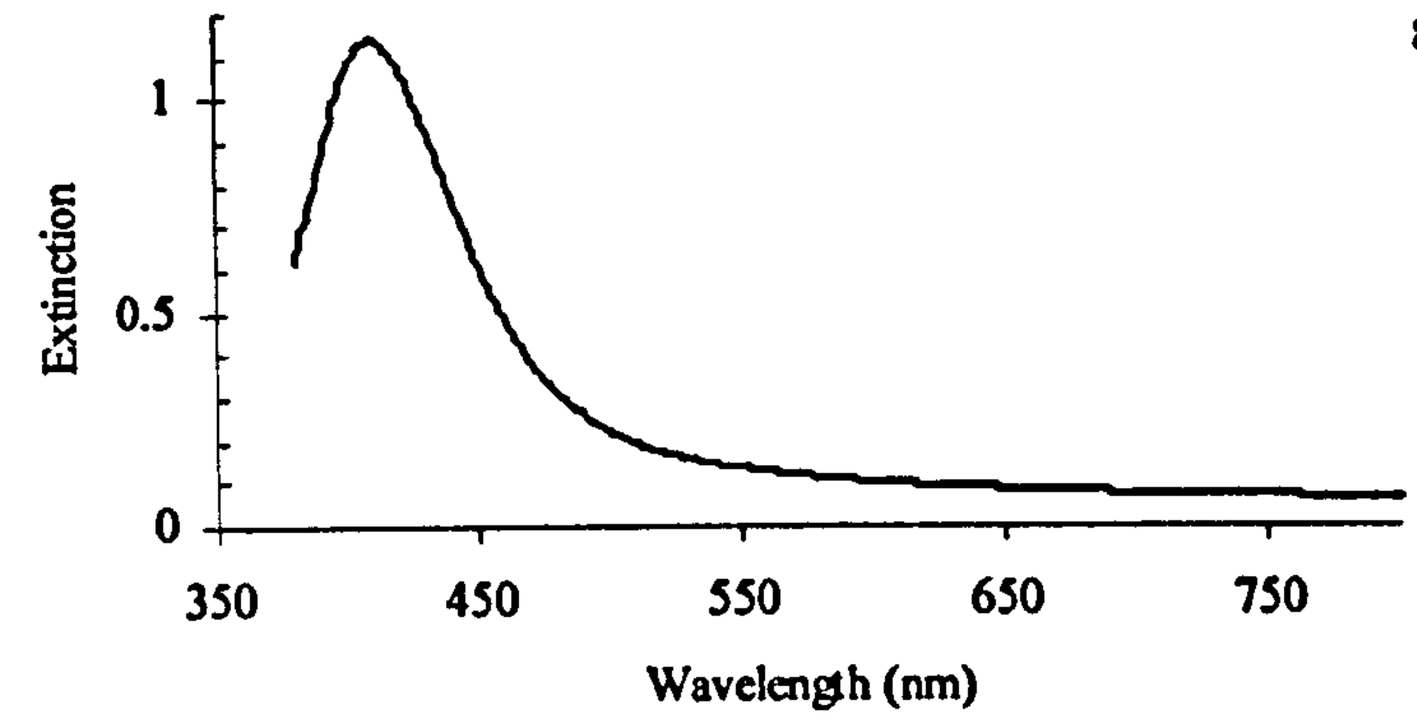

FIGURE 6.9. a) The extinction spectra of an unaggregated silver nanoparticles suspension with mercaptophenol and, b) The normalized SERS-intensity profile of the 1080 cm^{-1} peak of mercaptophenol adsorbed on unaggregated silver nanoparticles. All points are averages of 5 replicates.

A plot of the 1080 cm^{-1} band of mercaptophenol indicates that SERS cannot be detected under the conditions used with excitation close to the plasmon resonance frequency (figure 6.9. b). Relatively weak scattering is observed with longer excitation wavelengths probably due to the formation of a few clusters, some larger particles or rods, and, possibly, to collisions caused by Brownian motion.

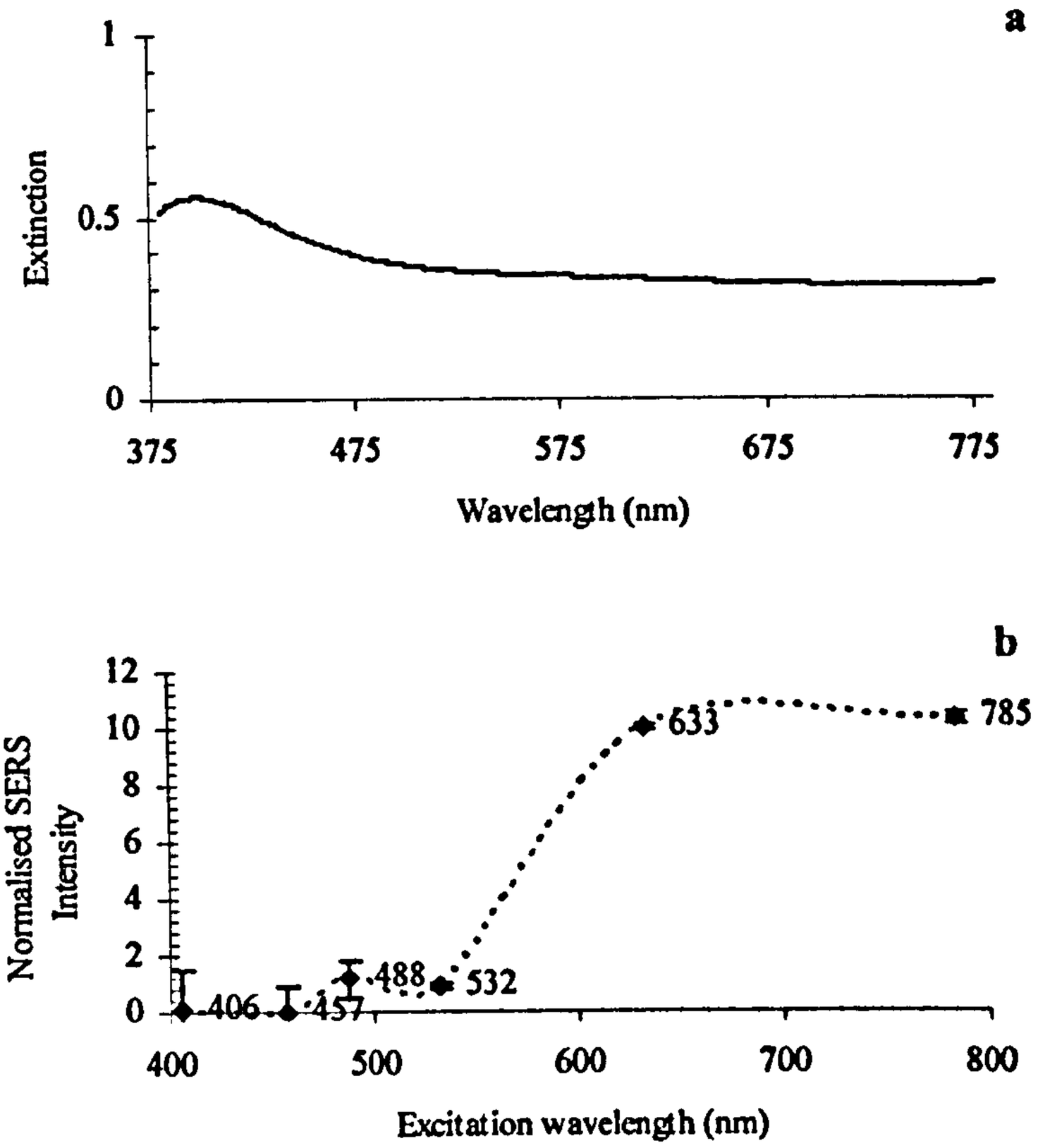

FIGURE 6.10. a) Extinction spectra of aggregated silver nanoparticles with mercaptophenol, b) The normalized SERS-intensity profile of the 1080 cm^{-1} peak of mercaptophenol adsorbed on aggregated silver nanoparticles. All points are averages of 5 replicates.

The extinction spectra from the aggregated silver suspension (figure 6.10 a), shows that the maximum extinction is still at 405-415 nm, but there is appreciable extinction at longer wavelengths, indicating the formation of clusters. The exact form of this spectrum is critically dependent on the state of aggregation since it will depend on the number and size of SERRS clusters formed

The highest SERS intensities are found with 633 nm and 785 nm excitation. The broad absorption at longer wavelengths suggests a range of aggregates with different plasmon resonance frequencies are formed. Since this will result in some aggregates being in resonance at each excitation frequency used, this will ensure a broad SERS response making the interpretation of the data easier.

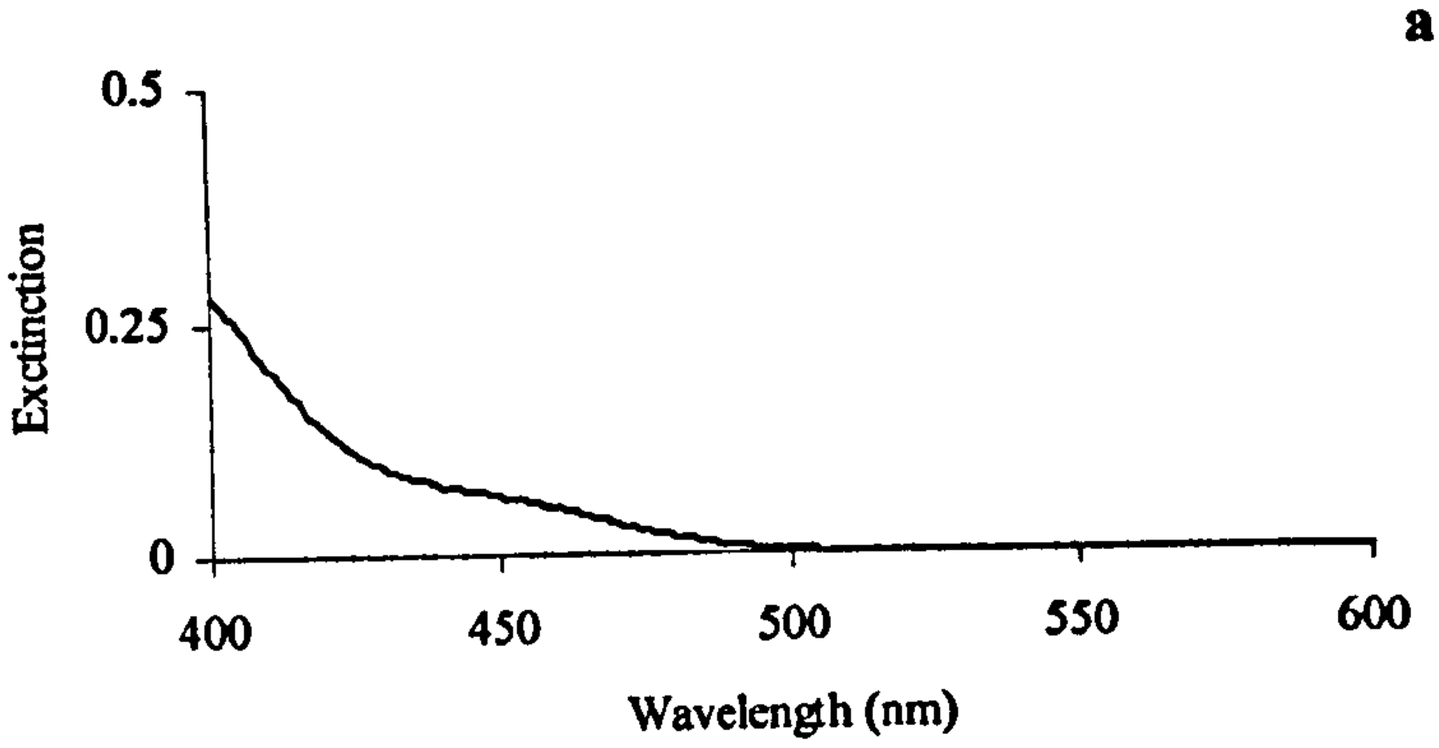

FIGURE 6.11. a) Extinction spectrum of dye A, b) Normalised SERRS intensity profile of the 1353 cm^{-1} peak of dye A adsorbed on unaggregated silver nanoparticle, c) Normalised SERRS intensity profile of the 1353 cm^{-1} peak of dye A adsorbed on aggregated silver nanoparticle. All points are averages of 5 replicates.

Dye A has a chromophore in the near ultraviolet with a peak at 380 nm which tails into the visible (figure 6.11.a). A typical SERS spectrum from this compound is given in figure 6.8. Previous studies have shown that an exact overlap of plasmon resonance and molecular absorption frequencies is not necessary for effective SERRS and since the plasmon resonance frequency is about 407 nm, this analyte should give effective SERRS from single particles. On addition of the analyte, the extinction spectrum, the zeta potential and the particle size were essentially unaffected suggesting that there is little to no aggregation.

In contrast to the results obtained with mercaptophenol, the spectrum shows a maximum for the 1353 cm^{-1} peak of the dye close to the maximum in the plasmon resonance frequency of the unaggregated nanoparticle suggesting single particle enhancement (figure 6.11.b). In addition there is a tail in the intensity towards the red, suggesting a similar SERS enhancement to that experienced by mercaptophenol on unaggregated nanoparticles. There is a clear shift in the excitation frequency which produces the greatest scattering when the nanoparticle is aggregated (figure 6.11.c). However, it is still at a short wavelength compared to the result found with mercaptophenol indicating the importance of the molecular resonance contribution. Since the chromophore does not absorb at all after 500 nm, the spectrum with longer excitation wavelengths will be due to SERS.

SERS and SERRS can be seen as two separate effects in the profile, with SERRS providing the greatest enhancement (figure 6.12).

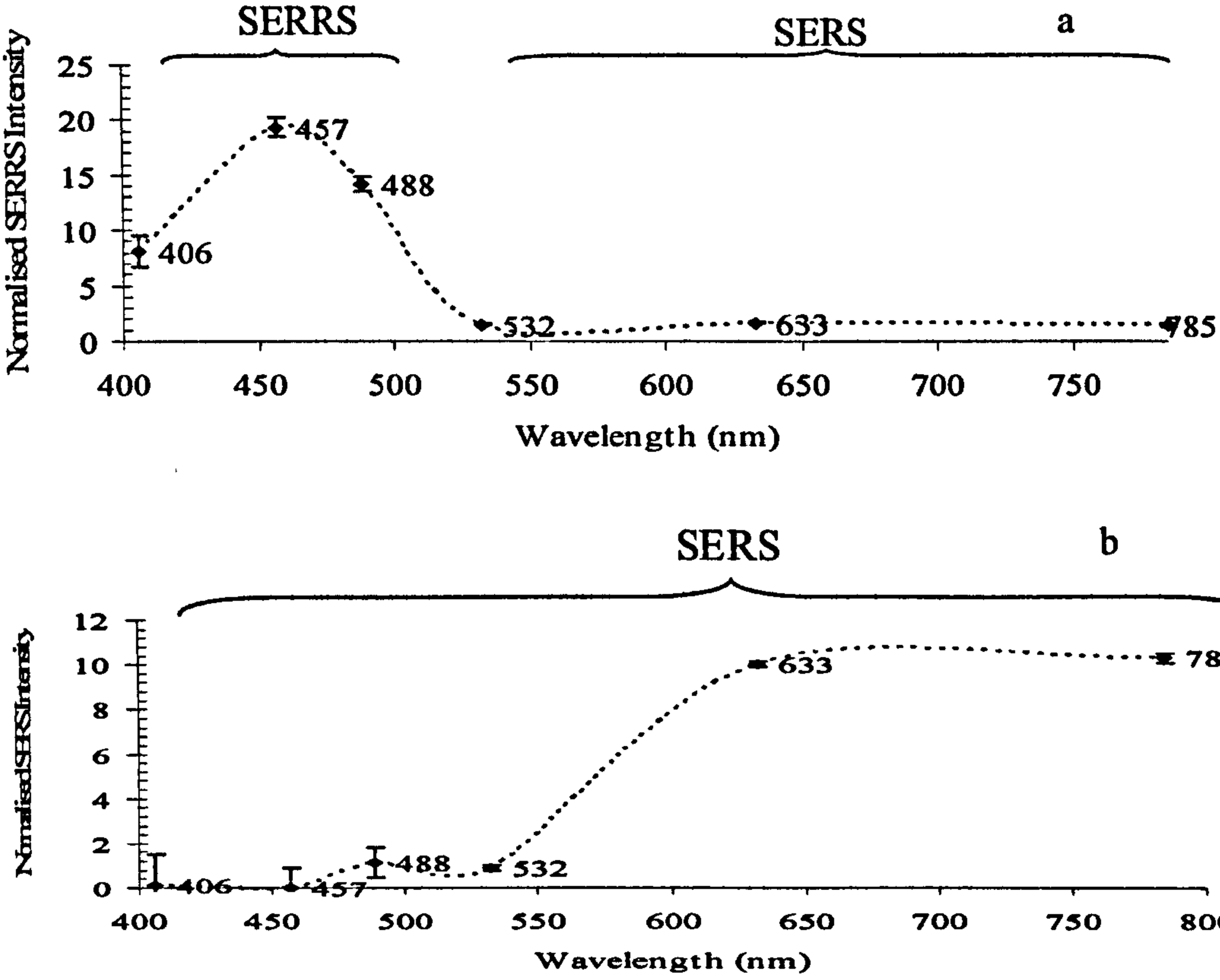

FIGURE 6.12. Illustration of the effect of the molecular resonance in a SERS/SERRS system. The chromophore (dye A) in a) is clearly visible up to 500 nm compared to the non resonant mercaptophenol in b). Note that the scales are different between the graphs. The profiles are from figures 6.11 c) (a) and 6.10 b) (b).

In addition, the SERS enhancement in aggregated nanoparticle is much higher for mercaptophenol indicating that it has a higher SERS cross section. However, the increased scattering with SERRS and not SERS in unaggregated nanoparticle at the plasmon resonance frequency is a striking difference suggesting a single particle enhancement mechanism for SERRS. Taking into consideration the SERS intensities at 633 and 785 nm for both analytes, and then comparing the SERS and SERRS at 457 nm or 407 nm, the effect of the cromophore in this experiment appears to be a factor of in the region 400times enhancement.

These conclusions are confirmed by the results using Mitoxantrone, (figure 6.13) an analyte with a chromophore absorbing at 550-650 nm. With unaggregated nanoparticle the maximum enhancement occurs with 633 nm excitation and when the nanoparticle is

aggregated a much larger enhancement is obtained with the same excitation wavelength. This is as expected from the previous discussion. In aggregated nanoparticles, the frequency of the electronic transition of Mitoxantrone and the surface plasmon resonance from an appreciable number of clusters are close to 633 nm and consequently the greatest enhancement is obtained at this excitation wavelength.

Since the absorbance of Mitoxantrone is less intense at 785 nm, SERRS drops significantly with this excitation wavelength. With unaggregated nanoparticle, the weaker enhancement centered around 633 nm is probably due as before to a few clusters, large particles, rods or collisions due to Brownian motion. Practically no enhancement is found at the plasmon resonance frequency where the scattering is effectively SERS.

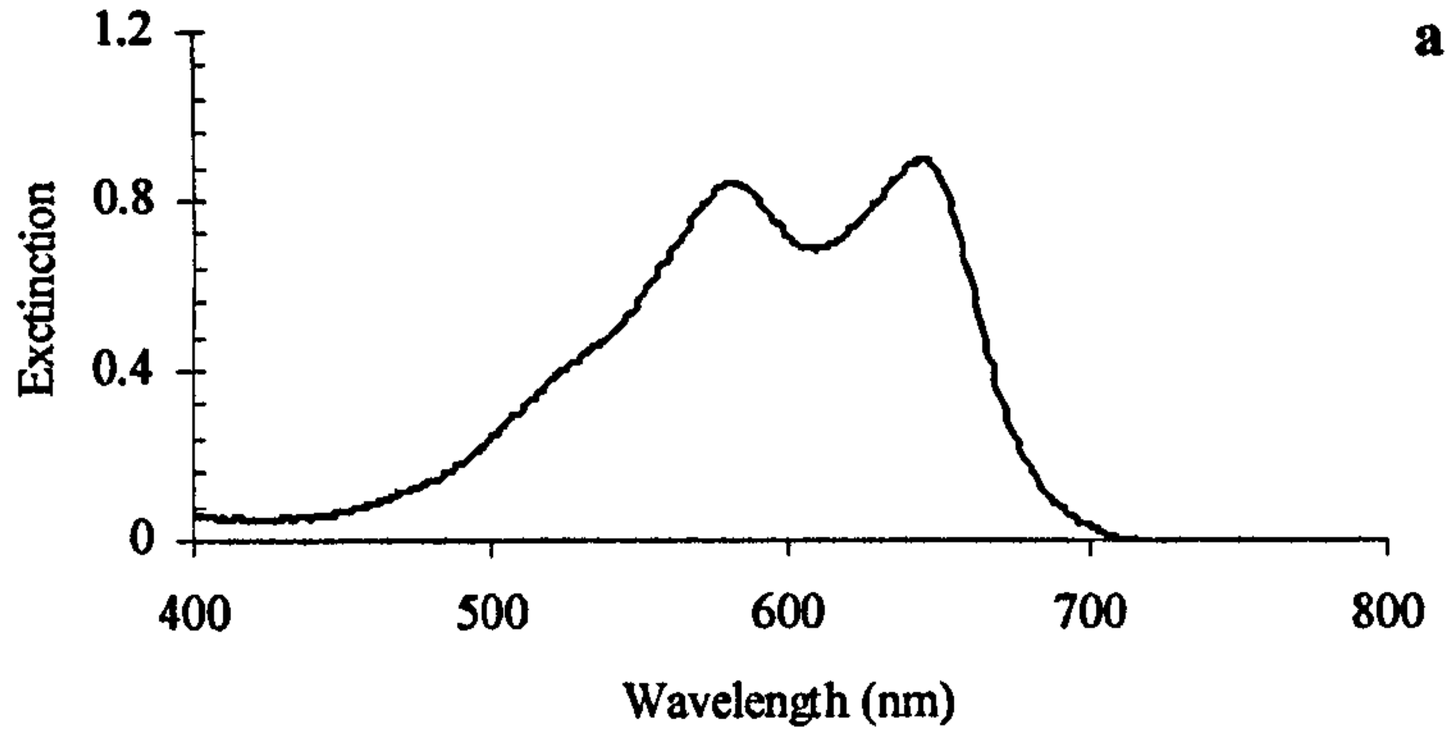

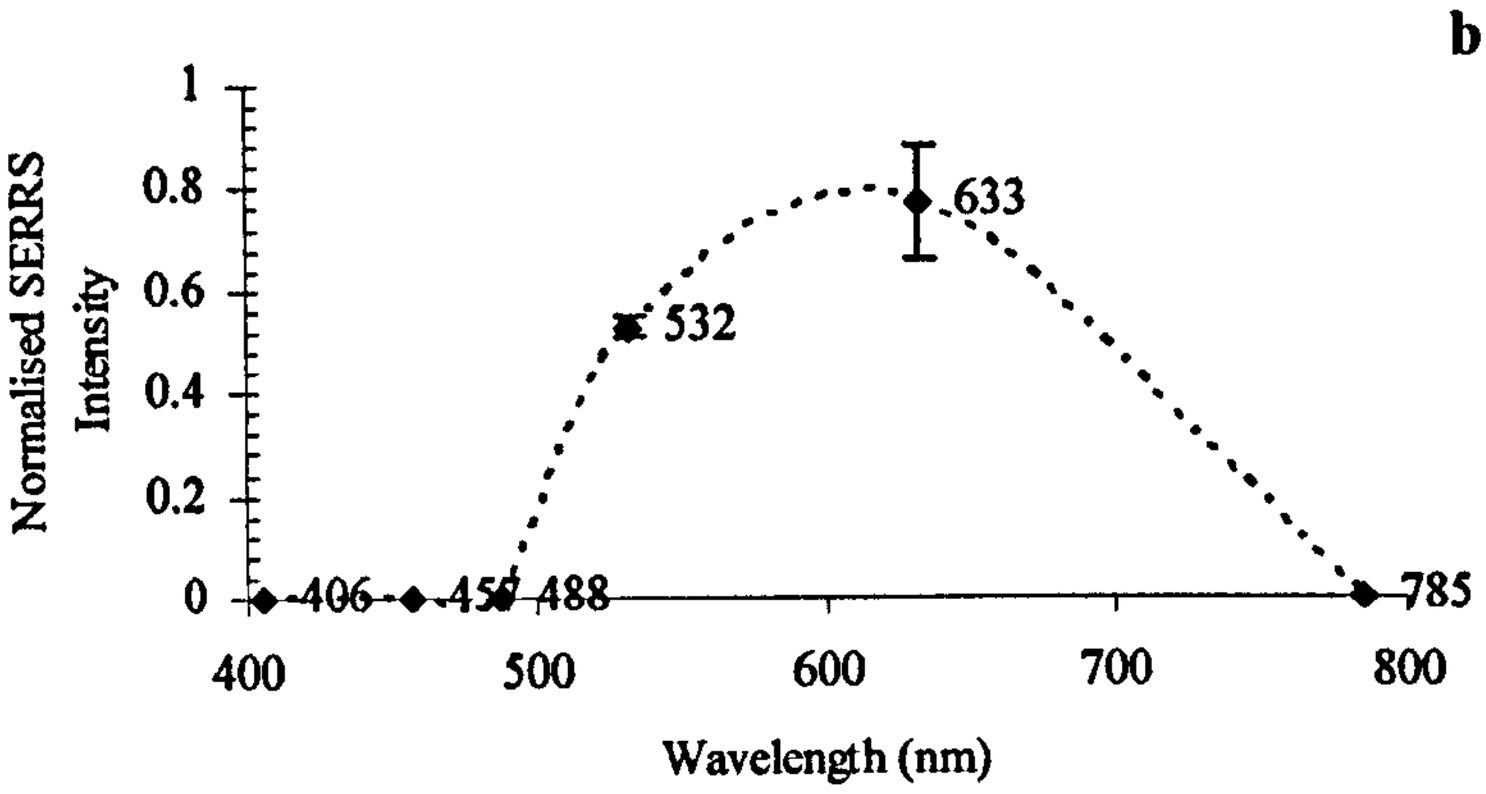

FIGURE 6.13 a) Extinction spectra of Mitoxantrone, b) Normalised SERRS intensity profile of the 1317 cm^{-1} peak of Mitoxantrone on unaggregated silver nanoparticle, c) Normalised SERRS intensity profile of the 1317 cm^{-1} peak of Mitoxantrone on aggregated silver nanoparticle. All points are averages of 5 replicates.

Since gold is the other most common metal used as SERS substrate, the same effect was investigated for gold nanoparticle solutions. Unaggregated Gold nanoparticle with

mercaptophenol did not give a detectable SERS signal under the conditions used. With the aggregation conditions used in these experiments, aggregated gold nanoparticles showed a decrease in absorbance towards 785 nm (6.14.a). Aggregating the nanoparticle enables detection of the signal, it is however still weak. Unlike for silver, the signal decreases for 785 nm compared to 633 nm. The UV-Vis spectra indicate a lower number of large species formed which may be a part of the explanation for this decrease.

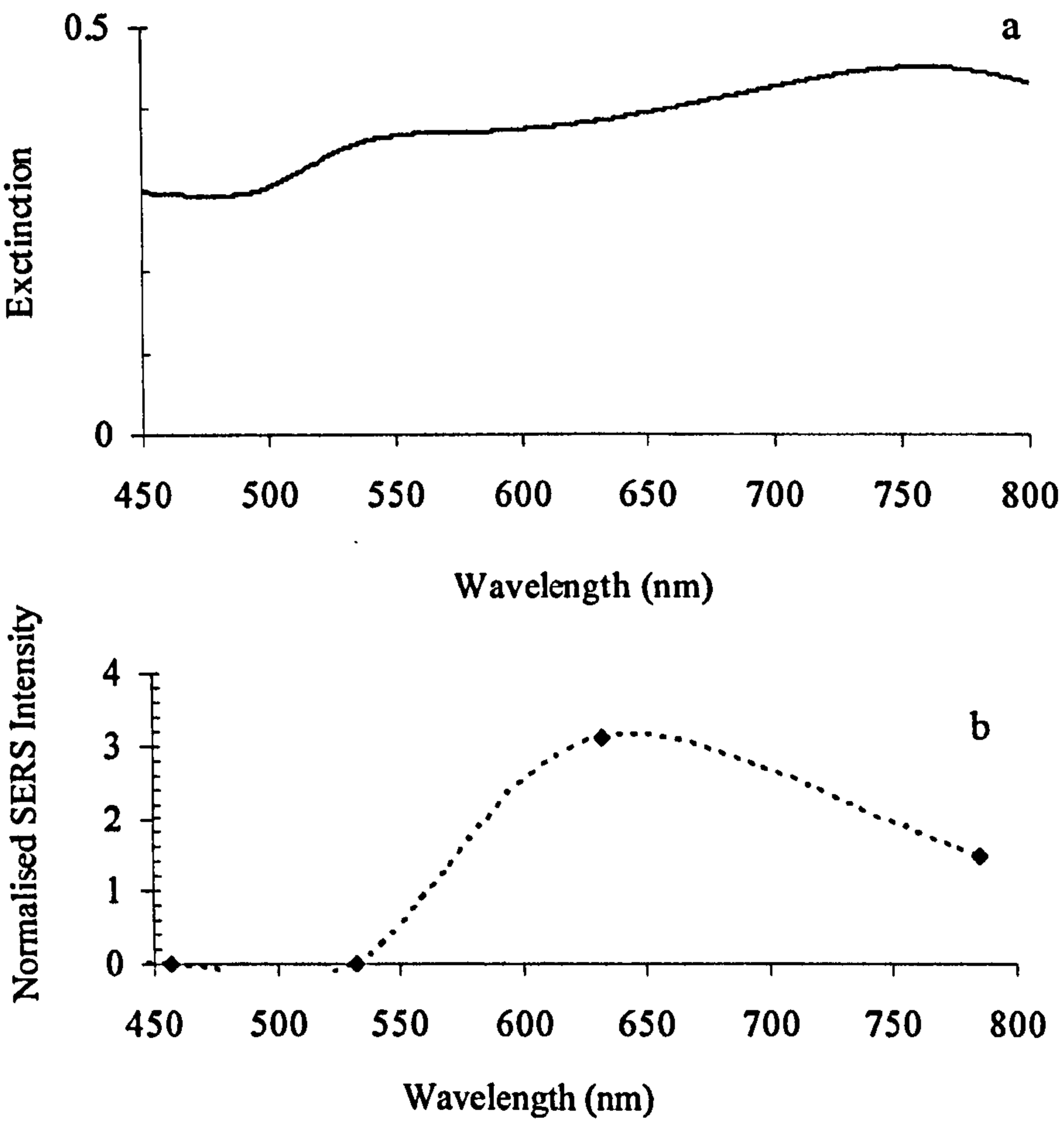

FIGURE 6.14) Extinction spectra of aggregated gold nanoparticle with mercaptophenol, b) The normalized SERS-intensity profile of the 1080 cm^{-1} peak of mercaptophenol adsorbed on aggregated gold nanoparticles. All points are averages of 5 replicates.

Using Victoria Blue instead of mercaptophenol, the presence of the chromophore (lambda-max ~610nm, figure 6.15 a) makes it possible to detect SERRS even for unaggregated gold nanoparticles (figures 6.15.b) and 6.15.c)). The reason for using

Victoria Blue instead of mitoxantrone in these experiments is that it attaches well to gold, unlike mitoxantrone.

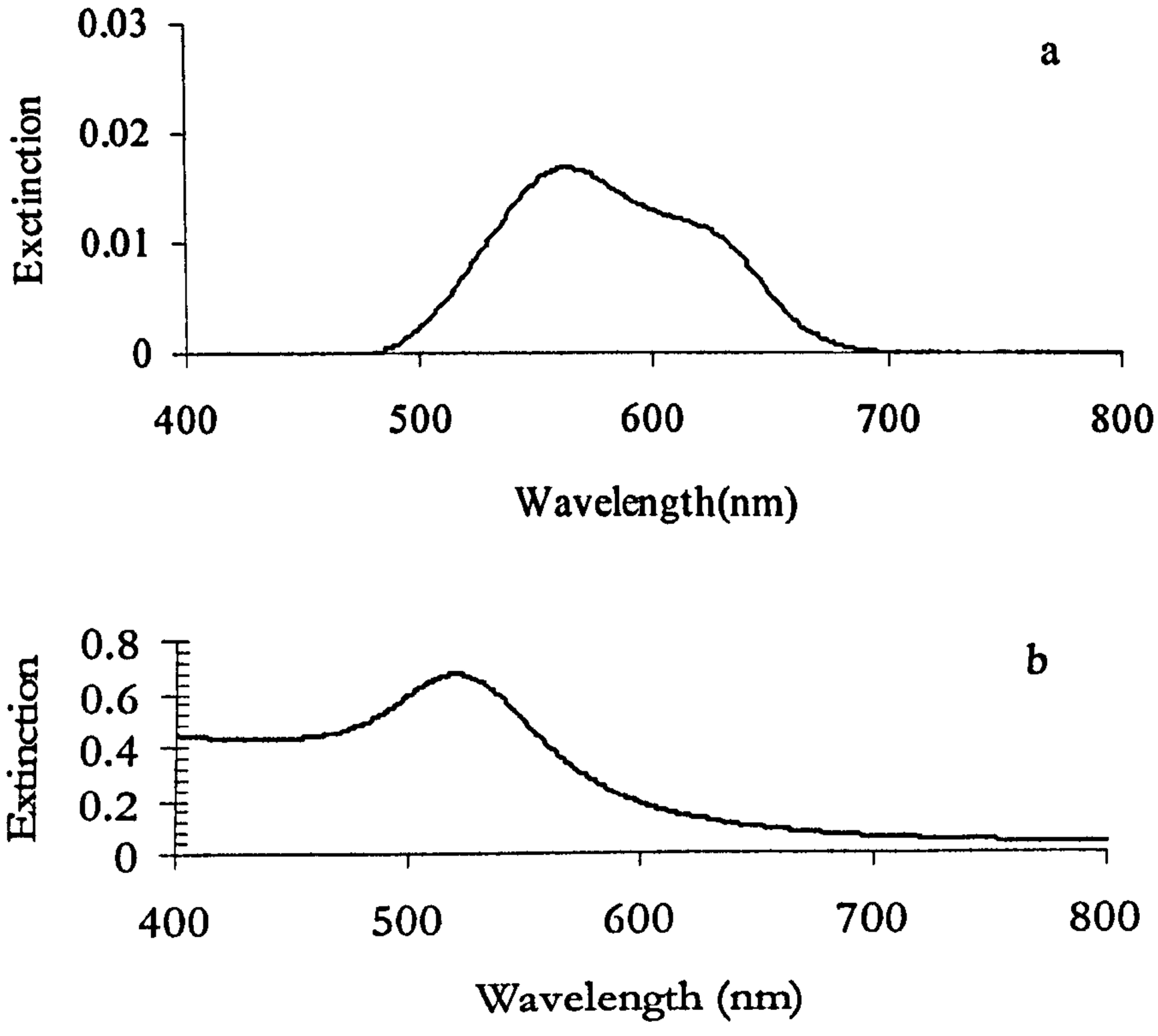

FIGURE 6.15 a) Extinction of Victoria Blue, b) extinction spectra of unaggregated gold nanoparticles, and c) SERRS intensity profile of the 1621 cm^{-1} peak of Victoria Blue on unaggregated gold nanoparticles. All points are averages of 5 replicates.

When aggregating the gold nanoparticles, the Raman signal becomes very strong at 633 nm as expected, as this excitation line coincides with both the chromophore of Victoria Blue and with the surface plasmon resonance of aggregated species of gold nanoparticles (figure 6.16).

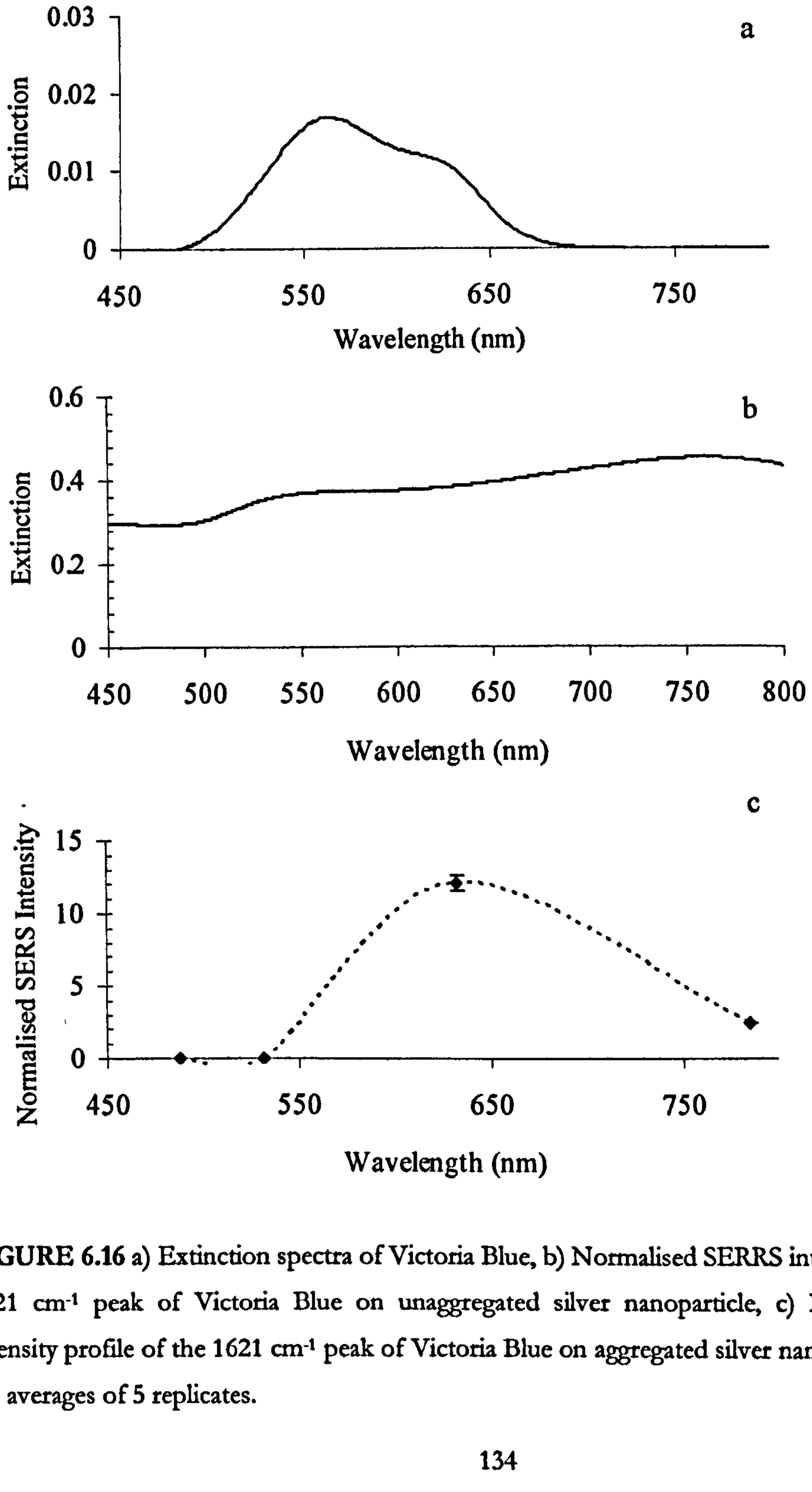

FIGURE 6.16 a) Extinction spectra of Victoria Blue, b) Normalised SERRS intensity profile of the 1621 cm^{-1} peak of Victoria Blue on unaggregated silver nanoparticle, c) Normalised SERRS intensity profile of the 1621 cm^{-1} peak of Victoria Blue on aggregated silver nanoparticle. All points are averages of 5 replicates.

6.4 DISCUSSION

Surface enhanced Raman scattering and surface enhanced resonance Raman scattering have been compared at several wavelengths over the visible region. The two effects have been separated, and the importance of overlap between the frequencies of surface plasmon resonance and molecular resonance is shown. The relative weakness of single particle enhancement on the Raman intensity is confirmed.

SERS from sols consisting of single nanoparticles appears to be a very weak phenomenon. Looking at previous studies on SERRS mapping of immobilized silver nanoparticles coated with ABT- DMOPA, 1-10 % of single nanoparticles show SERRS activity. SERS being a significantly less efficient technique would be expected to show even lower numbers of active particles. The results in this study confirm these findings. Using a very strong Raman scatterer, Mercaptophenol, without any chromophore in the visible region adsorbed on to silver nanoparticles, the SERS intensity profile over a number of excitation lines were probed. In this study, a silver nanoparticle solution is considered to be unaggregated if there can not be seen any change in Z-potential, UV/Vis spectra or dynamic light scattering (Z-sizer, HPPS) before and after the addition of dye/mercaptophenol.

Even for unaggregated nanoparticles the strongest intensities are found at 532 nm and 633 nm. In fact, it was not possible to detect any Mercaptophenol spectra at 407 nm excitation line, where single particles should be absorbing. This suggests that, even though the solution is considered to be unaggregated, the dominating SERS contribution comes from many-particle systems present in the solution. These systems would be likely to enhance raman scattering in a much higher degree than single nanoparticles due to the multiplicity of EM-fields around the particles.[29]

The results provide an indication of the combination of analyte and instrument conditions which are best suited to obtain the maximum enhancement from SERRS with silver nanoparticle. The importance of the chromophore in the analyte and of the aggregation condition of the nanoparticle is clear. Although much greater differences in

cross section between SERRS and SERS have been calculated, in practice the difference appears to be a factor of between 10 and 500 with these analytes under the conditions used. However, aggregation of the nanoparticle produces clusters of different sizes which will have different plasmon resonance frequencies and, as result, any one excitation frequency will excite the plasmon resonance in only a fraction of the clusters.

SERS enhancement from single particles is not conclusively observed with the conditions used in this study but in agreement with previous studies SERRS can be observed. Confirmatory evidence for this is the very different wavelength dependences for dye A and mercaptophenol. In unaggregated nanoparticle, dye A gives the greatest enhancement using excitation at the plasmon resonance frequency whereas SERS from mercaptophenol could not be detected under the conditions used

[1] C. McLaughlin, D. MacMillian, C. McCardle, W. E. Smith, *Analytical Chemistry* **2002**, *74*, 3160.

[2] K. L. Kelly, E. Coronado, L. L. Zhao, G. C. Schatz, *Journal Of Physical Chemistry B* **2003**, *107*, 668.

[3] T. R. Jensen, M. D. Malinsky, C. L. Haynes, R. P. Van Duyne, *Journal of Physical Chemistry B* **2000**, *104*, 10549.

[4] S. Nie, S. R. Emory, *Science* **1997**, *275*, 1102.

[5] K. Kneipp, Y. Wang, H. Kneipp, L. T. Perelman, I. Itzkan, R. R. Dasari, M. S. Feld, *Physical Review Letters* **1997**, *78*, 1667.

[6] X. L. Chen, P. S.; Holz, J. S. W.; Chi, Z. H.; Pajcini, V.; Asher, S.A.; Kelly, L.A., *Journal of the American Chemical Society* **1996**, *118*, 9705.

[7] F. T. Docherty, M. Clark, G. McNay, D. Graham, W. E. Smith, *Faraday Discussions* **2004**, *126*, 281.

[8] K. Faulds, W. E. Smith, D. Graham, *Analyst* **2005**, *130*, 1125.

[9] J. Gersten, A. Nitzan, *Journal of Chemical Physics* **1980**, *73*, 3023.

[10] Y. W. C. Cao, R. C. Jin, C. A. Mirkin, *Science* **2002**, *297*, 1536.

[11] A. J. Xu H., Käll M., Apell P., *Physical Review E* **2000**, *62*, 4318.

[12] D. D. Dlott, *Materials Science and Technology* **2006**, *22*, 463.

[13] K. C. Grabar, R. G. Freeman, M. B. Hommer, M. J. Natan, *Analytical chemistry* **1995**, *67*, 735.

[14] P. C. Lee, D. Meisel, *Journal of Physical Chemistry* **1982**, *86*, 3391.

[15] N. Leopold, B. Lendl, *Journal of Physical Chemistry B* **2003**, *107*, 5723.

[16] M. Moskovits, *103 Topics in Applied Physics* **2006**, 1.

[17] P. Hildebrandt, M. Stockburger, *Journal of Physical Chemistry* **1984**, *88*, 5935.

[18] A. M. Stacy, R. P. Van Duyne, *Chemical Physics Letter* **1983**, *102*, 365.

[19] A. M. Michaels, M. Nirmal, L. E. Brus, *Journal of the American Chemical Society* **1999**, *121*, 9932.

[20] S. Habuchi, M. Cotlet, R. Gronheid, G. Dirix, J. Michiels, J. Vanderleyden, F. C. De Schryver, J. Hofkens, *Journal of the American Chemical Society* **2003**, *125(28)*, 8446.

[21] K. Faulds, L. Stewart, W. E. Smith, D. Graham, *Talanta* **2005**, *67*, 667.

[22] K. Faulds, R. E. Littleford, D. Graham, G. Dent, W. E. Smith, *Analytical Chemistry* **2004**, *76*, 592.

[23] I. Khan, E. Polwart, D. W. McComb, W. E. Smith, *Analyst* **2004**, *129*, 950.

[24] V. A. Markel, V. M. Shalaev, P. Zhang, W. Huynh, L. Tay, T. L. Haslett, M. Moskovits, *Physical Review B* **1999**, *59*, 10903.

[25] H. Xu, J. Aizpurua, M. Kall, P. Apell, *Physical Review E* **2000**, *62*, 4318.

[26] I. Khan, D. Cunningham, R. E. Littleford, D. Graham, W. E. Smith, D. W. McComb, *Analytical Chemistry* **2006**, *78*, 224.

[27] I. Khan, D. Cunningham, D. Graham, D. W. McComb, W. E. Smith, *Journal Of Physical Chemistry B* **2005**, *109*, 3454.

[28] D. Cunningham, R. E. Littleford, W. E. Smith, P. J. Lundahl, I. Khan, D. W. McComb, D. Graham, N. Laforest, *Faraday Discussions* **2006**, *132*, 135.

[29] A. Campion, P. Kambhampati, *Chemical Society Review* **1998**, *27*, 241.

CHAPTER 7

CONCLUSIONS

7.1 CONCLUSIONS

In this thesis, the conditions to achieve surface enhancement effect in surface enhanced Raman scattering (SERS) using colloidal metal solutions is investigated and identified. Tools for synthesis and characterisation of gold and silver nanoparticles at different sizes are presented and evaluated. Also, gold and silver, the two metals most commonly used in this technique, are compared as SERS substrates at different wavelengths. Finally, the additional effect of molecular resonance in a SERS system is investigated.

A number of different protocols for synthesis of gold and silver nanoparticles have been investigated. The products have been characterised using scanning electron microscopy (SEM), atomic force microscopy (AFM) and electronic spectroscopy.

Methods to produce gold nanoparticles between 20 nm and 80 nm were obtained from literature. The products were found to be mostly spherical and relatively monodispersed (RSD = 20-25 %). The products were stable over long periods of time and were suitable for use in surface enhanced Raman spectroscopy. The surface plasmon of the nanoparticles peaked at around 520 nm for the small sizes (<30 nm) and was found to shift towards longer wavelengths as their diameter increased. The plasmon response was relatively broad.

The existing protocols for synthesis of silver nanoparticles were found to be inadequate to achieve a similar control as for that achieved with gold. One method based on citrate reduction of silver nitrate produced a very polydisperse particle suspension with a high number of rods and needles. One protocol using EDTA as reducing agent produced a high number of spherical particles of reasonable monodispersity, but could only produce one size. To provide a wider range of particle sizes, a new method based on seeded growth of EDTA reduced silver particles was developed. Particles of any size up towards 100 nm in diameter could be produced. The product was found to have a high ratio of spherical nanoparticles and particles of the desired size.

In connection with this, a study of different techniques used to characterise metal nanoparticles in the size range 20 nm to 100 nm diameters was carried out. It was found that the two most established techniques, scanning electron microscopy and atomic force microscopy, where in close agreement with each other. The least established technique, dynamic light scattering (DLS), was found to be a useful tool when dealing with nanoparticles in solution. Even though it is desirable to have some knowledge about the general properties of the nanoparticles analysed to fully interpret the light scattering data, it was found to give the size distribution of the particle solutions with a high degree of agreement compared to the particle distribution determined by SEM.

A method for the separation of scattering and absorption to the extinction of nanoparticle suspensions was developed. The method uses a standard fluorometer to measure the scattering at 90° angle from a very dilute nanoparticle suspension. The scattering is normalised against a Perylene standard and a scattering cross section can be calculated. From this and theoretical values of the extinction cross sections, the absorption contribution is calculated. The data acquired from these measurements correlates with theoretical predictions and gives an increased insight to the properties of the nanoparticle system and its interaction with light.

The manner that a surface structure interacts with light is intimately connected with its performance as a SERS substrate. By using the technique developed here, the differences in interaction with electromagnetic radiation between gold and silver nanoparticles were investigated. For gold nanoparticles, the extinction spectra were dominated by absorption over the entire spectrum. The silver nanoparticles in contrast were mostly radiative beyond 475 nm, with very low absorption. An increasing redshifting of the dipole resonance frequency with size, together with indications of higher order oscillations appearing at wavelengths on towards the blue spectra of illumination was discovered.

In the case of a nanoparticle solution with a single dipole plasmon resonance frequency, the strongest SERS intensity would be expected when the plasmon maxima is between the excitation wavelength and the Raman peak emission wavelength. As the solution is

aggregated the electronic response changes. The size and shape of the clusters formed will determine the electronic response of the aggregate and with this, to some degree, its properties as a SERS substrate. It is shown that it is possible to control and tune the maxima of the electronic response of the aggregated solution by changing the particle size and concentration. In chapter 4 the effect of the aggregation conditions on the SERS intensity has been investigated using sodium chloride as aggregating agent. We have shown that by varying the particle concentration and size it is possible to control the electronic response of gold and silver aggregates. If also the concentration and addition rate of aggregation agent to the nanoparticle solution is kept constant, this electronic response is reproducible.

The influence of self extinction of scattered light by the sample is concluded to have a major impact on the SERS intensity. There does not seem to be a clear connection between the magnitude of the electronic response and the SERS intensity obtained. Two different trends were identified at 633 nm and 785 nm excitation. At 633 nm, the trend was a decrease of SERS intensity with increasing electronic response at the excitation wavelength. At 785 nm the trend was the opposite. This is explained by the strong dependence on local geometry of the enhancement field. The difference in SERS intensity may suggest different types of clusters (such as fractal or compact) being resonant at the different wavelengths with different properties.

Finally, silver and gold were compared as SERS substrates. The results showed that gold was very inefficient at higher energies, most likely due to self absorption and plasmon damping by interband transitions, leading to a rapid dephasing of the plasmon and sample heating. At the 633 nm and 785 nm excitation wavelengths the SERS intensities of gold approached or surpassed the intensities achieved from silver. This is correlated with a decrease of nonradiative damping processes at lower energies for gold. The results suggest that at longer, 633 nm excitation frequencies and beyond, geometrical properties are more important than choice of metal.

Particles of different sizes are investigated. This means that the plasmon resonance frequency may have multiple peaks. In addition, the plasmon damping may differ over

the spectral range. In this research two excitation frequencies were used, 407 nm and 488 nm. At 407 nm a major part of the damping is through non radiative processes whereas at 488 nm the plasmon is dampened primarily through radiative processes.

The data strongly indicates that for unaggregated samples there is a direct correlation between the far field scattering efficiency and the near field responsible for the enhancement of the Raman scattering intensity. The scattering efficiency is dependent on the quality of the plasmon. The dephasing time of the plasmons is dependent on the damping processes involved. As the size of the particle increases, the polarisabililty of the particles increases and the plasmon damping due to collisions with the particle surface decreases. However, as the size increases beyond a point where higher order plasmons start to appear, other damping effects will occur, derived from the retardation effect that follow from this. This limit was investigated, and it was found that there was a strong dependence on the ratio between particle size and excitation wavelength. This dependence remained to some extent even as the particle solution was aggregated. From this it can be concluded that the "optimal" size of particle for maximum SERS intensity can be adjusted depending on what excitation wavelength is desired.

All data show a clear trend of initial increase in SERS enhancement with increasing diameter of the nanoparticles used as substrate for the surface enhancement. This correlates with an increase in polarization leading to an increase in optical response of the nanoparticle, as well as less damping from electrons colliding with the surface of the nanoparticle. However, for larger diameters, the SERS intensity tails off or decreases, suggesting damping of the plasmon as the particle size approaches the wavelength of the laser, causing the appearance of higher order oscillations. These higher order oscillations will bind up energy and be less radiative, and causing the localized electromagnetic field to be less efficient in polarizing the Raman scattering molecule, and contribute to heating of the sample.

The limit where the SERS intensity tails off is strongly correlated with the ratio V/λ^3, with an optimal ratio between 10^{-3} and 10^{-4}, depending aspect ratio of the SERS substrate. This correlation appears to remain even as the particles are aggregated and the

exciation source is 785 nm. This suggests that even though the plasmon resonance of the aggregates, and so preferred excitation wavelength for SERS, may not be close to any resonance of the individual nanoparticle making up the aggregate, the ratio between excitation wavelength and particle diameter is still a crucial parameter to achieve the strongest possible SERS signal. Some features of each individual nanoparticle plasmon are hence preserved upon aggregation, and has a significant impact on its properties.

Surface enhanced Raman scattering and surface enhanced resonance Raman scattering has been compared at wavelengths over the visible region. The two effects have been separated, and the importance of overlap between the frequencies of surface plasmon resonance and molecular resonance is shown. The relative weakness of single particle enhancement on the Raman intensity is confirmed.

SERS from single colloidal sols appears to be a very weak phenomenon. Looking at previous studies on SERRS mapping of immobilized silver colloids coated with ABT-DMOPA, 1-10 % of single colloids show SERRS activity. SERS being a significantly less efficient technique would be expected to show even lower numbers of active particles.

The results in this study confirm these findings. Using a very strong Raman scatterer, mercaptophenol, without any chromophore in the visible region adsorbed on to silver colloids, the SERS intensity profile over a number of excitation lines were probed.

In this study, a silver colloid solution is considered to be unaggregated if there is no registered change in Z-potential, UV/Vis spectra or dynamic light scattering (z-sizer, HPPS) before and after the addition of dye/mercaptophenol.

Even for unaggregated colloids the strongest intensities are found at 532 nm and 633 nm. In fact, it was not possible to detect any mercaptophenol spectra with 407 nm excitation, where single nanoparticles should be absorbing. This suggests that, even though the solution is considered to be unaggregated, the dominating SERS contribution comes from many-particle systems present in the solution. These systems would be

likely to enhance raman scattering in a much higher degree than single colloids due to the multiplicity of EM-fields around the particles and the higher ratio of active species.

PUBLICATIONS:

Practical control of SERRS enhancement

D. Cunningham, R. E. Littleford, W. E. Smith, P. J. Lundahl, I. Khan, D. W. McComb, D. Graham, N. Laforesta, *Faraday Discussions,* 2006, **132**, p.135 - 145

Quantitative enhanced Raman scattering of labelled DNA from gold and silver nanoparticles

R.J. Stokes, A. McAskill, P.J. Lundahl, K. Faulds, W.E. Smith, D. Graham

Small, 2007, **3**, p.1593 - 1601

Synthesis of unique nanostructures with novel optical properties using oligonucleotide mixed metal nanoparticle conjugates

D.G. Thompson, R.J. Stokes, R.W. Martin, P.J. Lundahl, K. Faulds, D. Graham

Small, (in press)

Synthesis and characterisation of monodispersed silver nanoparticles with controlled size ranges

P. J. Lundahl, R.J. Stokes, W. E. Smith, R.W. Martin, D. Graham *Micro & Nanoletters,* 2008, **3**, p.62 - 65

CONFERENCE CONTRIBTIONS:

Wavelength Dependence of SERRS (Oral Presentation)

P. J. Lundahl, W. E. Smith, *Pittsburgh Conference of Applied Spectroscopy and Analytical Chemistry*, 2007, Chicago, IL, USA